SYNTHESIS OF CROWDED TOLANES: MODELS FOR MOLECULAR RECOGNITION

Brett Lee Kite

Dissertation submitted to the Faculty of Virginia Polytechnic Institute and State University in partial fulfillment of the requirements for the degree of

Doctor of Philosophy

in

Chemistry

Richard D. Gandour, Chair

Karen Brewer

Neal Castagnoli

Joseph S. Merola

David G. I. Kingston

December 1, 2005

Blacksburg, Virginia

Keywords: Chemistry, Molecular Recognition, Diarylacetylene, Tolane

Copyright 2006, Brett L. Kite

SYNTHESIS OF CROWDED TOLANES: MODELS FOR MOLECULAR RECOGNITION

Brett Lee Kite

ABSTRACT

The development of suitable models to study and quantify the strengths of noncovalent interactions is a major goal of our group. With this goal in mind, we have synthesized octasubstituted diarylacetylenes (tolanes) as potential model systems to measure intramolecular noncovalent interactions.

The Stille cross-coupling reaction allowed synthesis of both arylacetylenes and tolanes from aryl iodides. The Stille reaction is usually slow for electron rich aryl iodides (such as these aryl iodides that are substituted resorcinol derivatives). However, these crowded penta-substituted aryl iodides underwent the Stille coupling reactions (typically 2-3 hours) at a significantly faster rate than the Stille couplings of the un-crowded tri-substituted aryl iodides (typically 24 hours). DFT calculations on 1,3-dimethoxy-2-iodobenzene (as a model system) indicate that this rate difference is mainly due to a decrease in the reduction potential of the crowded penta-substituted aryl iodides (~ 0.4 eV lower) relative to the tri-substituted aryl iodides.

The successful synthesis of the targeted crowded symmetrical tetra ester (**3.6**) produced a mixture of atropomers, which separated into two components with similar

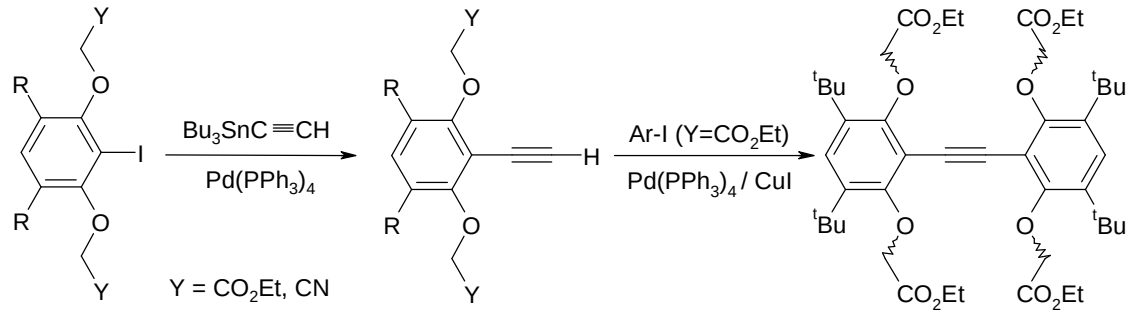

3.6

NMR and MS data. HF calculations on 4,4′,6,6′-tetra-*tert*-butyl-1,1′,3,3′-tetramethoxydiphenylacetylene (as a model system) showed that there are five possible atropomeric conformations. We separated the component which showed a green fluorescence when irradiated with UV (254 nm) light and grew a suitable single crystal.

The X-ray crystal structure revealed that this component is the syn-syn_anti atropomer. The remaining atropomers, which show blue fluorescence when irradiated with UV (254 nm) light, were not successfully separated. Comparison of the observed UV spectrum of the green-fluorescent atropomer (syn-syn_anti) with a calculated (ZINDO) UV spectrum of diphenylacetylene, with an interplanar angle of 0° between the arene rings, showed that the observed and calculated spectra closely matched. The calculated (ZINDO) UV spectrum of diphenylacetylene, with an interplanar angle of 60° between the arene rings, closely matched the observed spectrum for the blue-fluorescent component (mixture of atropomers). The combination of experimental and computational methods demonstrated the stereochemical complexities of the crowded symmetrical tetra ester (**3.6**).

ACKNOWLEDGEMENTS

Many people have helped me during the course of this research. I would especially like to thank the following people.

To my wife Kerri Ann thanks for all of your love, support and patience.

To my parents, Bert and Leisa Kite and Alice Murray and to my brother Bart Kite thanks for all of your support and faith.

A special thanks to my advisor, Dr. Richard Gandour, for your patience and loyalty.

Thanks to my former group members and friends Kevin Evans and Victor Rosas.

Thanks to Frank Fronczek and Dr. Joseph Merola for X-ray crystallography.

Thanks to the other members of my committee, Dr. Karen Brewer, Dr. Neal Castagnoli, and Dr. David Kingston for advice and assistance.

Thanks to the current members of the Gandour group, especially Richard Macri, Eko Winny Sugandi and André Williams.

DEDICATION

I would like to dedicate this work to the memory of and in honor of my grandparents: Harry Lowers, Frances Lowers, Bertram Wilson Kite, Sr. and Arbutus Kite.

"The end of a matter is better than its beginning, and patience is better than pride."
Ecclesiastes 7:8

TABLE OF CONTENTS

Page

ABSTRACT……..... ii

AKNOWLEDGMENTS……. iv

DEDICATION……..... v

LIST OF FIGURES…….. xi

LIST OF SCHEMES…… xiv

LIST OF TABLES…….…….. xv

I. BACKGROUND…….....… 1

I.1 Introduction…… 1

I.1.1 Substitutent Effects…… 2

I.1.2 Field Effect……...… 2

I.1.2.a Theory……... 2

I.1.2.b Experiments…… 3

I.1.2.c Comments…….. 6

I.1.3 Convergent Functional Groups……. 6

I.2 Models of Enzyme Catalysis…….. 8

I.2.1 Theories of Intramolecular Catalysis……..… 9

I.2.2 Orbital Steering…….. 10

I.2.3 Propinquity……... 11

I.2.4 Entropy Trapping…… 11

I.2.5 Stereopopulation Control……...….. 11

I.2.6 Spatiotemporal Hypothesis…….. 12

I.3 Previous Work in Gandour's Laboratory…….…….. 13

I.4 Tolanes as Building-Blocks……..…….. 17

I.4.1 Spacer / Linker…….. 17

I.4.2 Spools……..…... 18

I.4.3 Anchors……... 18

I.4.4 Proximity Models…….. 18

I.4.5 Tethered Tolanes…… 19

I.4.6 Applications of Tolanes as Molecular Machines and Devices……..…….. 19

I.5 Conclusions and Goals…….. 22

II. SYNTHESIS OF IODORESORCINOLS……... 23

II.1 Synthesis of Buttressed *O,O*-Dialkylated-2-Iodoresorcinols…… 24

II.1.a Synthesis of 4,6-di-*tert*-butylresorcinol……. 24

II.1.b Synthesis of 4,6-di-*tert*-butyl-2iodoresorcinol…… 24

II.1.c Attempted Synthesis of 4,6-di-*tert*-butyl-2-iodo-3-methoxyphenol…….. 26

II.1.d Dialkylation of 4,6-di-*tert*-butyl-2-iodoresorcinol…….. 27

II.2 Synthesis of Phenylcarbamate-4,6-di-*tert*-butyl-2-iodoresorcinol 29

II.3 Experimental…….. 31

II.3.a Preparation of 2-iodoresorcinol…….. 31

II.3.b Preparation of 4,6-di-*tert*-butylresorcinol…….. 31

II.3.c Iodination of 4,6-di-*tert*-butylresorcinol……... 31

II.3.d Iodination of 4,6-di-*tert*-3-methoxyphenol…… 32

II.3.e *O,O*-Dialkylation of iodoresorcinols, Method A…… 33

II.3.f *O,O*-Dialkylation of iodoresorcinols, Method B……. 33

II.3.g *O,O*-Dialkylation of iodoresorcinols, Method C…… 33

II.3.h 1,3-Bis-allyloxy-2-iodobenzene…….. 33

II.3.i (3-Cyanomethoxy-2-iodo-phenoxy)-acetonitrile…… 33

II.3.j 2-Iodo1,3,-di(*tert*-butyl-dimetyl)siloxybenzene…….. 34

II.3.k (2-Iodo-1,3-phenylenedioxy)diacetic acid diethyl ester… 34

II.3.l (4,6-di-*tert*-butyl-2-iodo-1,3-phenylenedioxy)diacetic acid diethyl ester (**2.1**) …….. 34

II.3.m (3-Cyanomethoxy-4,6,-di-*tert*-butyl-2-iodo-phenoxy) -acetonitrile (**2.2**) ……..…... 34

II.3.n 1,3-di-allyloxy-4,6-di-*tert*-butyl-2-iodobenzene (**2.4**) …

II.3.o (2-Azidoethoxy-4,6-di-*tert*-butyl-2-iodophenoxy)-2 -azidoethane (**2.3**)……..….. 34

II.3.p (4,6-di-*tert*-butyl-2-iodo-1,3-phenylenedioxy)di-*N*-phenylformamide)……..…. 35

III. SYNTHESIS OF ARYLETHYNES AND TOLANES…..…… 36

III.1 Synthesis of Arylethynes……..….. 36

III.2 Synthesis of Tolanes……..……... 38

III.3 Analysis of the Tetra Ester…….…. 39

III.4 Structure of Green-Fluorescent Component……..…..…. 41

III.5 Atropisomerism in Crowded Arenes……...…. 43

III.6 Summary……..…….….. 43

III.7 Experimental……..…….…. 45

III.7.a 1,3-Di-(2,3,-*O,O*-isopropylidine-1-propoxy)-2-benzethyne……..……..…….…. 45

III.7.b 1,3-Di-(ethoxycarbonylmethoxy)-2-benzethyne (**3.1**)…. 45

III.7.c 1,3-Di-(ethoxycarbonylmethoxy)-4,6-di-*tert*-butyl-2-benzethyne (**3.2**)……..……..…….…. 45

III.7.d 1,3-Di-(oxoacetonitrile)-2-benzethyne (**3.3**)……..... 46

III.7.e 1,3-Di-(oxoacetonitrile)-4,6-di-*tert*-butyl-2-benzethyne (**3.4**)……..……..…….…. 46

III.7.f 1,3-Di-(2-azidoethoxy)-4,6-di-*tert*-butyl-2-benzethyne (**3.5**) 46

III.7.g 2-[1,3-Di-(ethoxycarbonylmethoxy)-4,6-di-*tert*-butyl-2-benzethynyl]-1,3-di-(ethoxycarbonylmethoxy)-4,6-di-*tert*-butylbenzene (**3.6**)..... 47

III.7.h 1-[1,3-Di-(oxoacetonitrile)-2-benzethynyl]-2-(methoxycarbonyl)benzene..... 47

III.7.i 1-[1,3-Di-(2-azidoethoxy)-4,6-di-tert-butyl-2-benzethynyl]-2-(methoxycarbonyl)benzene..... 48

IV. CALCULATIONS..... 49

IV.1 Calculations on 2-Iodoresorcinols..... 49

IV.2 Calculations on the Tetra Ester..... 54

IV.3 Experimental..... 56

IV.3.a XYZ Data for the Anti (C_2) rotation of 1,3-dimethoxy-2-iodobenzene..... 56

IV.3.b XYZ Data for the Syn (C_S) rotation of 1,3-dimethoxy-2-iodobenzene..... 63

IV.3.c XYZ Data for the minimum conformations of 4,4′,6,6′-tetra-*tert*-butyl-1,1′,3,3′-tetra-methoxy-diphenylacetylene..... 70

V. CONCLUSIONS..... 85

V.1 Synthesis of pentasubstituted arenes..... 85

V.2 Synthesis of arylacetylenes..... 85

V.3 Unusual reactivity of crowded aryl iodides..... 86

V.4 Atropisomerism in crowded tolanes..... 86

V.5 Final Comments..... 86

References..... 88

Appendix A (Supplemental NMR Data)..... 95

Appendix B (Supplemental X-Ray Data)…….……..……. 109

VITA……..……..…..……..…….…….…. 133

LIST OF FIGURES

		Page
Figure 1.1	Types of Noncovalent Interactions…….……..	1
Figure 1.2	Transmission Factors for cyclohexyl, bicylo[2.2.1]heptyl and bicyclo[2.2.2]octyl 1-carboxylic acids……..	4
Figure 1.3	Hammett constants for arylnorbornene-2-carboxylic acids……	4
Figure 1.4	Ionization data of 5-substituted-triptycene-7-carboxylic acids…	5
Figure 1.5	Ionization data of bridged anthroic acids…….……..	5
Figure 1.6	Proximate diacids……..…..	6
Figure 1.7	Carboxylic acids in macrocyclic polyethers……..…	7
Figure 1.8	Proximate carboxylic acids and imidazoles……..…	7
Figure 1.9	Steric compression of *cis*-urocanic acids……..……	8
Figure 1.10	A cartoon representation of an enzyme…….……	8
Figure 1.11	Lactonization and thiolactonization (Orbital Steering)……	9
Figure 1.12	Rates of formation of anhydrides (Propinquity)……..…	10
Figure 1.13	Rates of formation of lactones, cyclic ethers and cyclic anhydrides (Stereopopulation Control)…….……	12
Figure 1.14	Rates of lactonization in norbornyl hydroxyacids (Spatiotemporal Hypothesis)…….…..……	12
Figure 1.15	Tethered stilbenes and tolanes…….……	13
Figure 1.16	Tethered dinaphthylacetylenes and diphenylacetylenes……	14
Figure 1.17	General base catalysis in 2-carboxy-2′-dichloroacetoxydiphenylethyne…….…….	14
Figure 1.18	Heterocyclic by-products formed during removal of methoxy groups…….…….….	15
Figure 1.19	Tolanes as molecular switches…….….	16
Figure 1.20	Previously synthesized molecules in the Gandour group…….	16
Figure 1.21	Rates of lactonization of diphenylacetylenic acids……..…..	17

Figure 1.22 •-turn anchor…… 18
Figure 1.23 Proximity model of Vedejs…… 19
Figure 1.24 Ruggli and Voegtle's tethered tolanes…… 19
Figure 1.25 Kelly's molecular brake…… 20
Figure 1.26 Phenylacetylene dendrimers…….. 20
Figure 1.27 Bistrityldiacetylene fluorescent chemosensor…… 21
Figure 1.28 Tolanes as molecular wires and caltrops…….. 21
Figure 1.29 Tolane retrosynthesis…… 22
Figure 2.1 Structure of (4,6-di-*tert*-butyl-1,3-phenylenedioxy)-diacetic acid diethyl ester…….. 23
Figure 2.2 Hemiquinone obtained during iodination of 4,6-di-*tert*-butyl-methoxyphenol…….. 27
Figure 2.3 Pool of *O*,*O*-dialkylated 4,6,-di-*tert*-butyl-2-iodoresorcinols…. 28
Figure 2.4 Formation of bis-imidazolines, bis-benzimidazoles and bis-acetonides……. 28
Figure 2.5 Bis-carbamate and allophanate……... 29
Figure 2.6 X-ray crystal structure of bis-carbamate…… 30
Figure 3.1 Catalytic cycle for the Stille cross-coupling reaction ……... 36
Figure 3.2 ^{1}H NMR spectra of green and blue-fluorescent components …. 39
Figure 3.3 UV spectra of green and blue-fluorescent components……. 40
Figure 3.4 AM1 structure of 2,2′,4,4′,6,6′-hexa-*tert*-butyldiphenylacetylene 41
Figure 3.5 X-ray crystal structure of the green-fluorescent component …... 42
Figure 3.6 Bürgi-Dunitz trajectory for nucleophilic attack……. 42
Figure 3.7 Axial chirality in crowded tolanes……. 43
Figure 4.1 LUMO energy versus methoxy torsions in 1,3-dimethoxy-2-iodobenzene…….. 51
Figure 4.2 LUMOs for anti (C_2) rotation…….. 52

Figure 4.3 LUMOs for syn (C_S) rotation……..…….. 53

Figure 4.4 Structural families of the tetra-ester (**3.6**)……..….. 54

Figure 4.5 Conformations and energies of 2,2′,4,4′-tetra-*tert*-butyl-1,1′,5,5′-tetramethoxydiarylacetylene……..…… 55

LIST OF SCHEMES

		Page
Scheme 1.1	Synthesis of arylacetylenes from acetophenones and aryl iodides	14
Scheme 3.1	Stille coupling of buttressed and unbuttressed iodoresorcinols…	37
Scheme 3.2	Synthesis of molecular switches……..……..	38
Scheme 3.3	Synthesis of tetra ester…….	38

LIST OF TABLES

Page

Table 2.1 pH dependence of the reduction potential of resorcinol…….. 26

Table 3.1 Synthesis of aryl ethynes…….. 37

CHAPTER I: Background

I.1 Introduction

Molecular recognition, *i.e.* the ability of molecules and functional groups to recognize and interact with each other, is fundamentally important for understanding many chemical phenomena, e.g., drug–receptors, enzyme–substrate recognition, adhesion of molecules to surfaces, self-assembly of molecules, etc. In order to understand and incorporate molecular recognition into the rational design of synthetic molecules, we must first understand and quantify the actual recognition events (forces).

Molecular recognition is largely driven by noncovalent interactions between molecules and their associated functional groups. The strengths of these noncovalent interactions are dependent on both distance (often very strongly) and orientation. A list of noncovalent interactions and how the energy of attraction (or repulsion) varies with distance is shown in Fig. 1.1.[1] Noncovalent interactions have been studied computationally. Because noncovalent interactions are largely electrostatic interactions, the use of the electrostatic potential (and derived quantities[2,3]) has been a logical and popular starting point for computational studies. Accurate and precise experimental

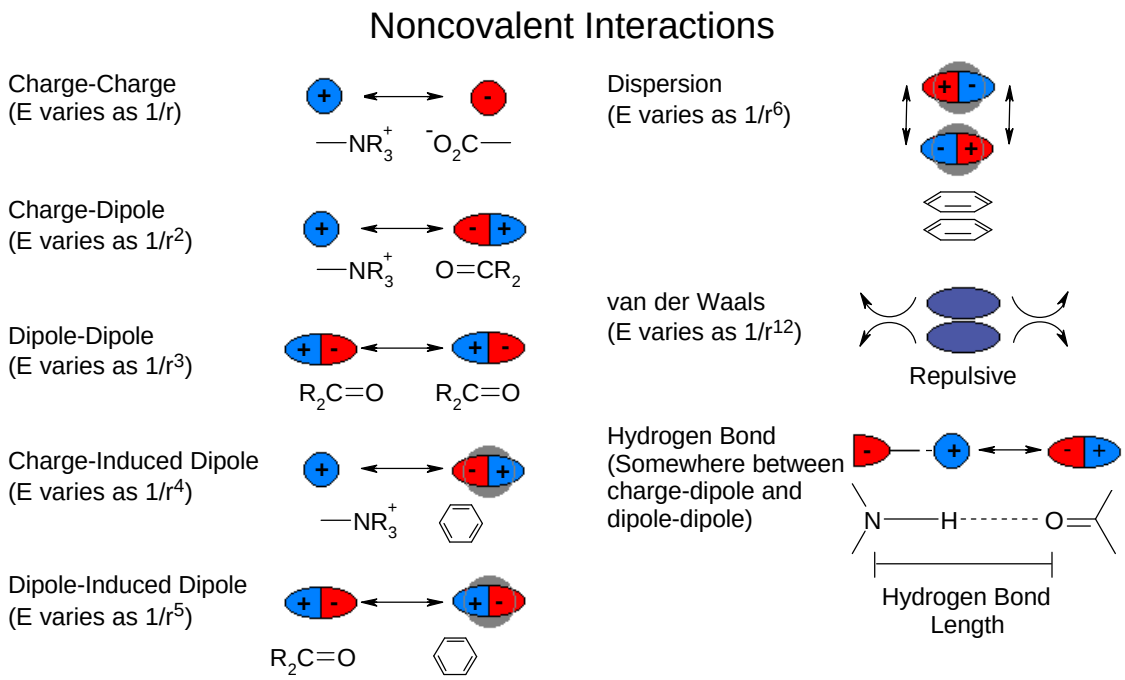

Figure 1.1. Types of noncovalent interactions and their distance dependence (reproduced in part from Mathews and Van Holde[1]). E is the electronic interaction and r is distance.

measures of noncovalent interactions as functions of distance, however, remain a considerable challenge even today.

I.1.1 Substitutent Effects

One approach to studying substituent effects is to anchor two groups on the same molecule and measure some property. Issues of orientation, distance, effect of molecular framework, etc. can then be systematically addressed. These same types of model systems might also mimic the intramolecular recognition between groups found in proteins.

The history of this approach began with Hammett's[4,5] classic studies of correlating reaction rates versus equilibrium constants.

$$R\text{–}COOCH_3 \;+\; N(CH_3)_3 \;\rightarrow\; R\text{–}COO^- \;+\; {}^+N(CH_3)_4$$

Because of the limitations of the aromatic molecular framework and the reaction used for the reference, researchers began defining substituent constants for several reactions. This practice reached the point where Swain commented that "…the number of sets of substituent constants now exceeding the average number of substituents in a set…"[6]. Swain[6,7] and co-workers proposed to define all substituent constants as composed of two contributions: field ($\mathfrak{I}$) and resonance ($\mathfrak{R}$). This approach stirred controversy and further experiments. However, the question of whether the field effect occurs through "space" (or solvent) or by polarization of the intervening bonds remained open to debate.

I.1.2 Field Effects

I.1.2a Theory

Most noncovalent interactions operate, by definition, through field effects. However the uncoupling of field (through space or solvent) and inductive effects (through bond) in order to obtain a quantitative picture of each has remained elusive. One of the major obstacles to a theoretical treatment of field effects is that of the geometry of the molecule in a solvent cavity. If the dipoles/charges are located at the ends of a long and slender molecule, the lines of force mostly pass through the bulk solvent. However if the dipoles/charges are located inside a bulky molecule, the lines of force mostly pass through the molecule itself. Kirkwood and Westheimer[8,9] have developed a treatment (Eq. 1.1 and 1.2) assuming an ellipsoidal (or spherical) cavity of

low dielectric constant surrounded by a higher dielectric constant medium (bulk solvent). This treatment, with some modifications, still constitutes the basis for the majority of the theoretical calculations.

$$\log(K/K^{o}) = \frac{Ze\mu\cos\theta}{2.303kTr^{2}(4\pi\varepsilon_{0}\,\varepsilon_{ef})} \qquad (1)$$

$$\log(K/K^{o}) = \frac{Z_{1}Z_{2}e^{2}}{2.303kTr(4\pi\varepsilon_{0}\,\varepsilon_{ef})} \qquad (2)$$

Equations 1.1 and 1.2. Z_1 and Z_2 are the charges, μ is the dipole moment, θ is the angle between the dipole vector and the distance r between the charge and the dipole, *k* is Planck's constant, T is temperature, ε_0 is the permittivity of free space, and ε_{ef} is the relative permittivity.

Two problems in particular still limit and cloud the issue with respect to the application of electrostatic field theory. The first is in the choice of an effective permitivity, ε_{ef}. This value lies somewhere between that of the bulk permitivity of the solvent and the intrinsic permitivity of the solute. Both of these permitivities are macroscopic properties; however, what is needed is a molecular permitivity. Therefore, the choice of effective permitivity is very subjective and arbitrary. The second problem is the effect of angular dependence on the calculated electrostatic field.[10] It has been shown that the electrostatic field values are overestimated (by 38% at $q = 80°$) or underestimated (by 25% at $q = 0°$) depending on the angle.[11]

Another source of error is the point-dipole approximation, in which the distances are measured from the center of the dipole length. The validity of the point-dipole approximation decreases as the interaction distance decreases and as the dipole length increases. Segurado and co-workers have developed equations free from the errors associated with point-dipoles, while retaining the use of dipole moments.[11]

I.1.2.b Experiments

A common evaluation of substituent effects is to compare experimental reaction constant data, ρ or ρ/ρ^{0}, with those predicted by various theoretical models for both inductive and electrostatic field effects. Charton[12] (Fig. 1.2) has compared the

reaction constants, ρ_i / ρ_i^o, for the ionization of cyclohexyl, bicyclo[2.2.1]heptyl, and bicyclo[2.2.2]octyl acids to the predicted inductive and electrostatic field values.

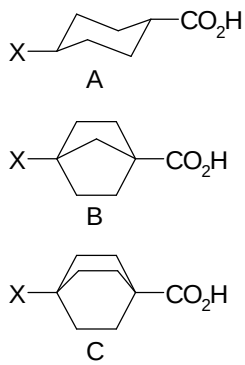

Transmission factors ρ_i / ρ_i^0

System	Exptl.	Calcd. (Inductive)	Calcd. (Electrostatic Field)
A	0.18	0.09	0.16
B	0.25	0.22	0.24
C	0.21	0.14	0.19

Figure 1.2. Hammett ρ_i/ρ_i^o values for the plots of pK_a vs σ_I for 4-cyclohexane-1-carboxylic acids (A), 4-bicyclo[2.2.1]heptane-1-carboxylic acids (B), and 4-bicyclo[2.2.2]octane-1-carboxylic acids (C). Note that ρ_i^o is the Hammett constant for substituted acetic acids.

Comparison of the experimental data with both calculated electrostatic field and calculated inductive values show the calculated electrostatic field values are in better agreement with the experimental data. Beugelman-Verrier et al[13] (Fig. 1.3) have studied the ionization of 3-arylnorbornene-2-carboxylic acids. The rigidity of the framework allows for good precision in the distance and angle between the carboxylic acid and the polar *para*-substituents. The calculated field effect values once again show better agreement with the experimental data (as compared calculated inductive effect values); however, the theoretical predictions only show minor differences between the two theoretical approaches.

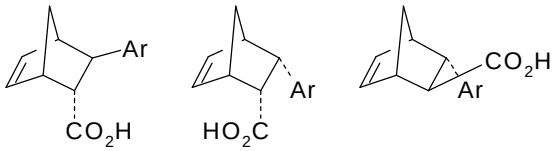

endo, *trans* *endo*, *cis* *exo*, *trans*

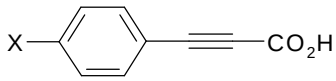

3-Arylpropargylic Acid (3-APA)

Hammett constants ρ / ρ^o

System (ρ)		Exptl.	Inductive Model	Field Model
endo, trans	(0.44)	1.0	1.0	1.0
exo, trans	(0.49)	1.1	1.0	1.0
endo, cis	(0.68)	1.5	1.0	1.3
3-APA	(0.37)	0.8	0.9	0.8

Figure 1.3. Hammett ρ/ρ^o values for plots of pK_a vs σ constans of arylnorbornene-2-carboxylic acids and 3-arylpropargylic acids. Note that ρ^o is the ρ value for the *endo, trans* isomer.

Others have examined ΔpK_a data as compared with predicted values. Acevedo and Bowden[14] (see Fig 1.4) have studied a series of 5-substituted triptycene-7-carboxylic acids and esters. The ionization data show a clear (although the effects are small) reversed dipolar substituent effect (*i.e.*, electron withdrawing substituents increase rather than decrease the acidity); however, the esterification and ester hydrolysis data are more complex.

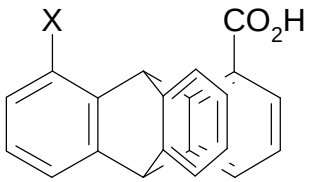

X	pK_a	Esterification k_2 (l mol $^{-1}$ min $^{-1}$)	Ester Hydrolysis k_2 (l mol $^{-1}$ min $^{-1}$)
H	6.88	0.626	0.266
Cl	7.04	0.982	0.181
CN	7.03	0.187	0.387
OMe	7.16	0.582	0.204

Figure 1.4. Ionization data for triptycene acids, pK_a data measured in 80% (w/w) 2-methoxyethanol–water. The esterification data is for esterification of the triptycene acids with diazodiphenylmethane at 30 °C, while the alkaline hydrolysis is for the methyl esters in 70% (v/v) dioxane–water at 30.4 °C.

Grubbs[15-18] and co-workers have studied chloro substituted 9,10-bridged 1- and 2-anthroic acids. These systems are attractive models as one predicts no difference in inductive effects among the four isomeric dichloroethano bridged systems (ortho b, meta b, and ortho c, meta c). That there is a difference in pK_a is strong evidence in favor of the electrostatic field theory. Also the angular disposition of the dipoles can account for the 'vanished' or reduced dipolar substituent effects noticed in Meta c, Ortho c, and Alkene c (Fig. 1.5).

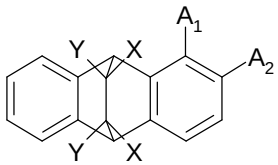

Meta (A_1=H, A_2=CO_2H)
a X = H, Y = H
b X = H, Y = Cl
c X = Cl, Y = H

Ortho (A_2=H, A_1=CO_2H)
a X = H, Y = H
b X = H, Y = Cl
c X = Cl, Y = H

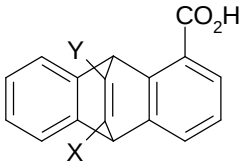

Alkene
a X = H, Y = H
b X = Cl, Y = H
c X = H, Y = Cl

ΔpK_a (rel to a)

Compound	Exptl.	Calcd.
Meta b	0.58	(Electrostatic Field)
Meta c	0.18	
Ortho b	0.47	0.36
Ortho c	0.02	0.01
Alkene b	0.22	0.29
Alkene c	0.04	0.13

Figure 1.5. Ionization data (namely ΔpK_a) for bridged anthroic acids.

I.1.2c Comments

The majority of these model systems suffer from the same disadvantage: the molecular framework of the models lies between the interacting ends (*i.e.* the rest of the molecule could act as a 'screen'). At best, a few models have the interacting groups side-by-side. Models that position groups head on (converging) could help to clarify our understanding of the magnitudes of field and inductive effects. Models in which the inductive and field effects operate in opposite directions (like the all trans fused model to the right proposed by Hine in 1975[19]) have attracted theoreticians but frustrated synthetic chemists.

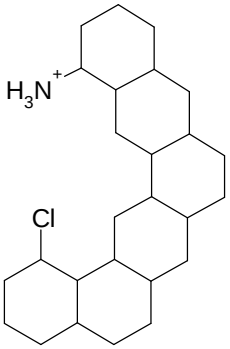

I.1.3 Convergent Functional Groups

Rebek et al.[20] (Fig. 1.6) have synthesized models that have two proximate carboxylic acids in a variety of orientations: convergent, divergent, and parallel. Also these models are part of an ongoing attempt to design synthetic enzymes. This was done not so much to study field effects, as it was to examine the stereoelectronics of the carboxylate groups (*i.e.* that the syn lone pair is more basic than the anti lone pair[21]). Rebek's data support this view; however the conclusions are not as simple as one would like.

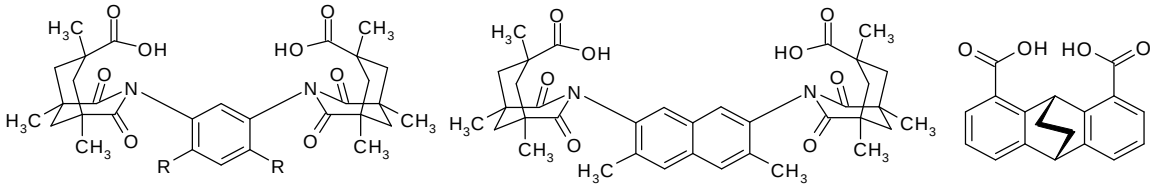

Figure 1.6. Effect of orientation on the ΔpK_a of proximate diacids.

Cram et al.[22] have synthesized a series of macrocylic polyethers (Fig. 1.7) in order to align "potentially complexing functional groups" [22]. The most relevant of these macrocylic polyethers align a carboxylic acid with either another carboxylic acid or a pyridine. The X-ray crystal structures show that the functional groups are indeed hydrogen-bonded. The models show that a proximate pyridine can significantly raise the

pK_a of a carboxylic acid. However, the diacid in solution is apparently not strongly associated, most likely due to the increased flexibility of the larger polyether.

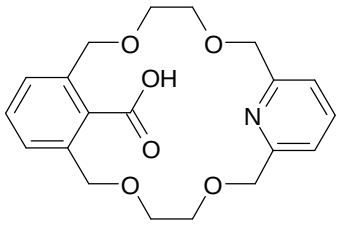

$pK_{a\ COOH}$ = 5.8 (H_2O)

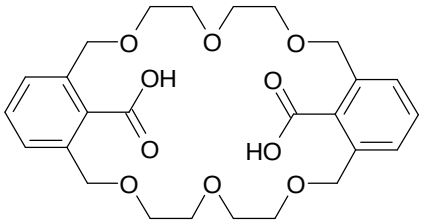

$pK_{a1\ COOH}$ = 6.3 (65:35 DMSO/H_2O)
$pK_{a2\ COOH}$ = 8.0 (65:35 DMSO/H_2O)

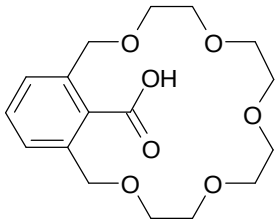

$pK_{a\ COOH}$ = 4.8 (H_2O)

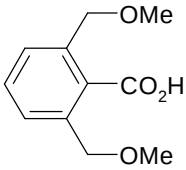

$pK_{a\ COOH}$ = 3.30 (H_2O)
$pK_{a\ COOH}$ = 6.65 (65:35 DMSO/H_2O)

Figure 1.7. Effect of proximity on the pK_a of carboxylic acids in macrocylic polyethers.

Zimmerman et al.[23,24] have synthesized models (based in part on the X-ray structures of Cram[22]) to study the histidine-aspartate couple found in enzymes such as serine proteases. The majority of these enzymes show the carboxylate of aspartate oriented syn onto a histidine. Zimmerman's models (see Fig 1.8) demonstrate that carboxylate can raise the pK_a of a proximate imidazole.

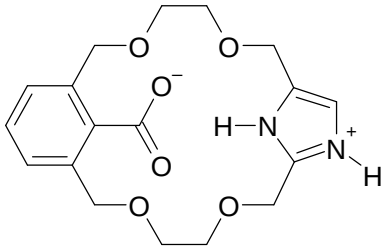

$pK_{a\ Imidazole}$ = 7.5

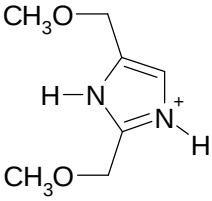

$pK_{a\ Imidazole}$ = 6.00

Figure 1.8. Effect of a proximate carboxylate on the pK_a of an imidazole.

Other researchers have examined the role of a low barrier hydrogen bond (short and presumably strong hydrogen bonds) between histidine and aspartate. Cloninger and Frey have examined the possibility of steric compression and LBHB formation (Fig

1.9).[25] The data show the *trans*-urocanic acids all have the same pK_a (6.0 ± 0.1). However, the *cis*-urocanic acids show a definite increase in pK_a. Cloniger and Frey attribute this increase to steric compression of the carboxylic acid and the imidazole ring. This would increase the hydrogen bond strength and consequently increase the pK_a.

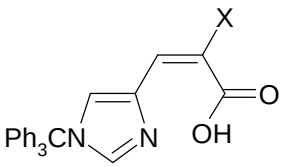

cis-Urocanic Acids

X	pK_a
H	6.78
Cl	7.81
Br	9.10

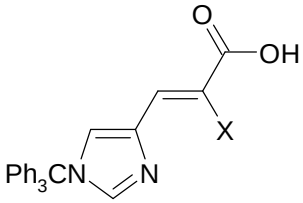

trans-Urocanic Acids

X	pK_a
H	5.92
Cl	6.02
Br	5.99

Figure 1.9. Effect of steric compression on pK_a of *cis*-urocanic acids.

I.2 Models of Enzyme Catalysis, Functional Groups that Interact Intramolecularly

Enzymes and enzymatic catalysis, in particular, have been widely studied, because enzymes are able to greatly accelerate reactions over their non-enzymatic counterparts. Enzymatic transformations are also much more selective, both in terms of stereoselectivity and chemoselectivity than their corresponding non-enzymatic transformations. Synthetic enzymes that catalyze many chemical transformations would help to increase the ease of synthesis and diversity of synthesized molecules.

The key to understanding enzymatic transformations is to understand the interactions between proximate functional groups. These functional groups can be proximate on the enzyme itself and between the enzyme and a substrate (see Fig 1.10). We know these interactions are critical for recognition and catalysis; however, the understanding of these interactions is still largely qualitative.

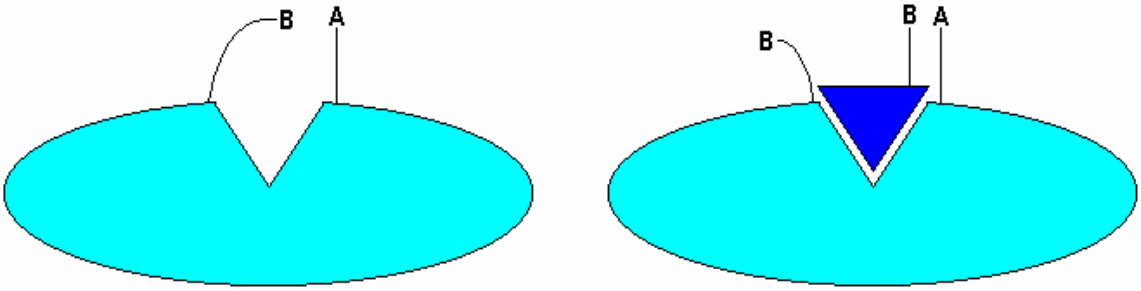

Figure 1.10. A cartoon representation of an enzyme (A and B are groups capable of interaction) and an enzyme with bound substrate.

Two major types of model systems have been developed and studied, host-guest and intramolecular. In the host-guest approach, one or two molecules are allowed to bind to a 'host' molecule (typically a cyclodextrin[26]). In the intramolecular approach, a single molecule is designed to incorporate all reactive/catalytic sites. Each model has its own advantages and disadvantages. In this review, we focus on intramolecular models.

I.2.1 Theories of Intramolecular Catalysis

Each proponent of a theory has used a unique set of models to develop their particular theory. The majority utilized intramolecular models to compare intramolecular vs. intermolecular transformations. This is a problem as one cannot directly compare the first order and second order rate constants obtained from the intramolecular (k_1) and intermolecular reactions (k_2), respectively. The usual solution is to compare the ratio of rate constants for the two reactions, k_1/k_2. The units of this ratio must be (1/s)/(1/M·s), which is equivalent to M. Therefore, this ratio has been called an effective molarity (abbreviated EM). For accurate EM's the intramolecular and intermolecular reactions must have the same mechanism, and the rates of the corresponding reactions measured under the same conditions. In general, these stringent conditions are unattainable, so the majority of EM's are obtained by comparing the intramolecular reaction rate constant, k_1, with the "rate constant for the closest equivalent intermolecular reaction under conditions which are as similar as possible."[27] A brief overview of some of the major theories and the intramolecular models studied is necessary. The early theories have been reviewed[28,29] previously in greater detail.

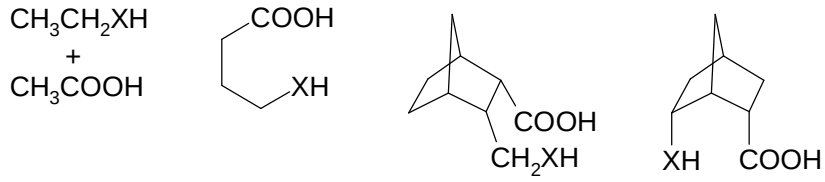

X=O				
Uncorrected Rel. Rate	1	79	6630	1.03×10^6
Corrected Rel. Rate	1	413	1590	1.87×10^4
X=S				
Uncorrected Rel. Rate	1	384	90	8.21×10^5
Corrected Rel. Rate	1	2020	5	1.5×10^4

Figure 1.11. Rates of lactonization and thiolactonization for intermolecular, acyclic and cyclic systems.

I.2.2 Orbital Steering

Storm and Koshland[30-32] (see Fig 1.11) suggested stereoelectronics, i.e. the orientation of orbitals in the reacting atoms (molecules), as the major factor contributing to the catalytic nature of enzymes. This "orbital steering" can account for rate enhancements up to 10^4 per reacting atom. However, in order to achieve such enhancements, each atom must be stringently oriented, thus reacting at only a fraction of its surface (reaction window).

Orbital steering has been widely attacked, mostly on the correction factors (which include proximity, torsional strain, and conformational isomers). Capon[33] disagrees with the magnitude of the strain correction (it's too small) and lack of an internal rotational entropy correction.

The reaction window is another argued point. Bruice[34] calculated that a window of 0.1° is necessary for a rate enhancement of 10^4. Storm and Koshland disagreed, pointing out that Bruice's value is for only one atom. Storm and Koshland[31] calculated that a 10° window achieved by two atoms gives the desired enhancement.

The proximity factor correction, with a value of 55 (the molar concentration of water in water), has raised the most controversy. Bruice[35] stated that experimental intra/intermolecular rate ratios exceed 55. Page and Jencks[36,37] calculated a value of 10^5 for the proximity factor.

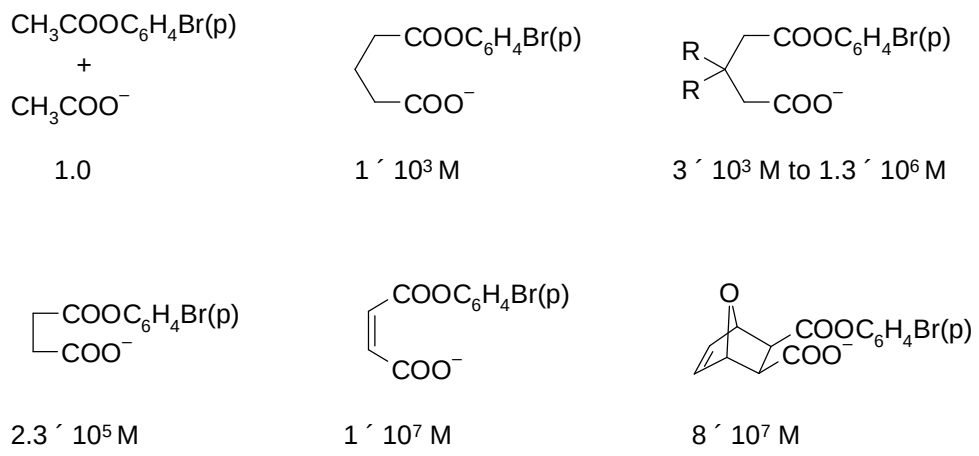

Figure 1.12. Rate of formation of anhydrides from monoesters.

I.2.3 Propinquity

Propinquity as proposed by Bruice and Pandit[38-41], states that the rate enhancement results from holding the reacting functional groups in close proximity. Bruice and co-workers measured the rate of formation of anhydrides from the monoesters of model diacids (Fig. 1.12). All rate enhancements can be attributed to the loss of translational entropy. Later Lightstone and Bruice[42] did some calculations that demonstrated that those compounds which had a greater mole fraction of "near attack conformation" reacted at an increased rate. Only the magnitude of the enhancement is debated, 10^5–10^6 (Page and Jencks[36]) vs. 10^8 (Bruice).

I.2.4 Entropy Trapping

Page and Jencks[36,43] attribute the rate enhancement of an enzymatic transformation to a loss of entropy, namely rotational and translational entropy. When a molecule is bound to an enzyme's active site, the entropy component of the reaction barrier is lowered, as compared to the unbound state. In effect the entropy is "frozen" out, thus lowering the barrier to reaction. Entropy trapping can account for enhancements up to 10^8.

I.2.5 Stereopopulation Control

Cohen[44-46] and co-workers proposed that suitable substituents could limit or freeze the molecule into the most productive rotamer conformation for reaction. This phenomenon of increasing the population of one conformation has been dubbed "stereopopulation control". Cohen utilized in his models a "trimethyl lock". As Fig. 1.13 shows, when both R4 and R5 are methyl groups the rate accelerations are quite impressive (on the order of 10^5). Stereopopulation control has also been criticized, mainly that the model systems are actually quite strained.[47,48] In my view, the X-ray data show no attraction between the functional groups in the monocyclic compounds; crowding the groups causes strain from repulsion. Covalent bond formation replaces this repulsion with a strong attractive force. This could explain the incredible acceleration ($\sim 10^{11}$) seen in the lactonization reactions.

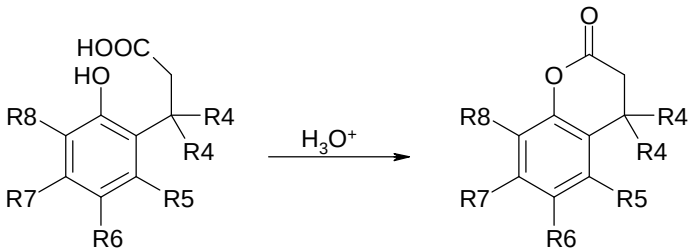

R4	R5	R6	R7	R8	Rel. Rate
H	H	H	H	H	1
H	CH_3	H	CH_3	H	6.8
CH_3	H	H	H	H	4,400
CH_3	H	H	H	CH_3	16,700
CH_3	CH_3	H	CH_3	H	8×10^{10}
CH_3	CH_3	H	H	CH_3	3×10^{11}
CH_3	CH_3	H	CH_3	CH_3	3×10^{11}

R4	R5	R6	R7	R8	Rel. Rate
H	H	H	H	H	1
H	H	H	CH_3	CH_3	3.5
H	CH_3	H	CH_3	CH_3	7
CH_3	H	H	H	H	3,100
CH_3	H	H	CH_3	CH_3	10,464
CH_3	CH_3	H	CH_3	CH_3	9×10^5

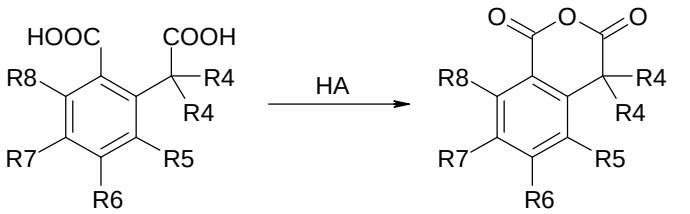

R4	R5	R6	R7	R8	Rel. Rate
H	H	H	H	H	1
H	H	H	H	CH_3	10
H	CH_3	H	H	H	52
H	CH_3	H	H	CH_3	50
CH_3	H	H	H	H	82,000
CH_3	CH_3	CH_3	CH_3	CH_3	8×10^5

Figure 1.13. Rate of formation of lactones, cyclic ethers, and cyclic anhydrides.

I.2.6 Spatiotemporal Hypothesis

Menger[49] proposed that the enhancements are due to the *time* the functional groups are within a *critical distance*. Also Menger suggests that distance is more important than orientation. Menger studied the lactonization of substituted norborynl hydroxyacids (Fig. 1.14). The O···C distances are very similar, but the angle between the alcohol oxygen and acid carbonyl varies (~10°). If Koshland's[30] orbital steering theory were correct then the 10° variation should lead to a rate difference of 10^4. However, Menger[50] found almost identical rates of lactonization, implying that distance

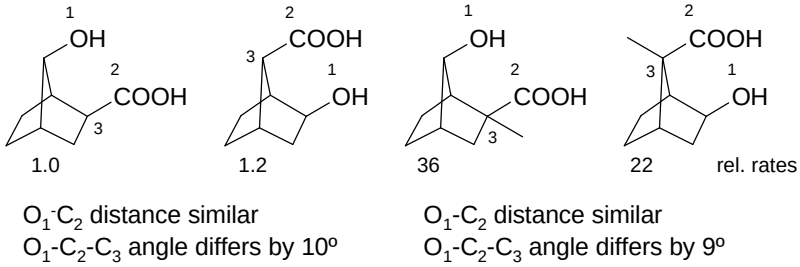

Figure 1.14. Rates of lactonization in substituted norborynols.

(not alignment) is the dominant factor.

I.3 Previous Work in Gandour's Laboratory

Previous efforts in our group were directed toward the design and synthesis of suitable models to study enzymatic catalysis. The original idea was to synthesize suitable tethered (namely macrocycles that link aromatic rings) systems, in order to study proximity effects, and intramolecular transformations in particular. The untethered intermediates would be available as useful controls for comparison.

The design concept was to vary the tether length and flexibility. This variation could provide a systematic variation of the distance and orientation between A and B. The advantage of these models would be that the molecular framework remained constant and the changes occur by rotation about carbon-carbon single bonds. Such models would enable the development of equations that describe an interaction as a function of distance.

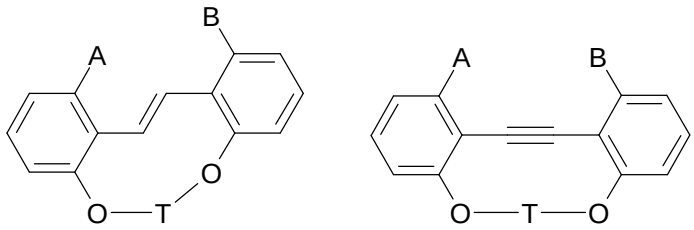

Figure 1.15. Tethered stilbene and tolanes (A and B groups capable of interaction).

The initial work in our laboratory on such model systems was based on stilbene and stilbene crowns (Fig. 1.15), where T = $(–CH_2CH_2O–)_n$.[51,52] Attempts to make stilbene crowns with substituents, A and B, involved many steps and, ultimately, ended in failure because A and B interfered with ring closure reactions.[53]

Later, we switched to acetylene-derived models, due mainly to the ability of acetylenic models to position groups more effectively (A and B) at a well-defined distance (R) based upon the length and flexibility of the tether. Also the tethered and even untethered systems could be utilized as molecular calipers (Fig. 1.16). This would be accomplished by synthesizing suitable fluorescent models in which the fluorescence would vary as the angle,ϕ, between the aromatic rings changes. So for example, if group A interacts with a protein binding site while group B interacts with a nearby binding site, the fluorescence

observed would correlate to a particular angle (ϕ), which would also correlate to a particular distance (R) between A and B.

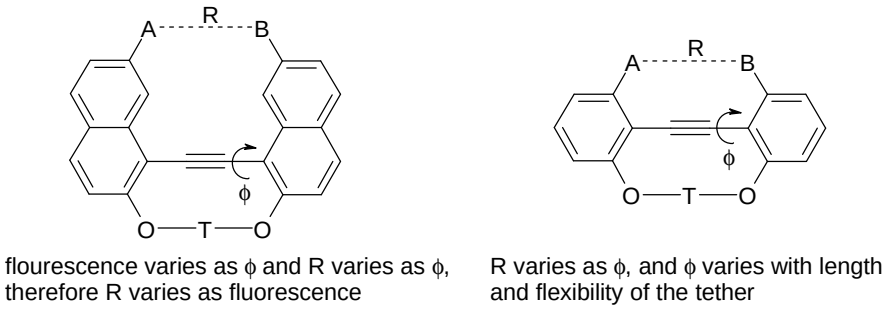

Figure 1.16. Tethered dinaphthylacetylenes and diphenylacetylenes as potential molecular calipers.

Oliver[54] synthesized 2-carboxy-2'-dichloroacetoxydiphenylethyne, which is an untethered model for interactions. He determined a pH-rate profile, which demonstrated intramolecular catalysis by the carboxylate (Fig. 1.17). This experiment confirmed the design concept that the groups are close enough for intramolecular interactions.

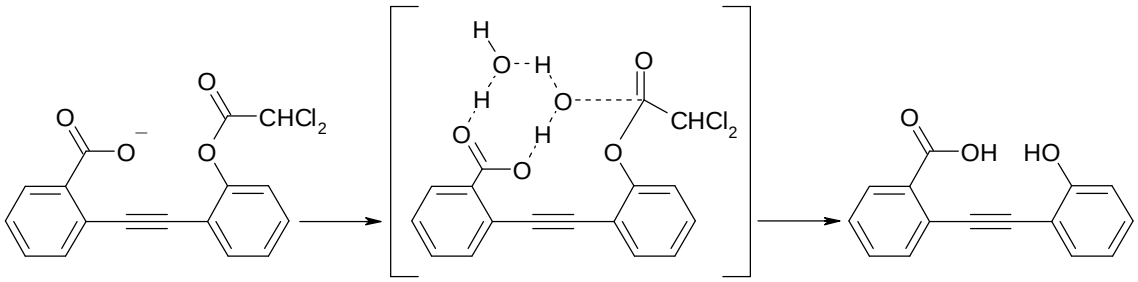

Figure 1.17. General base catalysis in 2-carboxy-2'-dichloroacetoxydiphenylethyne.

Evans[55] and Prince[56] continued the project with the goal of making tethered versions. A variety of methodologies were utilized in the syntheses. The first was based upon suitable acetophenones and their subsequent conversion into vinyl chlorides and

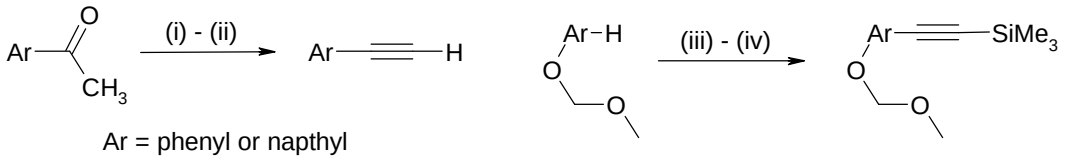

Scheme 1.1. Synthesis of arylacetylenes from acetophenones and aryl iodides. *Reagents and conditions:* (i) PCl_5 / PCl_3; (ii) LDA; (iii) LDA / I_2; (iv) $Bu_3SnC{\equiv}C{-}TMS$ / $Pd(PPh_3)_4$

eventually acetylenes (Scheme 1.1).

Later, ortho lithiation was utilized to synthesize iodo derivatives, which could be converted into acetylenes with standard Stille coupling conditions. The early synthetic strategy was to synthesize the diarylethyne framework early in the synthesis. These diarylethyne intermediates would then be deprotected and then elaborated further. However, elaboration of these early diarylethyne intermediates was fraught with major difficulties, due mainly to problems deprotecting the methoxy groups (Fig 1.18). The

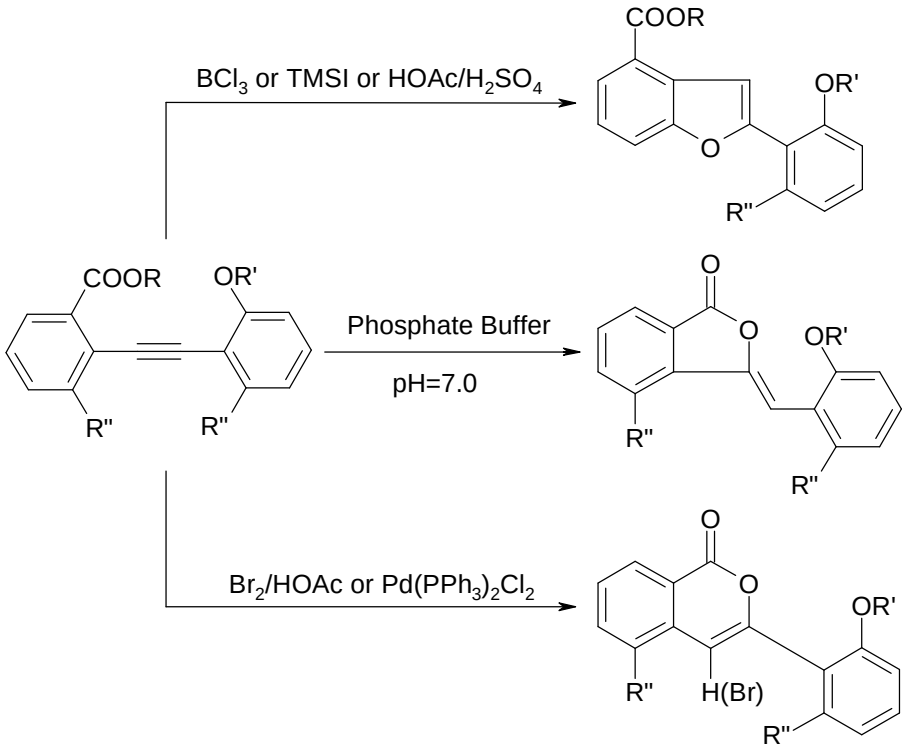

Figure 1.18. Heterocyclic by-products formed during removal of methoxy groups.

most common difficulty was that of the free hydroxy groups reacting with the acetylene to generate heterocyclic products (in particular benzofurans). Formation of heterocycles was only exacerbated by the strongly acidic methodologies employed for methoxy deprotection. Lactones were also formed in some cases.[57]

Later we proposed using diarylethynes as molecular switches (Fig. 1.19). These switches would take advantage of the low barrier to rotation along an acetylenic axle.[58] Synthesis of suitable diarylacetylene models would allow for the study and quantification of noncovalent interactions, in particular hydrogen bonding. This assumes some spectroscopic difference between the intramolecular interacting side of the switch and the

intermolecular interacting side of the switch. The energy of interaction would correspond to the temperature at which the switch freely rotates minus the intrinsic rotational barrier of the acetylene.

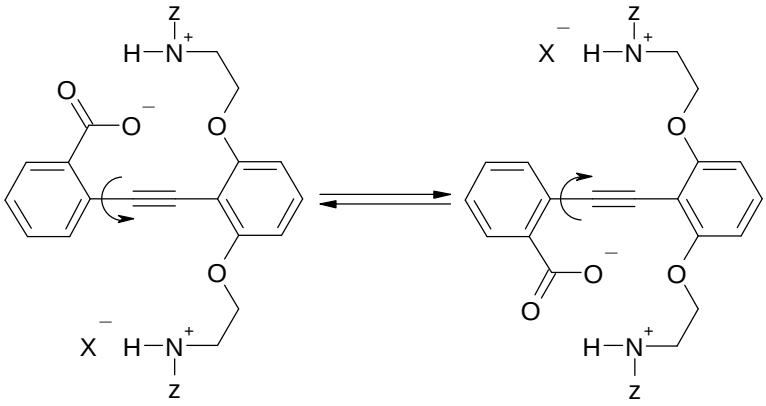

Figure 1.19. Tolanes as potential molecular switches.

Critiques of the proposal pointed out the conformational flexibility, i.e. floppiness, of the aminoethoxy side chains, which could adopt conformations that pointed away from the carboxylate. Two possible solutions immediately sprang to mind: (1) attach the amines to a ring or (2) place a buttresing group adjacent to the side chains in

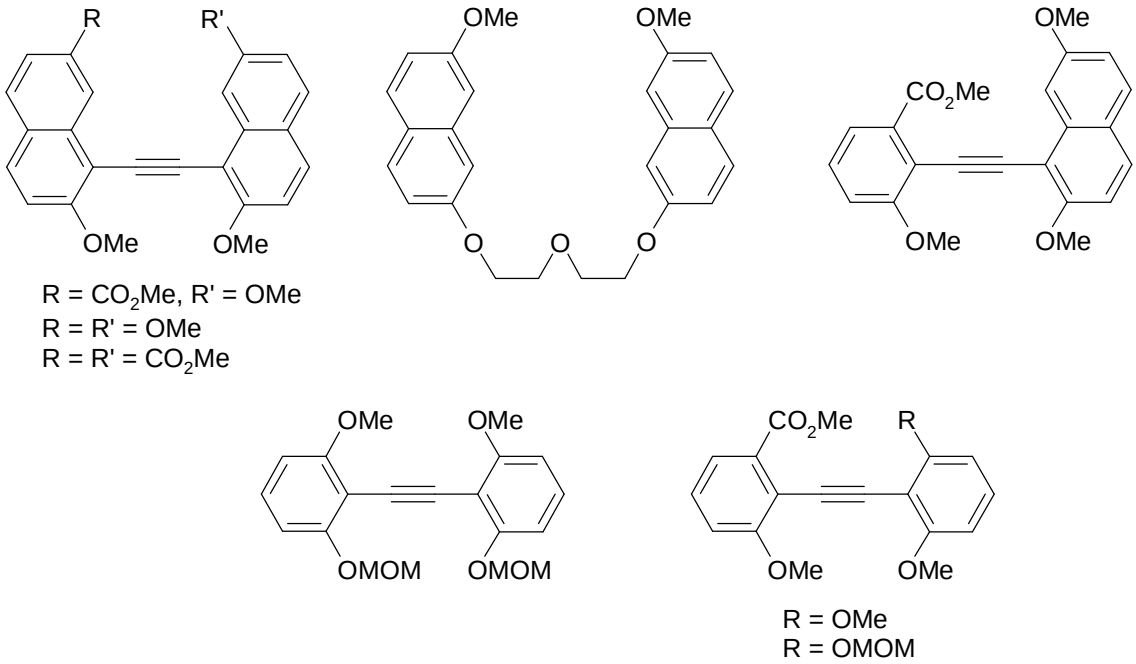

Figure 1.20. Representative sample of previously synthesized molecules in the Gandour group.

order to force the amine groups forward. For this dissertation, we chose to explore the latter strategy.

Before I state the goals, a brief review of tolane (*i.e.* diarylacetylenes) chemistry is in order.

I.4 Tolanes as Building-Blocks

The idea of using tolanes to study intramolecular interactions has a rich literature. Tolanes have become useful building blocks for molecular architects.

I.4.1 Spacer / Linker

The idea of utilizing tolanes as "spacers" dates back to Letsinger[59]. The original tolane spacer was a bis-boronic acid. The idea was to "space" the boronic acid groups as a way of designing new ligands for catalysis. However the tolane proved to be unstable, reacting with itself to form a boracycle. This result prompted Letsinger[60] and coworkers to synthesize the bis-carboxylic acid. As expected, the bis-carboxylic acid rearranged to a lactone (Fig. 1.21). They also compared the rate of lactonization of the 2,2'-dicarboxcylic acid with 2,4'-dicarboxylic acid and 2-carboxyclic acid. They found that 2,2'-dicarboxylic acid lactonized 11,000 times faster than the 2-carboxylic acid, while the 2,4'-dicarboxylic acid was only 2.3 times faster then the 2-carboxylic acid. This implied some type of cooperation (intramolecular) of the two carboxylic acids. Furthermore, the

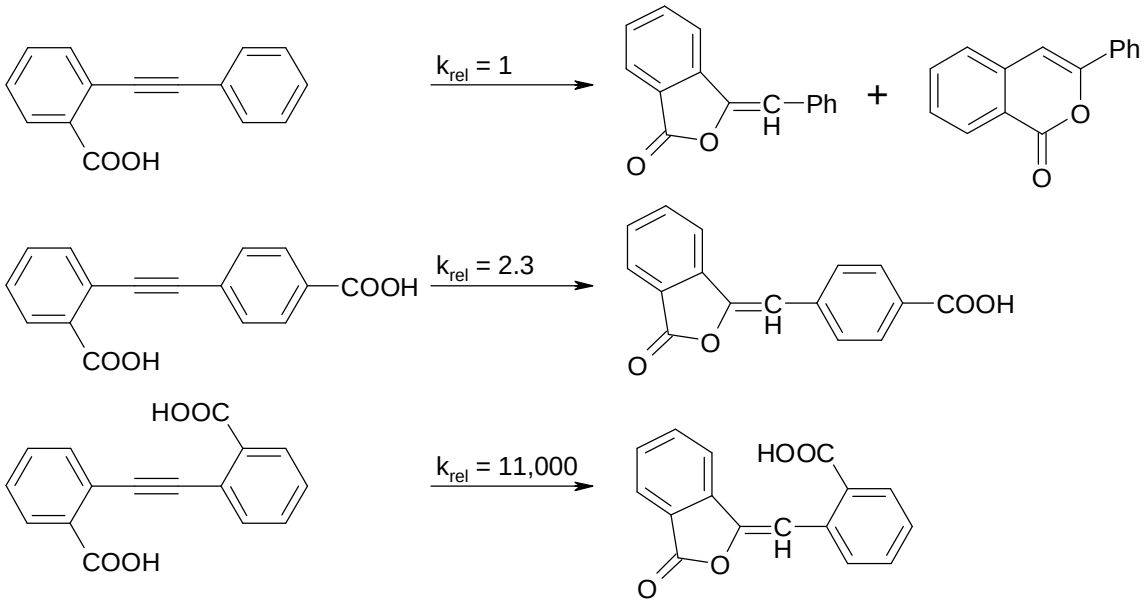

Figure 1.21. Relative rates of lactonization for diphenylacetylenic acids.

pH-rate profile showed an optimum rate at pH 4. This implies that one (but only one) of the carboxylic acids is actually ionized. The proposed mechanism has the carboxylate attacking the alkyne while the carboxylic acid donates its proton to the other side of the alkyne.

I.4.2 Spools

The major advantage of tolanes is their low rotational barrier, 0.578 kcal/mol.[58] This means that the aromatic rings can freely rotate about the axle to become "spools"[61]. Also since the rotational barrier is known, we can correct for the inherent barrier when measuring the interaction of the side chains.

I.4.3 Anchors

Tolanes can also be utilized as anchors (*i.e.* they can be used to enforce a particular structural motif). In particular, they have been utilized as •-turn anchors[62] (Fig. 1.22). The use of tolanes as •-turn anchors is viable due to the fact that the tolane is rigid and is geometrically appropriate for an anti-parallel sheet. Also the tolane anchor can act as its own built-in spectroscopic-reporter functionality.

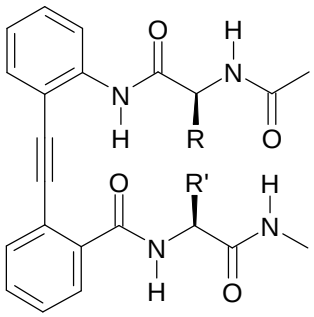

Figure 1.22. b-turn anchor.

I.4.4 Proximity Models

Tolanes have also been utilized to study proximity as aids to reactivity. Vedejs[63] synthesized *o*-acetoxy-*o´*-diphenylphosphanyltolane as a possible restricted mechanistic probe of the acylation of phosphanes with anhydrides (Fig. 1.23). They obtained the tolane however it proved to be unstable over time; yielding a red material (also obtained if heated in toluene at 95 °C). Also if the synthesis was stopped at the phenol stage, they obtained another red material or a benzofuran depending on the actual conditions. They propose that they indeed form the P-acyl zwitterion first, and that this undergoes a P-to-C alkylation to give an allene. This allene could then undergo an intramolecular [2+4] cycloaddition to afford the red materials.

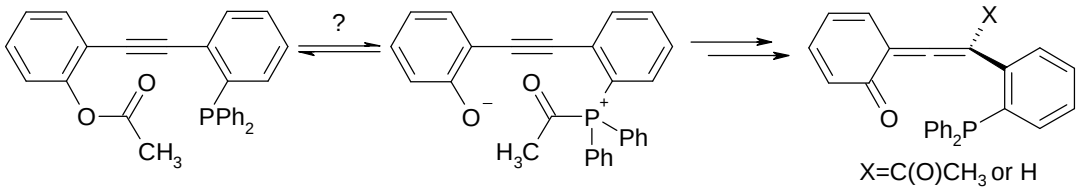

Figure 1.23. Vedejs' proximity model.

Tolanes have also been utilized as scaffolds for convergent multidentate Lewis acids.[64] Wuest et al. were able to synthesize the appropriate bisphenol, which has the phenolic protons symmetrically doubly π-bonded to the acetylene. However when the bisphenol was treated with Al(*i*-Bu)$_3$, they obtained the cyclic dimer and not the desired convergent 'unassociated' bidentate Lewis acid.

1.4.5 Tethered Tolanes

Ruggli[65-67] first synthesized tethered tolanes ninety years ago, during his work on rings containing acetylenes (Fig. 1.24). Later a large number of tethered tolanes were synthesized during work on annulenes.[68] Recently tethered tolanes have been designed to study steric interactions with the "π cloud" of the triple bond (Fig. 1.24).[69]

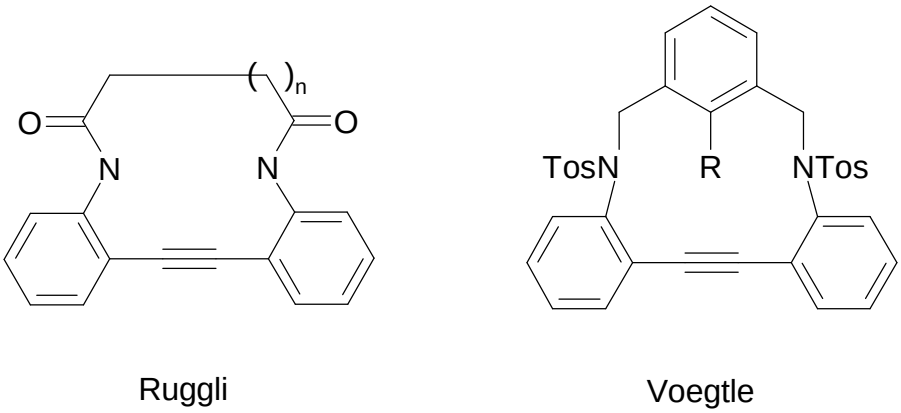

Figure 1.24. Ruggli and Voegtle's tethered tolanes.

1.4.6 Applications of Tolanes as Molecular Machines and Devices

Tolanes have also been utilized in the design and synthesis of molecular machines. A tolane (or tolane equivalent) could be the freely rotating axle for a molecular brake (Fig 1.25).[70] Kelly hoped that the braking of the freely rotating triptycene could be activated by addition of a metal ion to the bipyridine segment.

Unfortunately the desired braking action was not achieved, the axle was apparently not rigid enough. This allowed the triptycene "blades" to push the brake out of the way.

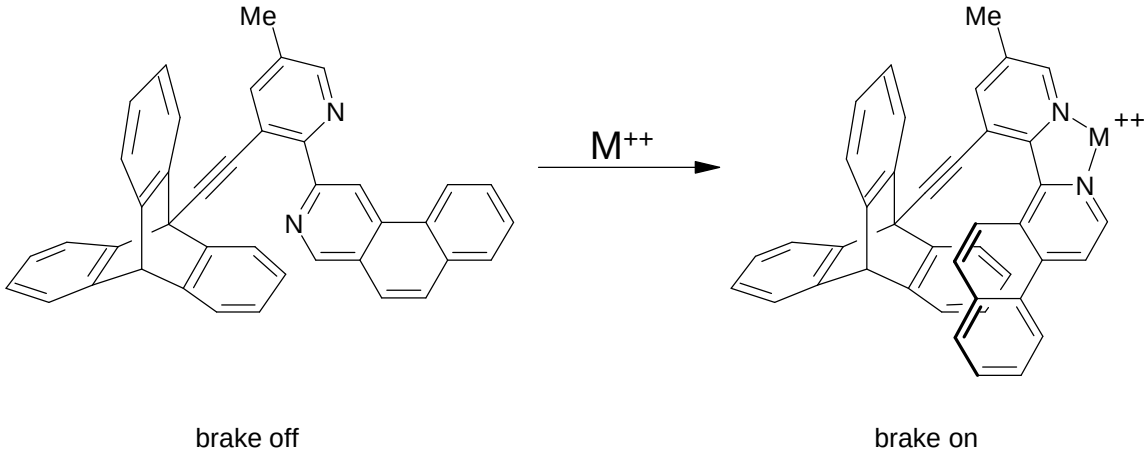

Figure 1.25. Kelly's molecular brake, with a bipyridine binding site and triptycene "blades".

Also researchers have studied and utilized phenylacetylene dendrimers (Fig. 1.26) as potential new materials (in particular as molecular antennae).[71,72] The extended dendrimers show enhanced energy funneling toward the perylenic core. However, the compact dendrimers transfer energy from the perylenic core out to the dendrimeric periphery. Linear-substituted *m*-phenylene ethynylene oligomers have also been studied

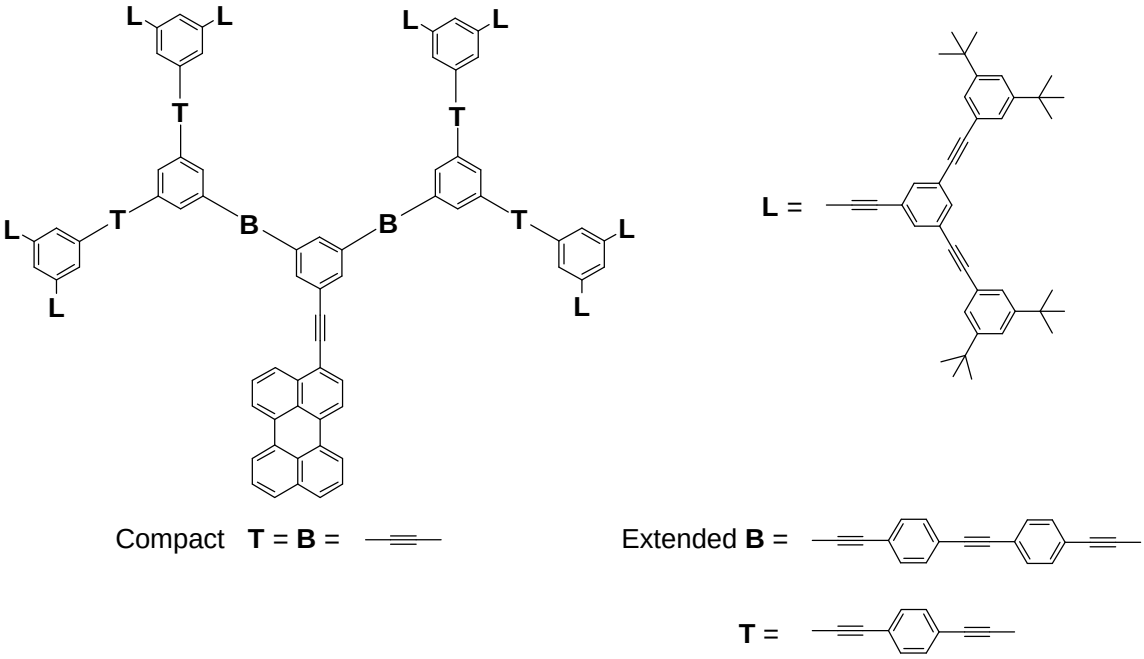

Figure 1.26. Phenylacetylene dendrimers as molecular antennae.

due to their tendency to adopt helical conformations in solution.

Tolanes or tolane-like molecules are also attractive as chemosensors (Fig 1.27). In particular bistrityldiacetylene models with increased fluorescence in the presence of metal ions have been recently reported.[73]

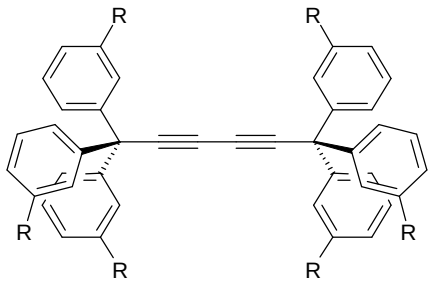

Figure 1.27. A flourescent chemosensor based on bistrityldiactylene core.

Tolanes (in particular polytolanes) are particularly attractive as molecular wires and terminals for electronic devices (Fig 1.28).[74,75] Tolanes have also been utilized in "molecular caltrops",[76] which are potential scanning probe microscopy tips (Fig 1.28).

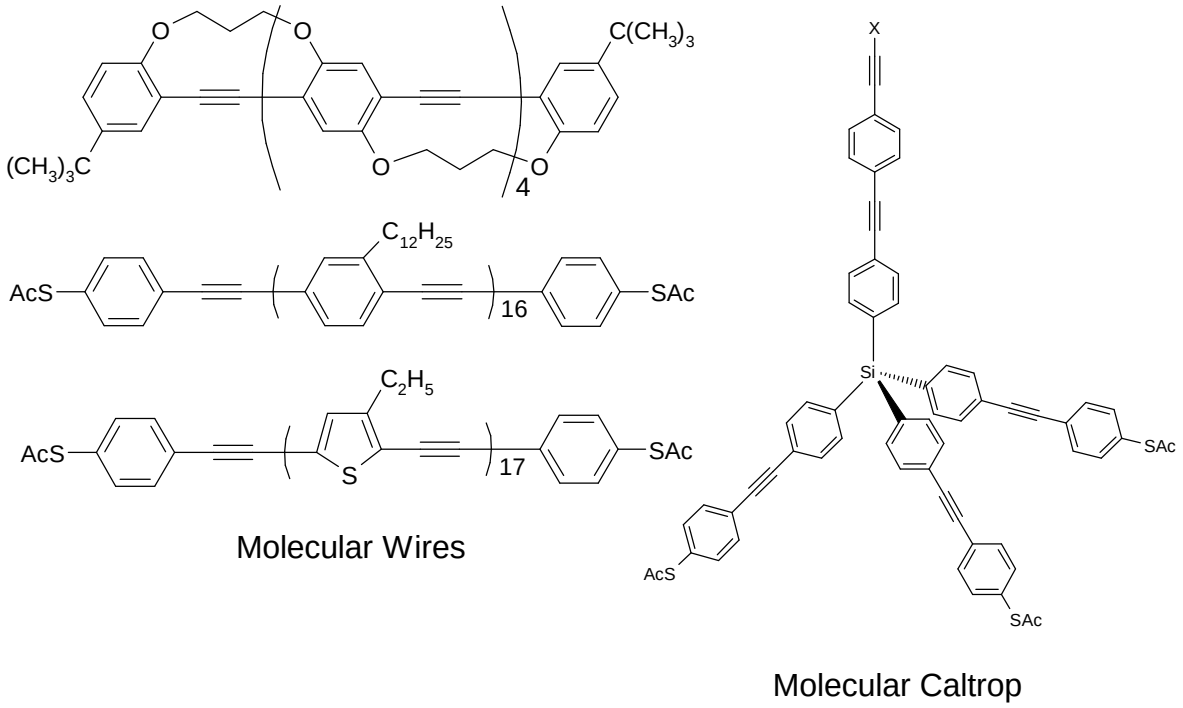

Figure 1.28. Tolanes as molecular wires and caltrops.

1.5 Conclusions and Goals.

Tolanes can be used in a variety of applications from models for the study of intramolecular interactions to molecular machines. Gandour et al. have specialized in synthesizing *o,o,o',o'*-tetrasubstituted tolanes with the goal of tethering between *o* and *o'* groups. This goal is still being pursued by Professor Scott Davis at Mercer University. In this dissertation, I take a different approach to enforce intramolecular interactions. I plan to develop syntheses of tolanes where groups in the meta positions will impose conformational restraints on the groups attached at the ortho positions. As shown in Figure 1.29, I need to construct appropriately functionalized pentasubstituted aromatics. The assembly of these units into tolanes creates a novel class of molecules with potentially unusual properties.

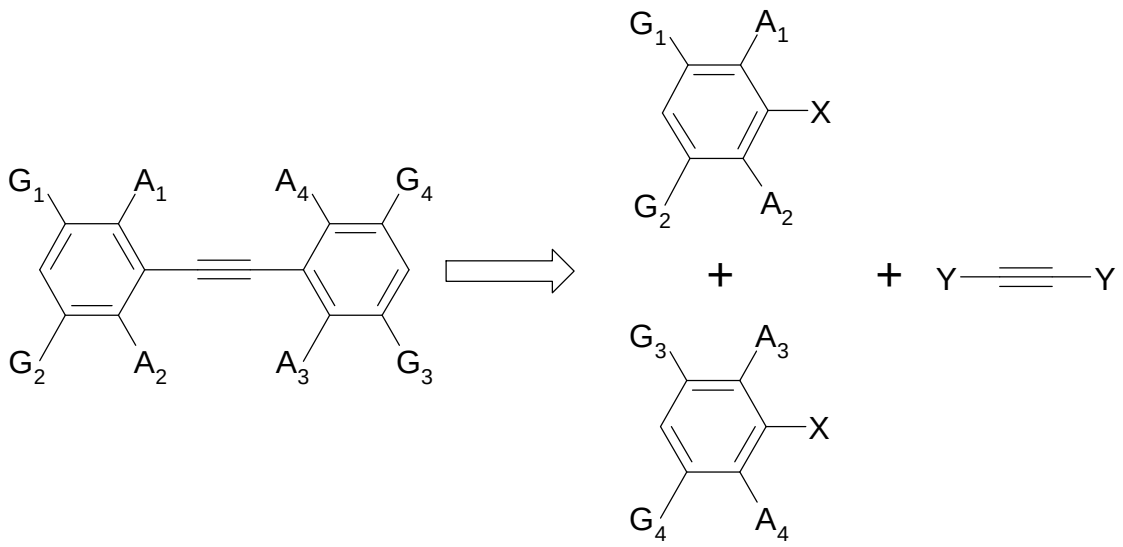

Figure 1.29. Tolane retrosynthesis and disconnection.

This work has the following specific goals:

1) The synthesis of pentasubstituted aromatics suitable for the construction of tolanes by coupling methods.
2) The feasibility of coupling such crowded molecules into tolanes.
3) The study of any unusual reactivity during the construction of these tolanes.
4) The study of any unusual structural features and/or properties of these tolanes.

CHAPTER II: Synthesis of Iodoresorcinols

II.1 Synthesis of Buttressed *O,O*-Dialkylated-2-Iodoresorcinols

One drawback to utilizing *O,O*-dialkylated-2-iodoresorcinols, is that the side chains prefer to point back away from the iodo substituent (the 180°, 180° conformation) when R1 = H. We want the side chains to point toward each other in diarylacetylenes across the acetylene axle (the 0°, 0° conformation), so we need to block the 'backside' with a bulky 'buttressing' group. The simplest buttressing group for R1 is the *tert*-butyl group, which can easily be introduced by Friedel–Crafts alkylation.

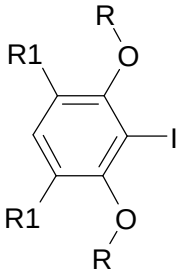

180º, 180º

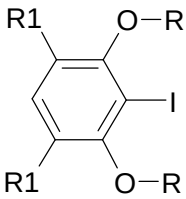

0º, 0º

To examine the 'buttressing' concept, we synthesized (4,6-di-*tert*-butyl-*m*-phenylenedioxy)diacetic acid diethyl ester[77] (R1 = *t*-Bu, R = CH_2COOEt) and the corresponding free acid (R1 = *t*-Bu, R = CH_2COOH). The diacid was synthesized

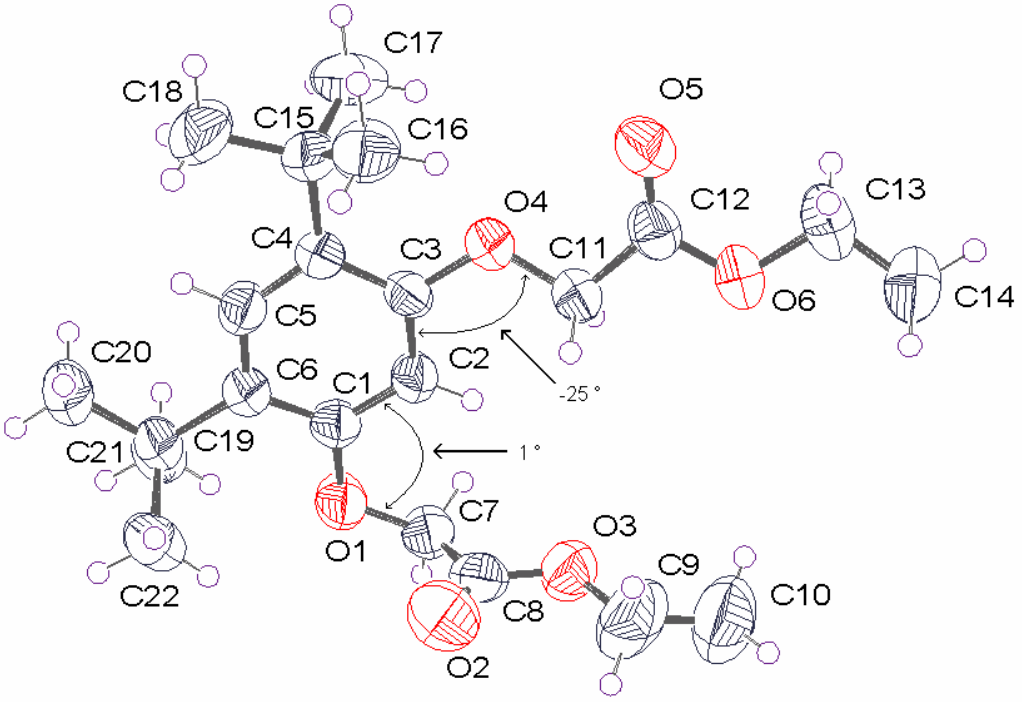

Figure 2.1 X-ray crystal structure[77] (thermal ellipsoids at 50% probability) of (4,6-di-*tert*-butyl-*m*-phenylenedioxy)diacetic acid diethyl ester. The C2-C1-O1-C7 torsion angle is -25° and the C11-O4-C3-C2 torsion angle is 1°.

to see if there was any effect on the pK_a of the two carboxylic acids when crowded together. Preliminary titration data[78] (in 5:1 ethanol/water) showed a difference of 1.3 pK_a units for the two carboxylic acids. Also, we were able to obtain an X-ray crystal structure of the diester, that showed the 'side' chains pointed forward (one in the aromatic plane at 1°, the other torqued up at 25°). These data verify the buttressing concept, namely that the side chains are directed forward.

II.1.a Synthesis of 4,6-di-*tert*-butylresorcinol

Our approach to the synthesis of buttressed *O,O*-dialkylated-2-iodoresorcinols began with resorcinol, which was efficiently alkylated with *tert*-butyl alcohol in acetic acid with sulfuric acid. This procedure was a modification of that reported by Korneev et al.[79] Later, we also used phosphoric acid as the acid catalyst,[80] but the reaction time was longer (10 hours vs. 2 hours) and required external heat. The phosphoric acid catalyzed product required the same amount of purification as the sulfuric acid procedure, so we returned to using sulfuric acid as the catalyst. Recrystallization of the crude material from ethanol/water yielded 4,6-di-*tert*-butylresorcinol as a white crystalline solid.

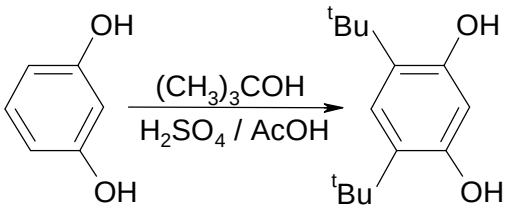

II.1.b. Synthesis of 4,6-di-*tert*-butyl-2-iodoresorcinol

Purification of the 4,6-di-*tert*-butylresorcinol was critical for the next step, which was the iodination following the procedure that Thomsen and Torssell[81] developed for resorcinol. We had numerous problems with highly colored material(s) (usually some shade of orange) being formed during the iodination.

First, we tried further purification of 4,6-di-*tert*-butylresorcinol with multiple recrystallizations from ethanol/water; however, this did not always work. Next, we dried (under high vacuum) the 4,6-di-*tert*-butylresorcinol and recrystallized the anhydrous material from hexanes. We then tried recrystallizing the anhydrous material from cyclohexane. All methods still left material that did not reproducibly give an uncolored product after iodination.

Next, we turned our attention to the iodination protocol. We changed the base (from $NaHCO_3$ to K_2CO_3, $KHCO_3$, and Li_2CO_3) and the method used to dissolve the 4,6-di-*tert*-butylresorcinol. The 4,6-di-*tert*-butylresorcinol was dissolved in ethanol and an aqueous solution of the base was added to afford either a milky suspension or a homogeneous solution, depending on the base. Still, we had the same problem with reproducibility.

Finally, we passed the crude (only recrystallized once from methanol/water) 4,6-di-*tert*-butylresorcinol through a column of silica gel followed by recrystallization from cyclohexane. This yielded a material that could be reproducibly iodinated without generating colored impurities.

The purified 4,6-di-*tert*-butylresorcinol was iodinated with iodine and potassium carbonate in ethanol/water to yield 4,6-di-*tert*-butyl-2-iodoresorcinol in high yield. In comparison, the iodination of resorcinol yields 2-iodoresorcinol plus small amounts of the multiple iodination products 2,4-di-iodoresorcinol and 2,4,6-tri-iodoresorcinol. The di-iodo and tri-iodo compounds can be removed through appropriate chromatography to afford pure 2-iodoresorcinol.

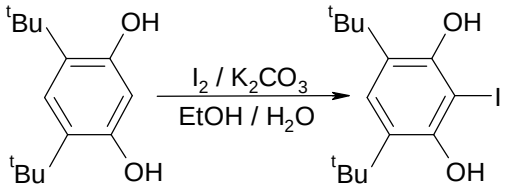

Later, we rationalized that the problems with production of colored material might be due to phenolic radical coupling products. Phenols are easily oxidized (to phenolic radicals) and, in fact, butylated phenols are utilized as anti-oxidants (BHT and BHA) in the food industry. The pH dependence of the reduction potential of resorcinol has been previously reported.[82]

From the published data, it was obvious that pH has a very pronounced effect on the potential oxidation of resorcinol (Table 2.1), with high pH's favoring the oxidation to produce phenolic radicals. The base we had been using, potassium carbonate, has a pKa of 10.5. Therefore, the pH of the reaction mixture would be high enough to favor the formation of phenolic radical species. These radicals could lead to the formation of highly colored impurities. We would expect 4,6-di-*tert*-butylresorcinol to show a similar pH dependence (as compared to resorcinol) of its reduction potential.

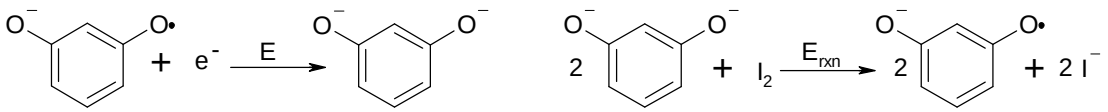

pH	[a]E	E_{rxn}	DG
0	1.130	-1.188	27.4
1	1.071	-1.070	24.67
2	1.012	-0.952	21.95
3	0.953	-0.834	19.23
4	0.894	-0.716	16.51
5	0.835	-0.597	13.78
6	0.774	-0.475	10.96
7	0.699	-0.327	7.53
8	0.597	-0.122	2.81
9	0.485	0.103	-2.37
10	0.388	0.296	-6.82
11	0.327	0.417	-9.63
12	0.303	0.466	-10.76
13	0.299	0.475	-10.95

a) E values taken from ref 82

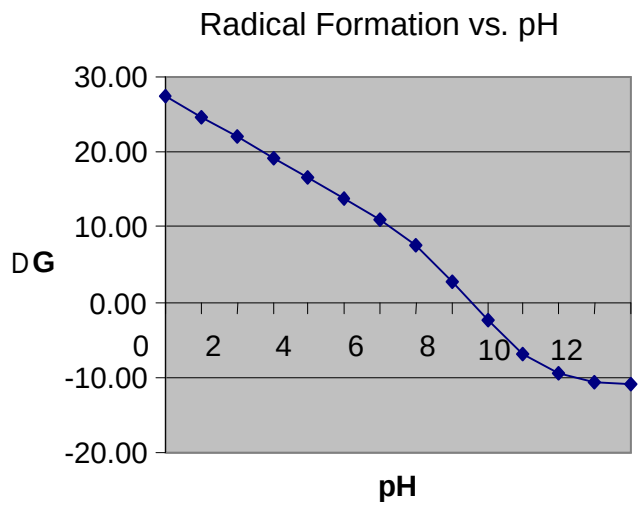

Table 2.1. The pH dependence of the reduction potential (E in eV)[82] of resorcinol and subsequent free energy (ΔG in kcal/mol) of the reduction of resorcinol by iodine.

In order to test the pH dependence of the iodination step, we decided to perform a simple test. We performed the same iodination reaction of 4,6-di-*tert*-butylresorcinol with iodine; however, one reaction was buffered at pH 7.2 and another reaction buffered at pH 8.0 (both buffers prepared from KH_2PO_4). The reaction run at pH 8.0 yielded an orange colored solid. However, the reaction run at pH 7.2 yielded a cream colored solid. Based on these results, we further decreased the pH down to 4.8 (using NaH_2PO_4 as the buffer), with both good yields and little color (off-white to cream).

II.1.c Attempted Synthesis of 4,6-di-*tert*-butyl-2-iodo-3-methoxyphenol

In an attempt to synthesize an unsymmetric buttressed iodoresorcinol, we alkylated 3-methoxyphenol with *tert*-butyl alcohol using the same conditions as for resorcinol. This yielded the desired 4,6-di-*tert*-butyl-3-methoxyphenol in good yield. However, the iodination of 4,6-di-*tert*-butyl-3-methoxyphenol yielded only a trace (~10%) of the desired iodo compound. The major product was a coupled hemiquinone as

identified by NMR (^{1}H NMR shows 4 distinct *tert*-butyl signals and 2 methoxy signals) and literature precedent[83] (see Figure 2.2). As this reaction was only run at a high pH, it may be possible to eliminate formation of the hemiquinone product by control of the pH (in an analogous manner as for the iodination of 4,6-di-*tert*-butylresorcinol).

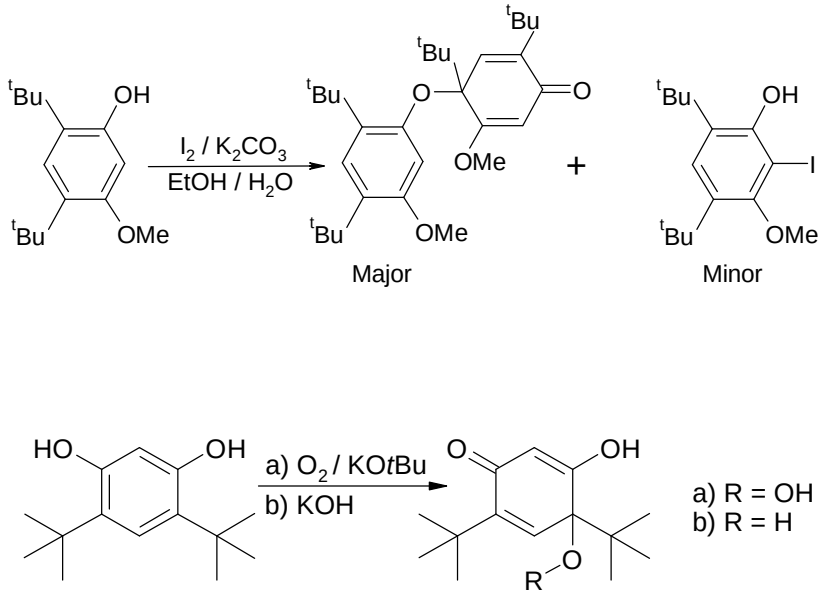

Figure 2.2. Hemiquinone obtained during attempted iodination of methoxyphenol (top) and reported (reference 83) hemiquinones obtained in the presence of molecular oxygen (bottom).

II.1.d Dialkylation of 4,6-di-*tert*-butyl-2-iodoresorcinol

The major hurdle to buttressed *O*,*O*-dialkylated-2-iodoresorcinols is the alkylation of di-*tert*-butyl-iodoresorcinol to attach the 'side chains'. The crowding caused by the bulky groups slows alkylation. To overcome this rate retardation, one needs to search for an effective base, a good solvent, and an active electrophile, such as an alkyl halide adjacent to a π-bond.

Initially, we treated the iodoresorcinol with potassium carbonate and the appropriate electrophile in DMSO at room temperature. This works reasonably well for 2-iodoresorcinol (reaction times of 2–3 days), but is unfeasible for 4,6-di-*tert*-butyl-2-iodoresorcinol (reaction times of 2–3 weeks). It was necessary to heat (80–95 °C) the alkylation reactions of 4,6-di-*tert*-butyl-2-iodoresorcinol. This reduced the reaction times to 3–5 days. Later, we discovered that cesium carbonate with heating (~90 °C), reduced reaction times to 2–3 days.

Another limitation in the alkylation is that, in general, only reactions with activated electrophiles give good yields. When the alkylation is carried out with 1-azido-2-(toluene-4-sulfonyloxy)ethane, for example, the yield is poor (36%).

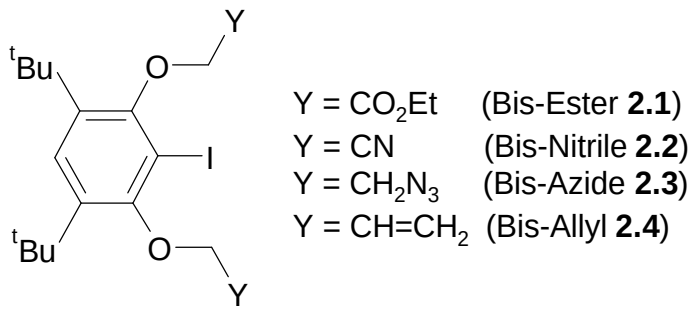

Figure 2.3. Pool of *O,O*-dialkylated 4,6,-di-*tert*-butyl-2-iodoresorcinols.

Utilizing this methodology, we were able to prepare a number of *O,O*-dialkylated 4,6-di-*tert*-butyl-2-iodoresorcinol building blocks (see Figure 2.3). A number of these blocks could be used right away (notably the bis-ester and bis-azide); however, others could (or must) be further functionalized before being coupled into tolanes. Thus the bis-allyl derivative undergoes deallylation in the presence of palladium.

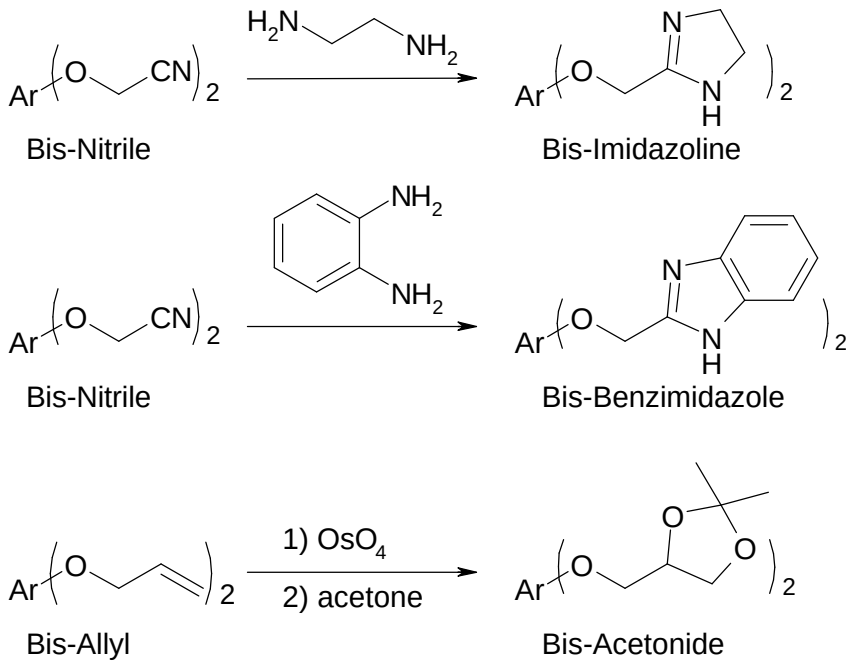

Figure 2.4. Formation of bis-imidazolines, bis-benzimidazoles and bis-acetonides.

The bis-nitrile analog was treated with ethylene diamine and 1,2-phenylenediamine to yield a bis-imidazoline and a bis-benzimidazole,[84] respectively (see Figure 2.4). These would be suitable nitrogen bases to interact with carboxylic acids. The bis-nitrile could also be directly coupled into the tolanes. However, reduction of the nitriles to amines was problematic, even before it was coupled.

The bis-allyl derivative was oxidized to the tetraol, which could be protected to give a bis-acetonide (see Figure 2.4). We also attempted to prepare the bis-epoxide, but it appeared that we oxidized the iodine instead. The oxidation of aryl iodides to iodoso compounds is well-documented.[85] The bis-allyl derivative did not react under Stille coupling conditions to give arylethynes. Instead, it underwent deallylation to give mostly the mono-allyl compound.

II.2. Synthesis of (4,6-di-*tert*-butyl-2-Iodo-1,3-phenylenedioxy)di-*N*-phenylformamide

We decided to change our side arm connector from an aryl ether to an aryloxy ester, as this would bias the system toward non-planarity. Unlike aryl ethers, aryloxy esters do not adopt a planar conformation. For example phenyl acetate adopts, as its ground state conformation, a conformation with the ester group nearly perpendicular to the aromatic plane (73° for the *s*-trans and 92° the *s*-cis conformations, at the RHF level of theory).[86]

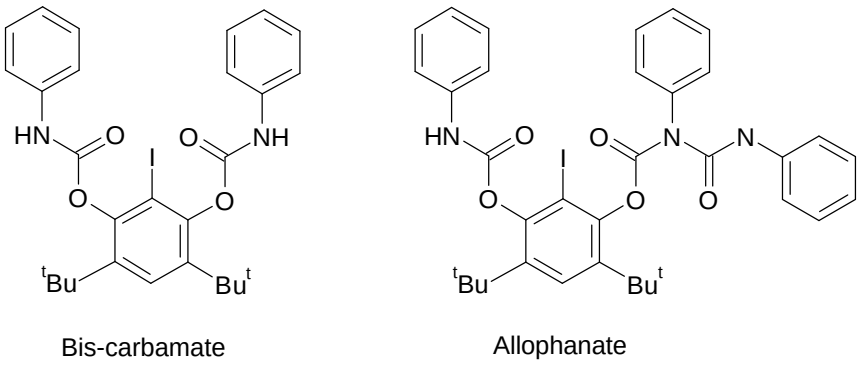

Figure 2.5 The desired bis-carbamate and possible allophanate by-product.

Because resorcinol is such a poor nucleophile, switching to a more reactive electrophile (such as an isocyanate) should improve reaction times. To this end we acylated 4,6-di-*tert*-butyl-2-iodoresorcinol with phenylisocyanate. This yielded a mixture

of the desired bis-carbamate (possibly two different bis-carbamates), unreacted starting material, mono-carbamate, and possibly some allophanate (see Figure 2.5). Separation and purification of one of the bis-carbamates yielded suitably clean material to grow a single crystal for X-ray analysis (see Figure 2.6). The X-ray crystal structure showed that the carbamate side chains were twisted (torqued) out of the aromatic resorcinol plane, with one side chain up and the other down (anti or C_2). The other bis-carbamate (presumably the syn or C_s conformer) was much more difficult to purify and a suitable single crystal was never obtained. In an attempt to obtain a more crystalline product, the same reaction was carried out with 4-methoxyphenyl-isocyanate. However, we were still unable to obtain a suitable single crystal of the C_s material.

In summary, we were able to prepare a number of buttressed iodo resorcinols. The major hurdle to synthesis is the alkylation to afford aryl ethers.

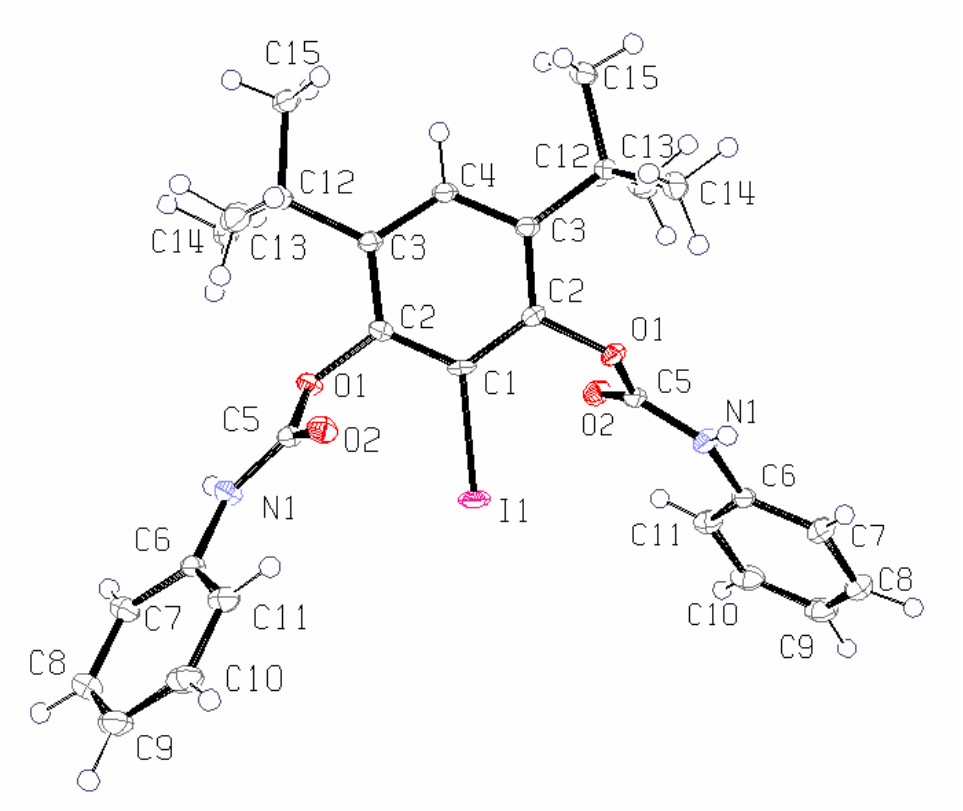

Figure 2.6. X-Ray crystal structure (thermal ellipsoids at 50% probability) of the C_2 isomer of the bis-carbamate. The C1-C2-O1-C5 torsion is 72.9°.

II.3 Experimental.

II.3.a Preparation of 2-iodoresorcinol.[81] To an ice cold (0 °C) solution of resorcinol (11.0 g, 100 mmol) in H_2O (100 mL), was added simultaneously I_2 (26.6 g, 105 mmol) and $NaHCO_3$ (9.24 g, 110 mmol). The resulting orange to tan slurry was stirred at 0 °C for 30 min. The reaction mixture was filtered to obtain a tan solid and an amber filtrate. The tan solid was dissolved in diethyl ether (300 mL) and washed successively with $Na_2S_2O_3$ (2 × 50 mL), H_2O (1 × 50 mL), saturated NaCl (1 × 50 mL), and dried ($MgSO_4$). Rotary evaporation yielded 14.80 g of a white solid. The original amber filtrate was extracted with diethyl ether (4 × 100 mL), and the combined ether layers were washed with $Na_2S_2O_3$ (2 × 50 mL), H_2O (1 × 50 mL), saturated $NaHCO_3$ (1 × 50 mL), and dried ($MgSO_4$). Rotary evaporation yielded an additional 5.75 g (87% total yield) of a slightly tan solid. Removal of the di-iodo and tri-iodo by-products (as detected by ^{1}H NMR) was accomplished with flash chromatography (silica gel; $CHCl_3$ – MeOH, 19:1) on small batches (3 – 5 g) to give 2-iodoresorcinol as a white solid: ^{1}H NMR (270 MHz, $CDCl_3$, agrees with literature[81]) δ 5.28 (s, 2H, OH), 6.57 (d, 2H), 7.12 (t, 1H).

II.3.b Preparation of 4,6-di-*tert*-butylresorcinol.[79] To a solution of resorcinol (20.0 g, 182 mmol) in acetic acid (40 mL) was added 2-methyl-2-propanol (44 mL, 460 mmol). Then a mixture of acetic acid (20 mL) and concentrated H_2SO_4 (12 mL) was added. The resulting dark red solution was stirred at rt for 2 h. A solution of NaOH (56 g in 100 mL H_2O) was added and stirred for 30 min, after which $NaHCO_3$ (satd, 80 mL) was added and stirred for an additional 30 min. The reaction mixture was vacuum filtered, and the resulting yellowish-white solid was washed with H_2O (6 × 250 mL). The crude product was recrystallized from MeOH / H_2O (200 mL / 350 mL) to afford ~53 g of 4,6-di-*tert*-butylresorcinol as its white crystalline dihydrate. The dihydrate was purified by flash chromatography (silica gel; hexanes – ethyl acetate, 3:1), and recrystallized from cyclohexane to afford ~30 g (75%) anhydrous 4,6-di-*tert*-butylresorcinol: ^{1}H NMR (270 MHz, $CDCl_3$, agrees with lit.[79]) δ 1.39 (s, 18H, *t*-Bu), 4.63 (s, 2H, OH), 6.07 (s, 1H), 7.15 (s, 1H).

II.3.c Iodination of 4,6-di-*tert*-butylresorcinol. *Unbuffered*: To a solution of anhydrous 4,6-di-*tert*-butylresorcinol (2.00 g, 9.00 mmol) in ethanol (14 mL) was added a solution

of $KHCO_3$ (0.93 g, 9.3 mmol) in H_2O (14 mL). To this light violet solution, was added dropwise a solution of I_2 (2.27 g, 8.94 mmol) in DMF / ethanol (4 mL / 2 mL). After addition, the reaction was stirred at rt for 5 h. A 10% $Na_2S_2O_3$ (6 mL) was added and the reaction stirred for an additional 30 min. The reaction mixture was vacuum filtered and the resulting solid washed with H_2O (2 × 50 mL) and vacuum dried to afford 2.8 g (90%) of 2-iodo-4,6-di-*tert*-butylresorcinol as an off-white solid: ^{1}H NMR (270 MHz, $CDCl_3$) δ 1.36 (s, 18H, *t*-Bu), 5.15 (s, 2H, OH), 7.18 (s, 1H);); IR: (solid) 3627, 3502, 2998, 2953, 1601, 1587 cm^{-1}; HRMS(FAB+) calcd for $C_{14}H_{21}IO_2$ $[M]^+$: *m/z* 348.0586, found 348.0591.

Buffered: To a solution of minimally purified (recrystallized once from ethanol/water, made anhydrous, and then recrystallized once from hexanes) anhydrous 4,6-di-*tert*-butylresorcinol (1.00 g, 4.50 mmol) in ethanol (10 mL) was added 10 mL of a K_2HPO_4 buffer solution (prepared by dissolving 1.30 g of K_2HPO_4 in 10 mL of water, and adding ~5M NaOH to adjust to either pH 7.2 or pH 8.0). To this solution was added I_2 (1.14 g, 4.49 mmol) all at once. The reaction was then allowed to stir at rt for 4 h. The reaction was quenched with 10% $Na_2S_2O_3$ (10 mL), vacuum filtered and washed with H_2O (2 × 20 mL) to afford 1.38 g (88%) of a light cream colored solid (pH 7.2) or 1.41 g (90%) of an light orange solid (pH 8.0).

II.3.d Iodination of 4,6-di-*tert*-butyl-3-methoxyphenol. To a solution of 4,6,-di-*tert*-butyl-3-methoxyphenol (2.00 g, 8.46 mmol) in ethanol (33 mL), was added $KHCO_3$ (0.87 g, 8.69 mmol) dissolved in water (14 mL). To the resulting milky suspension was added dropwise I_2 (2.12 g, 8.35 mmol) dissolved in DMF (4 mL) and ethanol (2 mL). After addition, the reaction was stirred at rt for 5 h. A solution of 10% $Na_2S_2O_3$ (8 mL) was added and reaction stirred for 30 min. Vacuum filtration yielded 1.98 g of a slightly beige solid. Chromatography (silica gel; hexanes – ethyl acetate, 6:1) afforded 0.3 g (10 %) of the desired 4,6-di-*tert*-butyl-2-iodo 3-methoxyphenol as a slightly yellow solid: ^{1}H NMR (270 MHz $CDCl_3$) δ 1.40 (s, 9H), 1.42 (s, 9H), 3.32 (s, 3H), 5.77 (s, 1H), 7.33 (s, 1H).

Another fraction contained 1.45 g (73%) of the hemiquinone as a white sticky solid: ^{1}H NMR (400 MHz $CDCl_3$) δ 1.15 (s, 9H), 1.28 (s, 9H), 1.31 (s, 9H), 1.47 (s, 9H),

3.47 (s, 3H), 3.61 (s, 3H), 5.68 (s, 1H), 6.47 (s, 1H), 6.68 (s, 1H), 7.19 (s, 1H); ^{13}C NMR (100 MHz $CDCl_3$) δ 26.4, 29.3, 29.8, 30.4, 32.3, 32.35, 33.0, 42.9, 55.5, 55.9, 83.3, 99.1, 105.8, 124.9, 128.2, 128.8, 143.7, 146.7, 154.2, 156.4, 174.1, 186.8; IR ($CHCl_3$, cm^{-1}) 2945, 1644, 1590, 1360, 1010, 911, 740.

II.3.e *O,O*-Alkylation of iodoresorcinols, Method A. To a slurry of K_2CO_3 (2.5 eq) in DMSO (15 mL) was added iodoresorcinol (6 – 9 mmol) dissolved in DMSO (15 mL). The reaction mixture was stirred for 30 min, then a solution of the electrophile (2.5 eq) in DMSO (30 mL) was added dropwise. The reaction was then stirred at rt for 2 – 3 d. The reaction mixture was poured into H_2O (50 mL) and extracted into diethyl ether (4 × 50 mL). Then the combined ether extracts were washed with saturated NaCl (2 × 50 mL) and dried ($MgSO_4$).

II.3.f *O,O*-Alkylation of iodoresorcinols, Method B. To a solution of iodoresorcinol (6 – 9 mmol) in DMSO (30 – 50 mL) was added K_2CO_3 (3.5 – 4 eq), then the electrophile (2.2 eq). The reaction mixture was heated and stirred for 3 – 5 d. The same workup was used as for method A.

II.3.g *O,O*-Alkylation of iodoresorcinols, Method C. To a solution of iodoresorcinol (6 – 9 mmol) in DMSO (30 – 50 mL) was added Cs_2CO_3 (3.5 – 4 eq), then the electrophile (2.2 eq). The reaction mixture was heated to 95 °C and stirred for 2 – 3 d. The same workup was used as for method A.

II.3.h 1,3-Bis-allyloxy-2-iodo-benzene. Method A (3 d, allyl bromide), 2.16 g (81%) of a white solid. ^{1}H NMR (400 MHz, $CDCl_3$) δ 4.61 (dt, *J* = 5 Hz, *J* = 1.5 Hz, 4H), 5.31 (dd, *J* = 10.6 Hz, *J* = 1.6 Hz, 2H), 5.55 (dd, *J* = 15.5 Hz, *J* = 1.6 Hz, 2H), 6.02 – 6.11 (m, *J* = 15.5 Hz, *J* = 10.6 Hz, *J* = 5 Hz, 2H), 6.47 (d, *J* = 12 Hz), 7.20 (t, *J* = 12 Hz) ; ^{13}C (100 MHz, $CDCl_3$) δ 69.8, 79.1, 105.6, 117.5, 129.6, 132.7, 158.6.

II.3.i (3-Cyanomethoxy-2-iodo-phenoxy)-acetonitrile. Method A (1 d, bromoacetonitrile), 2.0 g (75%) of a white solid. ^{1}H NMR (400 MHz, $CDCl_3$) δ 4.85 (s, 4H), 6.77 (d, *J* = 12 Hz), 7.41 (t, *J* = 12 Hz); ^{13}C (100 MHz, $CDCl_3$) δ 54.8, 79.7, 108.3, 114.2, 130.5, 157.2; MS *m/z* M^+ 314(43), 274(13), 246(10), 206(18), 160(15), 134(12), 107(100), 79(43); IR 2240, 905, 728. Anal. Calcd for $C_{10}H_7N_2O_2I$: C, 38.24; H, 2.25; N, 8.92; I, 40.41. Found: C, 38.34; H, 2.00; N, 8.96; I, 40.71.

II.3.j 2-Iodo-1,3-di(*tert*-butyl-dimethyl)siloxybenzene. Method A (DMF instead of DMSO, imidazole instead of K_2CO_3,1 d, *tert*-butyl-dimethyl-chlorosilane), 90%. ^{1}H NMR (400 MHz, $CDCl_3$) δ 0.28 (s, 12H), 1.07 (s, 18H), 45 (d, *J* = 12 Hz, 2H), 7.03 (t, *J* = 12 Hz, 1H); ^{13}C NMR (100 MHz, $CDCl_3$) δ -4.2, 18.4, 25.9, 87.6, 111.3, 128.7, 156.8.

II.3.k (2-Iodo-1,3-phenylenedioxy)diacetic acid diethyl ester. Method A (6 d, ethyl bromoacetate), 1.90 g (91%) of a white solid. ^{1}H NMR (270 MHz, $CDCl_3$) δ 1.13(t, *J* = 7.1 Hz, 6H), 4.10 (q, *J* = 7.1 Hz, 4H), 4.55 (s, 4H), 6.27 (d, *J* = 10 Hz, 2H), 7.04 (t, *J* = 10 Hz, 1H).

II.3.l (4,6-Di-*tert*-butyl-2-iodo-1,3-phenylenedioxy)diacetic acid diethyl ester (2.1). Method A (13 d, ethyl bromoacetate), 2.54 g (85%); method B (3 d, 95 °C, ethyl bromoacetate), 2.75 g (92%); method C (2 d, 50 °C, ethyl bromoacetate), 2.39 g (80%) of a white solid: mp 87.2 – 87.9 °C; ^{1}H NMR (400 MHz, $CDCl_3$) δ 1.34 (t, *J* = 7.1 Hz, 6H), 1.38 (s, 18H), 4.32 (q, *J* = 7.1 Hz, 4H), 4.62 (s, 4H), 7.36 (s, 1H); ^{13}C (100 MHz, $CDCl_3$) δ 14.4, 31.2, 35.6, 61.4, 70.1, 92.2, 127.6, 139.7, 156.0, 168.5. Anal. Calcd for $C_{22}H_{33}O_6I$: C, 50.78; H, 6.39; I, 24.39. Found C, 50.94; H, 6.42; I, 24.18. HRMS(FAB+) calcd for $C_{22}H_{33}O_6I$ $[M]^+$: *m/z* 520.1322, found 520.1330.

II.3.m (3-Cyanomethoxy-4,6-di-*tert*-butyl-2-iodo-phenoxy)-acetonitrile (2.2). Method A (18 d, bromoacetonitrile), 3.60 g (65%) of a white solid; method B (4 d, 85 °C, bromoacetonitrile): mp 155.5 – 156.2 °C; ^{1}H NMR (400 MHz, $CDCl_3$) δ 1.41 (s, 18H), 4.82 (s, 4H), 7.42 (s, 1H); ^{13}C (100 MHz, $CDCl_3$) δ 31.3, 35.7, 58.2, 91.1, 114.9, 128.1, 141.3. Anal. Calcd for $C_{18}H_{23}N_2O_2I$: C, 50.72; H, 5.44; N, 6.57; I, 29.77. Found C, 50.66; H, 5.41; N, 6.50; I, 29.93. HRMS(FAB+) calcd for $C_{18}H_{23}N_2O_2I$ $[M]^+$: *m/z* 426.0804, found 426.0801.

II.3.n 1,3-Di-allyloxy-4,6-di-*tert*-butyl-2-iodo-benzene (2.4). Method A (18 d, allyl bromide), 55%: ^{1}H NMR (270 MHz, $CDCl_3$) δ 1.39 (s, 18H), 4.52 (dd, *J* = 5 Hz, *J* = 1.5 Hz, 4H), 5.31 (dd, *J* = 10.6 Hz, *J* = 1.6 Hz, 2H), 5.53 (dd, *J* = 15.5 Hz, *J* = 1.6 Hz, 2H), 6.09 – 6.23 (ddt, *J* = 15.5 Hz, *J* = 10.6 Hz, *J* = 5 Hz, 2H), 7.34 (s, 1H).

II.3.o (2-Azidoethoxy-4,6-di-*tert*-butyl-2-iodo-phenoxy)-2-aziodethane (2.3). Method B (3 d, 75 °C, 2-azido-tosylethane[1]), 1.03 (36%) of a slightly yellow solid: mp 118.8 – 119.8 °C; ^{1}H NMR (400 MHz, $CDCl_3$) δ 1.41 (s, 18H), 3.74 (t, *J* = 5.3 Hz, 4H), 4.15 (t, *J*

= 5.3 Hz, 4H), 7.37 (s, 1H); ^{13}C NMR (100 MHz, $CDCl_3$) δ 31.4, 35.7, 51.2, 71.8, 93.6, 127.6, 139.4, 145.6, 156.5. Anal. Calcd for $C_{18}H_{27}N_6O_2I$: C, 44.45; H, 5.60; N, 17.28; I, 26.09. Found C, 45.36; H, 5.69; N, 16.28; I, 25.58. HRMS(FAB+) calcd for $C_{18}H_{27}N_6O_2I$ $[M]^+$: *m/z* 486.1240, found 486.1211.

II.3.p (4,6-Di-*tert*-butyl-2-Iodo-1,3-phenylenedioxy)di-*N*-phenylformamide. Method A (DMF instead of DMSO, 5% DMAP instead of K_2CO_3, 2.5 d, phenylisocyanate), 1.48 (52%) of a white solid. ^1H NMR (360 MHz, CD_3COCD_3) δ 1.40 (s, 18H), 7.09 (t, *J* = 6 Hz, 2H), 7.35 (t, *J* = 6 Hz, 4H), 7.56 (s, 1H), 7.67 (d, *J* = 6 Hz, 4H). Crystal data: orthorhombic, a = 26.419(5) Å, b = 9.774(2) Å, c = 10.195(2) Å, • = 90°, • = 90°, • =90°. V = 2632.5(9) $Å^3$, Z = 4, T = 100 K, R_1 = 0.0327, wR_2 = 0.0804, GOF = 1.014 for 223 parameters and 3824 total reflections. Graphite monochromator Mo K• (• = 0.71073 Å) radiation, structure solved by direct methods and refined by full matrix least squares against F^2 for all data using SHELXL software. The CIF file is included in Appendix B.

CHAPTER III: Synthesis of Arylethynes and Tolanes

III.1 Synthesis of Arylethynes

Now that we had a suitable pool of aryl iodides, we needed to synthesize the aryl ethynes. We chose to utilize the Stille[87] palladium cross-coupling reaction (see Figure 3.1) of aryl iodides with tin acetylides. While we could have employed other cross-coupling reactions, the Stille coupling reaction was attractive because of its robustness. The rate determining step is usually the addition of the aryl iodide to the palladium. This addition is a reduction of the aryl iodide and so consequently electron-rich aryl halides (because of their higher reduction potentials) are slow to react[88] . Furthermore, we had experience[89,90] with the reagents (namely tributyltin acetylide) and protocols necessary to perform Stille cross-coupling reactions. Also, the work of Saá et al.[91] suggested that reactions of hindered electron-rich aryl iodides with organostannanes (although they employed aryl triflates instead of aryl iodides) should be feasible, but sluggish.

The Stille coupling reaction of the unbuttressed dialkylated iodoresorcinols with tributyltin acetylide in the presence of palladium tetrakistriphenylphosphine,

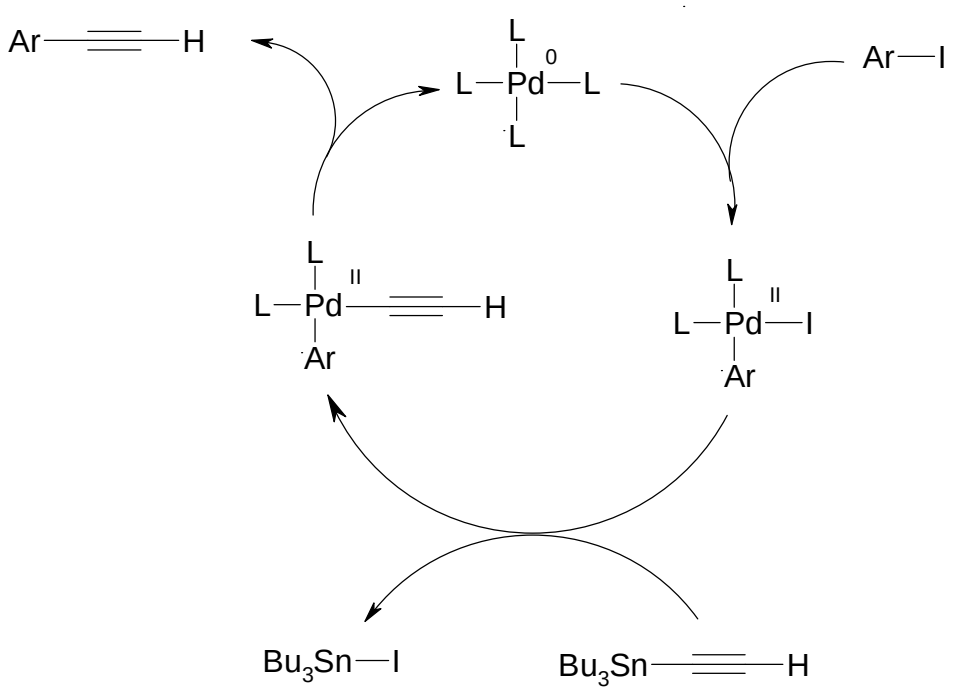

Figure 3.1 Catalytic cycle for the Stille cross-coupling reaction.

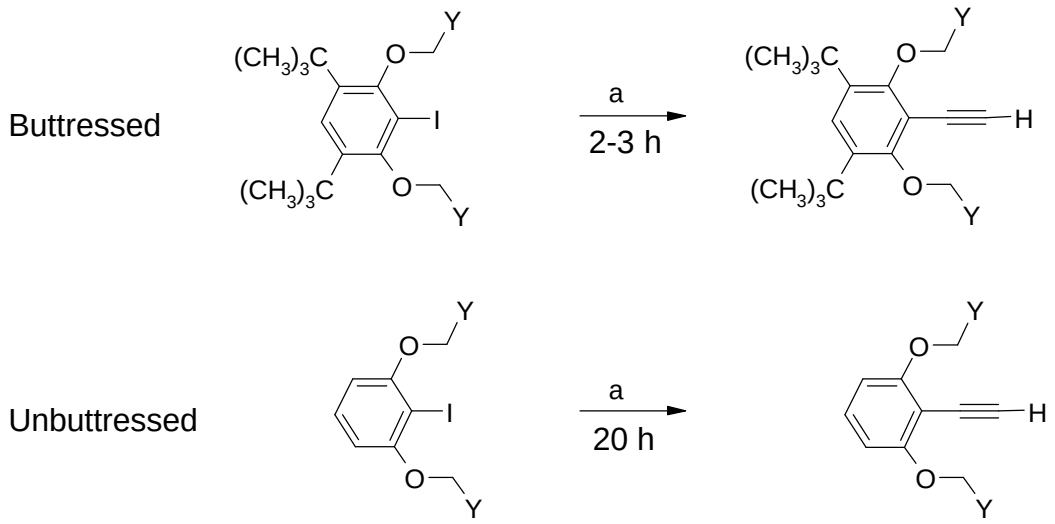

Scheme 3.1 Stille coupling of buttressed and unbuttressed iodoresorcinols. *Reagents and conditions*: (a) $Bu_3SnC\bullet CH$, $Pd(PPh_3)_4$, benzene, 80 °C

afforded the desired aryl acetylenes in modest yields. The reaction typically took about 12–18 hours, which is longer than most Stille coupling reactions, because we were using electron rich (unactivated) aryl iodides. The Stille coupling reaction of buttressed dialkylated iodoresorcinols with tributyltin acetylide occurred much faster (5–10 times)

Table 3.1 Synthesis of aryl ethynes.

Aryl Ethyne	Time	Yield[a]
3.1	20 h	31%[b]
3.2	2 h	71%[b]
3.3	20 h	50%
3.4	4 h	55%
3.5	24 h	62%

[a] After chromatography
[b] After chromatography and recrystallization

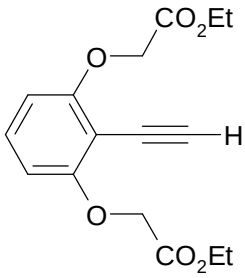

3.1

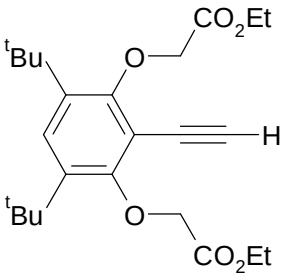

3.2

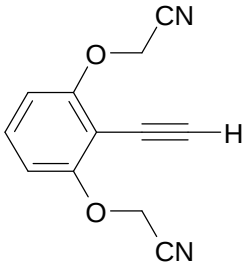

3.3

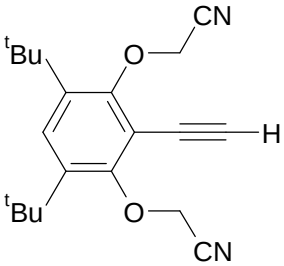

3.4

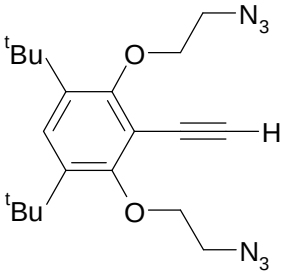

3.5

than the corresponding reaction with unbuttressed dialkylated iodoresorcinols (see Scheme 3.1 and Chapter 4 for an explanation). With this protocol, we synthesized several aryl ethynes (see Table 3.1).

III.2 Synthesis of Tolanes

Palladium/copper catalyzed coupling of aryl iodides with arylethynes yielded the desired tolanes in moderate yields. The first compounds prepared were the unsymmetrical tolanes. These molecules were envisioned as potential molecular switches (see Scheme 3.2). Now, all we needed were methods to generate the free amines from the cyano or azido groups and hydrolyze the ester.

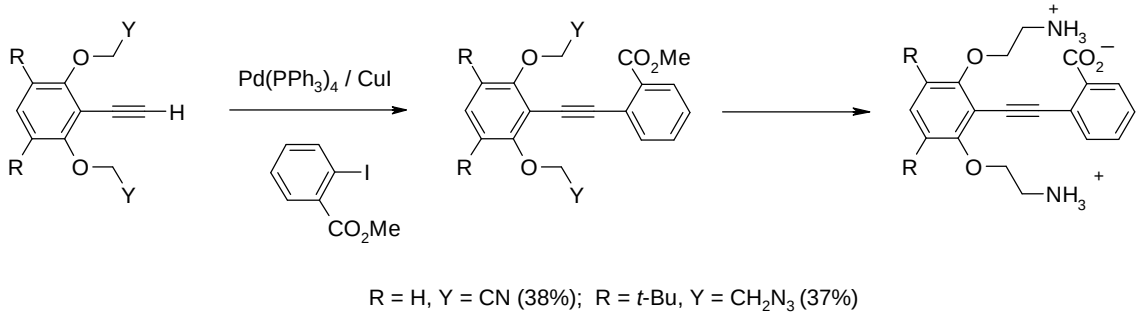

Scheme 3.2 General scheme for the synthesis of molecular switches.

The bis-nitrile (**3.4**) proved very difficult to reduce and isolate (both as the monoacetylene and diarylacetylene). The bis-azide (**3.5**) was treated with triphenylphosphine and water in THF and, this yielded the amine in low yield (35%). An attempt was then made to hydrolyze the ester; however, the amount of material recovered was insufficient to warrant further work.

With the ease of the Stille coupling reactions to afford aryl ethynes (especially

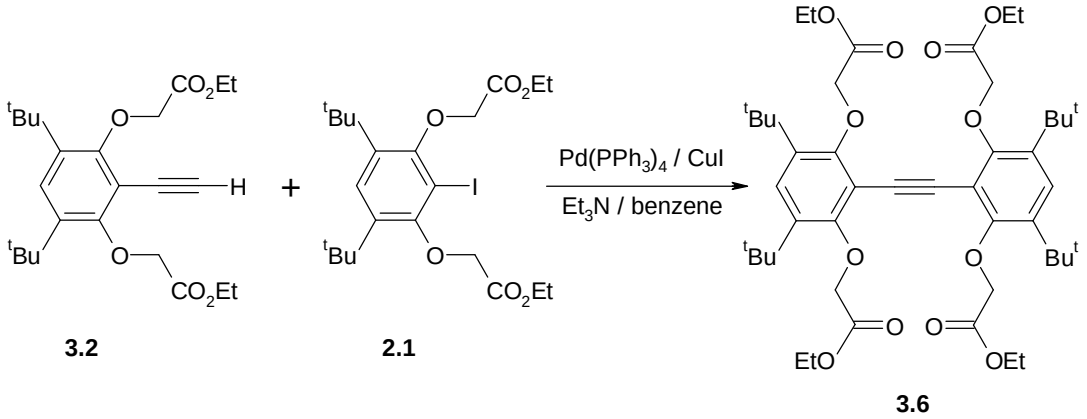

Scheme 3.3 Synthesis of the symmetrical tetra ester (**3.6**).

3.2), we decided to see if the copper/palladium couplings of **3.2** with its aryl iodide precursor (**2.1**) (Scheme 3.3) to afford the symmetrical tetra ester was accelerated (in an analogous manner as the Stille couplings). While the copper/palladium coupling did proceed (5–12 h with a 20% isolated yield), there did not appear to be any significant rate acceleration.

III.3 Analysis of the Tetra Ester

We had anticipated that the bis-carbamate (see section **II.2**) might manifest itself as a pair of atropomers. So, we were excited when we saw two long wave (254 nm) fluorescent components—one fluoresced blue (**3.6b**) and the other fluoresced green (**3.6a**)—in the TLC of the crude reaction product of the tetra ester. Separation (preparatory TLC) of the two components yielded a green-fluorescent material and a

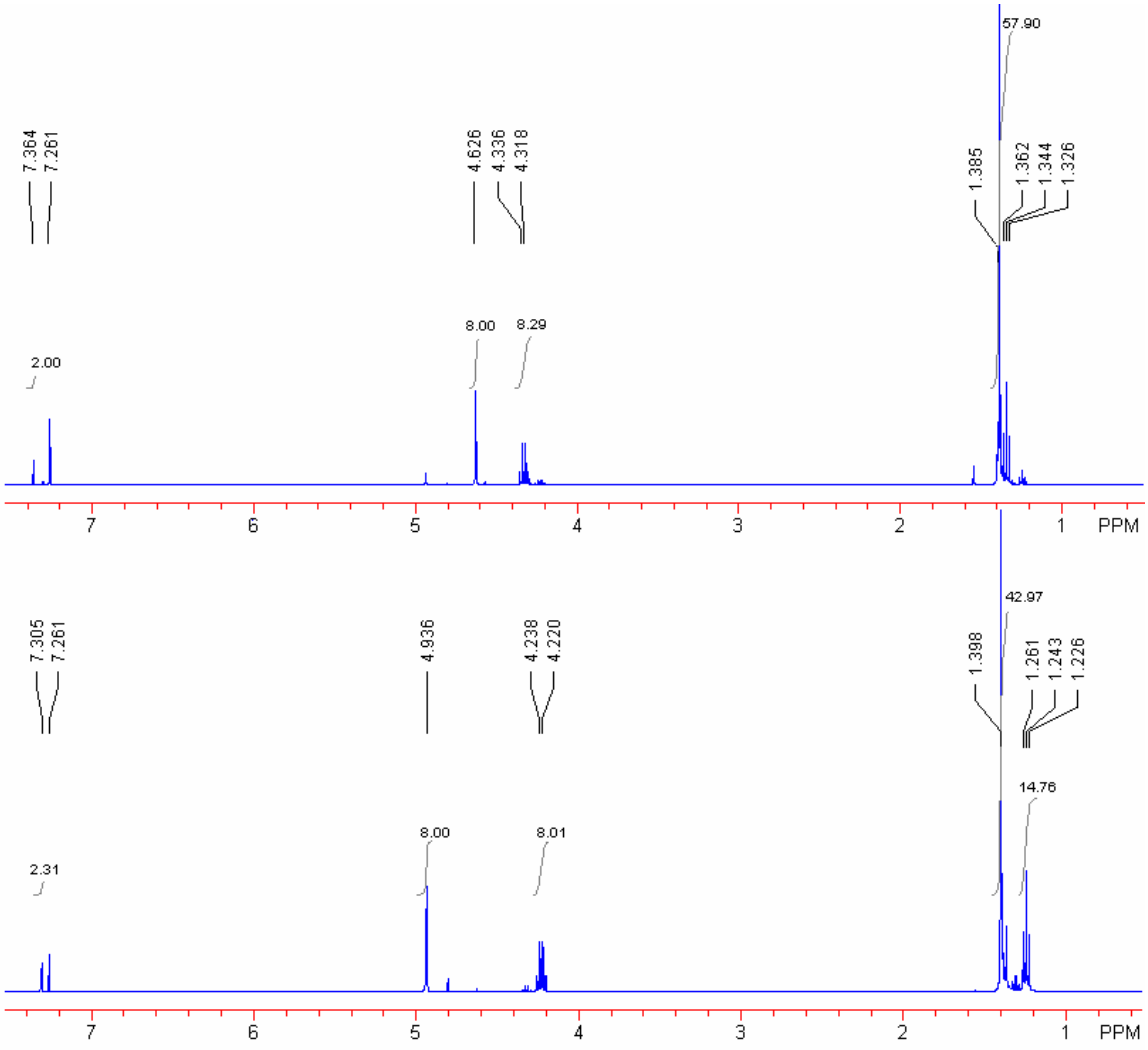

Figure 3.2. ^{1}H NMR (400 MHz, $CDCl_3$) spectra of **3.6b** (top) and **3.6a** (bottom).

blue-fluorescent material. The high resolution mass spectrum of the blue-fluorescent material showed an M^+ peak at 810.4556 (calculated is 810.4553), which confirmed the isomeric relationship.

Both materials have very similar ^{1}H (see Figure 3.2) and ^{13}C NMR spectra. The position of the *tert*-butyl signals remains nearly constant in both ^{1}H spectra. However, the methylenes of the "side chains" shift dramatically, from 4.61 ppm in **3.6b** to 4.93 ppm in **3.6a**. The other signals shift slightly *upfield* from **3.6b** to **3.6a** (the aromatic *para*-H shifts from 7.37 ppm to 7.30 ppm, and the ethyl ester signals shift from 4.32 and 1.33 ppm to 4.22 and 1.24 ppm). Analysis of the ^{13}C spectra shows the two spectra to be nearly identical. These data are consistent with different conformations (possibly atropomers) for **3.6a** and **3.6b**.

Furthermore, major differences appeared in the UV spectra (Figure 3.3). Comparison of the UV spectra with that reported for diphenylacetylene[92] (see Figure 3.3 inset), indicated that the UV spectrum of the green-fluorescent component (**3.6a**) matched the fine structure of the UV spectrum of diphenylacetylene. The UV spectrum of the blue-fluorescent (**3.6b**) component showed a complete lack of fine structure – just one major peak at 284 nm. The reported UV spectrum of the orthogonally constrained 2, 2´, 4, 4´, 6, 6´-hexa-*tert*-butyldiphenylacetylene (see Figure 3.4) also showed only a

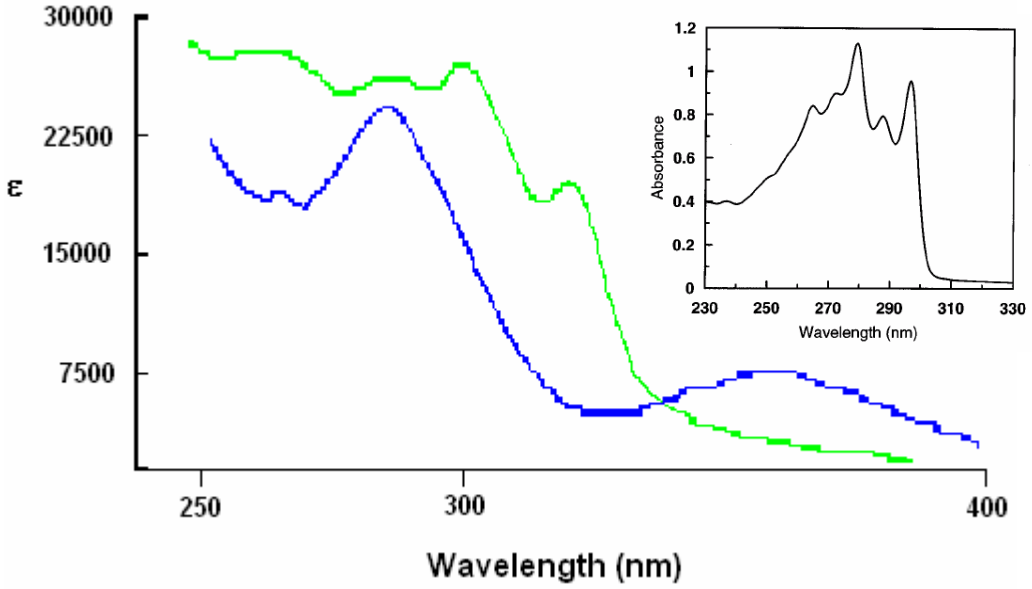

Figure 3.3 Overlay of UV spectra of the blue-fluorescent (blue) and green-fluorescent (green) components along with the UV spectrum of diphenylacetylene (from reference 92).

single strong UV absorption at 257 nm.[93] These results along with the other data (see below) suggested that we were dealing with conformational diastereomers that are actually atropomers.

From the UV data, we expected the green material to have the aromatic rings in the same plane (as this would allow maximum overlap of the π systems). This would suggest that the blue material would have the aromatic rings perpendicular (more or less) to each other.

We performed a simple ZINDO (as implemented in CAChe) calculation on AM1-optimized (also from CAChe) diphenylacetylene where we changed the angle between the aromatic ring planes. From these data, we calculated (angle, λ_{max}) UV spectra for diphenylacetylene at various twist angles: 0°, 304 nm; 30°, 290 nm; 60°, 283 nm; and 90°, 240 nm. The calculated λ_{max} of 304 nm at 0° matched up very well with the observed λ_{max} of 300 nm for the green component; however, the blue component λ_{max} of 284 nm actually matched up better with the value calculated for 60°.

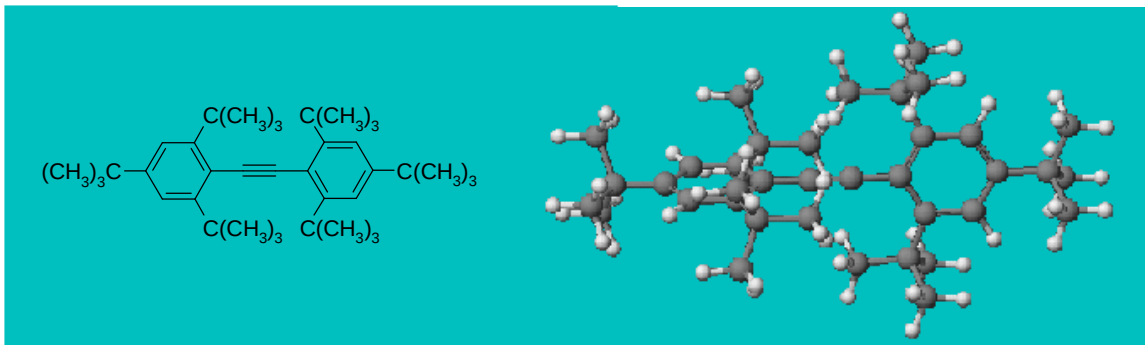

Figure 3.4 2, 2′, 4, 4′, 6, 6′-Hexa-*tert*-butyldiphenylacetylene and a ball and stick picture of an AM1-optimized structure showing that the aromatic rings are nearly perpendicular (actual value is ≈ 85°).

Fortuitously, a suitable single-crystal for X-ray analysis grew in the NMR tube of the green-fluorescent component. Unfortunately, a suitable X-ray crystal was never obtained (the analysis of the crystals revealed twinning).

III.4 Structure of Green-fluorescent Component

The X-ray crystal structure of the green-fluorescent material (see Fig 3.5) shows a center of inversion at the midpoint of the triple bond. The two ester-containing side arms on each ring have very similar conformations, angles, and distances, but are not

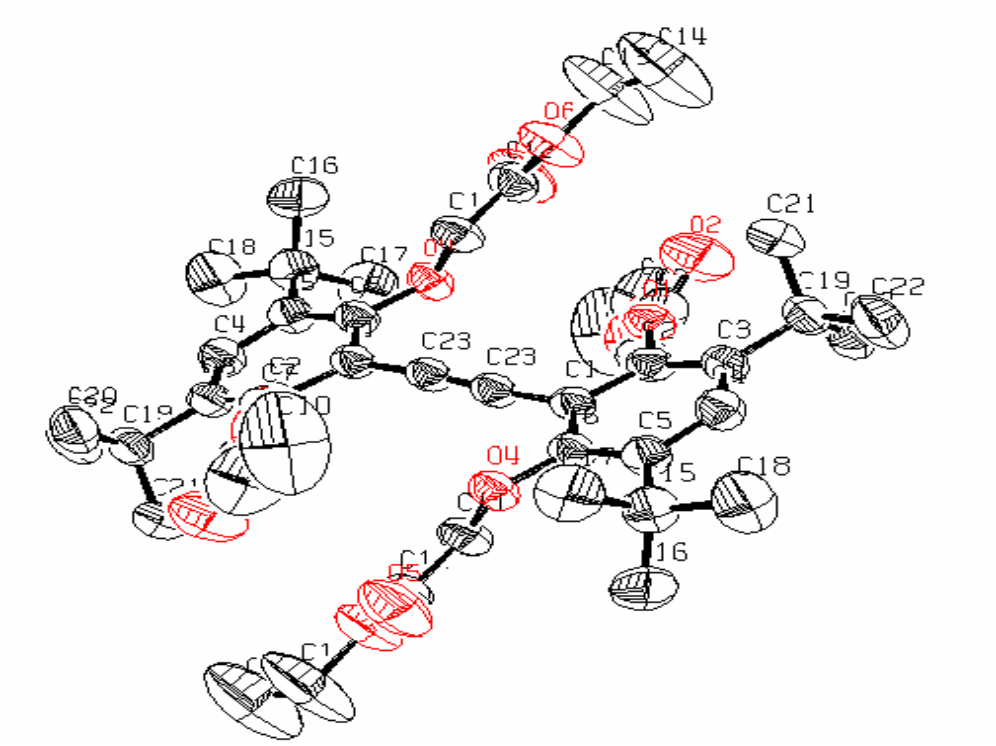

Figure 3.5 X-ray structure (thermal ellipsoids at 50% probability)of the green-fluorescent isomer of the tetra-ester. Note the large ellipsoids for the ester side chains (especially C9, C10, C13 and C14).

symmetric (also there is a fair amount of disorder in the side chains, as evident in the large thermal ellipsoids, especially toward the ethyl ester ends). The two aromatic rings reside in nearly parallel planes. The carbon atoms of the ring form a slight half-chair conformation with C1 slightly (~ 6°) out of the plane defined by the other five atoms (C2–C6). As a consequence, the carbon atom (C23) of the triple bond lies significantly below the two oxygens (O1 and O4) attached to the aromatic ring. These oxygens reside in the plane defined by C2–C6. The closest contact between two side arms on opposite rings is 3.27 Å, the distance between O2 (a carbonyl oxygen), and C12 (a carbonyl carbon). The O2-C12-O5 angle of ~79° is too acute to lie on the Bürgi-Dunitz trajectory[94] (see Fig 3.6) for nucleophilic attack on a carbonyl.

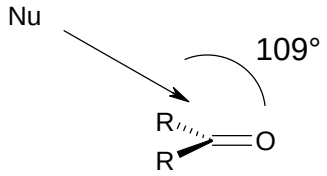

Figure 3.6. In the Bürgi-Dunitz trajectory, the nucleophile attacks the carbonyl at an angle of 100–110° (typically 109°).

III.5 Atropisomerism in Crowded Arenes.

A discussion of the atropisomerism in these compounds is in order. There are potentially four (maybe five) axes that have restricted rotation with barriers large enough to produce atropomers. The structure below (Fig 3.7) illustrates the point with the four chirality axes of the C—O bonds attached to the benzene rings. The analysis predicts 3 meso and 5 racemates. Four of the five racemates are related by symmetry, as the numbering of the axes is arbitrary. Consequently, there are five energetically unique conformations.

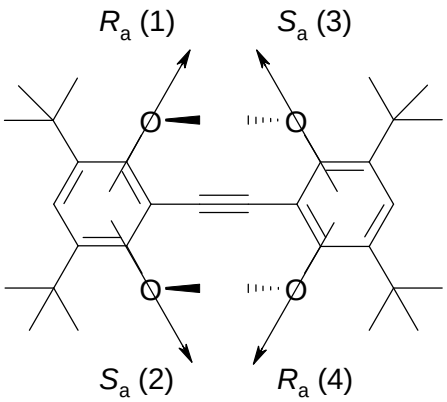

Possible Stereoisomers
(Axis **1**, Axis **2**, Axis **3**, Axis **4**)

$R_a\,S_a\,S_a\,R_a$	meso	Syn-Syn_Anti
$R_a\,S_a\,R_a\,S_a$	meso	Syn-Syn_Syn
$R_a\,R_a\,S_a\,S_a$	meso	Anti-Anti_Anti
$R_a\,R_a\,R_a\,R_a$	$S_a\,S_a\,S_a\,S_a$	Anti-Anti_Syn
$R_a\,R_a\,R_a\,S_a$	$S_a\,S_a\,S_a\,R_a$	Syn-Anti
$R_a\,R_a\,S_a\,R_a$	$S_a\,S_a\,R_a\,S_a$	Syn-Anti
$R_a\,S_a\,R_a\,R_a$	$S_a\,R_a\,S_a\,S_a$	Syn-Anti
$S_a\,R_a\,R_a\,R_a$	$R_a\,S_a\,S_a\,S_a$	Syn-Anti

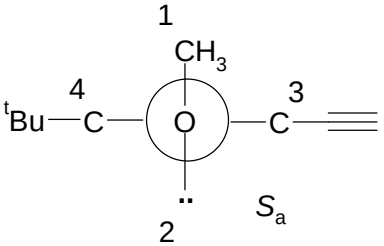

Looking down axis **2**

Figure 3.7 Assignment of axial chirality along the C—O bond and potential stereoisomers (with both absolute and relative configuration indicated) of a compound containing four such chiral axes.

III.6 Summary

The Stille coupling reactions of the unbuttressed dialkylated iodoresorcinols, while relatively slow, yielded the desired acetylenes in reasonable yields. However, the Stille coupling reactions of the buttressed dialkylated iodoresorcinols proved to be

remarkably fast (approximately an order of magnitude faster than that for the unbuttressed iodoresorcinols) and efficient.

Synthesis of the tolanes was similar for both buttressed and unbuttressed mono-aryl acetylenes. Elaboration of the tolane products remains a problem. The tetra ester yielded a mixture of separable (at least partially) fractions. The ^{1}H NMR spectra showed minor differences between the blue and green fractions. However, the UV spectra were very different (as well as their fluorescent behavior upon TLC analysis). These data support the notion that the tetra ester exhibits atropoisomerism.

The potential number of atropomers is quite large (3 meso and 5 pairs of enantiomers). With such a large number of stereoisomers, computations on a simpler model system may be able to provide valuable insight. While the assignment of axial chirality is unambiguous, the notation is not very convenient for describing the relative stereochemistry. For simplicity, we will employ the syn/anti designations.

III.7 Experimental.

III.7.a 1,3-Di-(2,3-*O*,*O*-isopropylidine-1-propoxy)-2-benzethyne. To a solution 1,3-di-(2,3-*O*,*O*-isopropylidine-1-propoxy)-2-iodobenzene (0.570 g; 1.23 mmol) in benzene (10 mL), was added tributyltinacetylide (0.580 g; 1.84 mmol), and tetrakis(triphenylphosphine) palladium (0.11 g; 0.095 mmol). The reaction mixture was heated to reflux and refluxed for 70 h. The crude mixture passed through a column (silica gel; hexanes–ethyl acetate, 2:1) to obtain 0.39 g (87%) of a reddish solid. ^{1}H NMR (270 MHz, $CDCl_3$) δ 1.37 (s, 6H), 1.44 (s, 6H), 3.42 (s, 1H), 3.92–4.20 (m, 8H), 4.44–4.48 (m, 2H), 6.47 (d, 2H), 7.18 (s, 1H).

III.7.b 1,3-Di-(ethoxycarbonylmethoxy)-2-benzethyne (3.1). To a solution 1,3-di-(ethoxycarbonylmethoxy)-2-iodobenzene (1.00 g; 2.45 mmol) in benzene (10 mL), was added tributyltinacetylide (0.920 g; 2.92 mmol), and tetrakis(triphenylphosphine) palladium (0.170 g; 0.147 mmol). The reaction mixture was refluxed for 46 h. The crude reaction mixture was concentrated, dissolved in acetonitrile (20 mL) and washed with hexanes (3 × 25 mL). The acetonitrile layer was concentrated and the residue passed through a column (silica gel; chloroform–hexanes–methanol, 19:10:1) and recrystallized from ethanol to obtain 0.23 g (31%) of brownish crystals. ^{1}H NMR (400 MHz, $CDCl_3$) δ 1.26 (t, J = 7.1 Hz, 6H), 3.56 (s, 1H), 4.22 (q, J = 7.1 Hz, 4H), 4.70 (t, J = 7.1 Hz, 4H), 6.43 (d, J = 10 Hz, 2H), 7.16 (t, J = 10 Hz, 1H).

III.7.c 1,3-Di-(ethoxycarbonylmethoxy)-4,6-di-*tert*-butyl-2-benzethyne (3.2). To a solution 1,3-di-(ethoxycarbonylmethoxy)-4-6-di-*tert*-butyl-2-iodobenzene (**2.1**) (1.00 g; 1.92 mmol) in benzene (10 mL), was added tributyltinacetylide (0.730; 2.32 mmol), and tetrakis(triphenylphosphine) palladium (0.11 g; 0.095 mmol). The reaction mixture refluxed for 2 h. The crude mixture was passed through a column (silica gel; hexanes–ethyl acetate, 3:1) and then recrystallized from ethanol to obtain 0.57 g (71%) of a slightly yellow-brown solid: mp 111.3 – 111.9 °C; ^{1}H NMR (400 MHz, $CDCl_3$) δ 1.33 (t, J = 7.1 Hz, 6H), 1.37 (s, 18H), 3.60 (s, 1H), 4.30 (q, J = 7.1 Hz, 4H), 4.81 (s, 4H), 7.29 (s, 1H); ^{13}C NMR (100 MHz, $CDCl_3$) δ 14.4, 30.8, 35.1, 61.3, 69.8, 89.3, 110.5, 126.9, 137.7, 158.3, 169.1. Anal. Calcd for $C_{24}H_{34}O_6$: C, 68.88; H, 8.19. Found C, 68.01; H, 8.1 (this is consistent with the ethyne being contaminated with 5% of the starting aryl

iodide, supported by the ^{1}H NMR). HRMS(FAB+) calcd for $C_{24}H_{34}O_6$ $[M]^+$: *m/z* 418.2355, found 418.2360.

III.7.d 1,3-Di-(oxoacetonitrile)-2-benzethyne (3.3). To a solution 1,3-di-(oxoacetonitrile)-2-iodobenzene (2.28 g; 7.26 mmol) in benzene (25 mL), was added tributyltinacetylide (3.200 g; 10.16 mmol), and tetrakis(triphenylphosphine) palladium (0.50 g; 0.43 mmol). The reaction mixture was refluxed for 20 h. The crude reaction mixture was concentrated, dissolved in acetonitrile (50 mL), and washed with hexanes (4 × 50 mL). The acetonitrile layer was concentrated, and the residue passed through a column (silica gel; chloroform–hexanes–methanol, 19:10:1) to obtain 1.0 g (50 %) of a brown solid. ^{1}H NMR (270 MHz, $CDCl_3$) δ 3.59 (s, 1H), 4.87 (s, 4H), 6.79 (d, *J* = 12 Hz, 2H), 7.37 (t, *J* = 12 Hz, 1H).

III.7.e 1,3-Di-(oxoacetonitrile)-4,6-di-*tert*-butyl-2-benzethyne (3.4). To a solution 1,3-di-(oxoacetonitrile)-4-6-di-*tert*-butyl-2-iodobenzene (**2.2**) (1.00 g; 2.35 mmol) in benzene (10 mL), was added tributyltinacetylide (0.770 g; 2.44 mmol), and tetrakis(triphenylphosphine) palladium (0.14 g; 0.12 mmol). The reaction mixture was refluxed for 4 h. The crude mixture passed through a column (silica gel; hexanes–ethyl acetate, 3:1) to obtain 0.42 g (55%) of a slightly brown solid: mp 155.1 – 155.6 °C; ^{1}H NMR (270 MHz, $CDCl_3$) δ 1.40 (s, 18H), 3.91 (s, 1H), 5.00 (s, 4H), 7.34 (s, 1H). Anal. Calcd for $C_{20}H_{24}N_2O_2$: C, 74.05; H, 7.46; N, 8.63. Found C, 73.43; H, 7.46; N, 8.55 (this is consistent with the ethyne being contaminated with 3% of the starting aryl iodide, supported by the ^{1}H NMR). HRMS(FAB+) calcd for $C_{20}H_{24}N_2O_2$ $[M]^+$: *m/z* 324.1838, found 324.1829.

III.7.f 1,3-Di-(2-azidoethoxy)-4,6-di-*tert*-butyl-2-benzethyne (3.5). To a solution 1,3-di-(2-azidoethoxy)-4,6-di-*tert*-butyl-2-iodobenzene (**2.3**) (2.00 g; 4.11 mmol) in benzene (25 mL), was added tributyltinacetylide (1.36; 4.32 mmol), and tetrakis(triphenylphosphine) palladium (0.24 g; 0.21 mmol). The reaction mixture was refluxed for 24 h. The crude mixture passed through a column (silica gel; hexanes–ethyl acetate, 5:1) to obtain 0.99 g (62%) of an orange-yellow solid. ^{1}H NMR (270 MHz, $CDCl_3$) δ 1.38 (s, 18H), 3.66 (t, *J* = 5 Hz, 4H), 3.70 (s, 1H), 4.37 (t, *J* = 5 Hz, 4H), 7.31 (s, 1H).

III.7.g 2-[1,3-Di-(ethoxycarbonylmethoxy)-4,6-di-*tert*-butyl-2-benzethynyl]-1,3-di-(ethoxycarbonylmethoxy)-4,6-di-*tert*-butylbenzene (3.6). To a solution of the diethyl 1,3-di-(ethoxycarbonylmethoxy)-4,6-di-*tert*-butyl-2-benzethyne (**3.2**) (0.550 g, 1.31 mmol) and 1,3-di-(ethoxycarbonylmethoxy)-4,6-di-tert-butyl-2-iodobenzene (**2.1**) (0.680 g, 1.31 mmol) in benzene (5 mL) was added tetrakis(triphenylphosphine) palladium (0.076 g , 0.066 mmol), cuprous iodide (0.013 g, 0.065 mmol), and triethylamine (3 mL). The reaction mixture was refluxed for 5 h. After concentration, the crude material was placed on a preparatory TLC plate (eluted with hexanes–ethyl acetate 4:1) and two major fractions were obtained.

One fraction yielded 0.070 g of a very slightly yellow solid (**3.6a**) (green-fluorescent material): mp 194.2 – 195.4 °C; ^{1}H NMR (400 MHz, $CDCl_3$) δ 1.24 (t, *J* = 7.1 Hz, 12H), 1.40 (s, 36H), 4.22 (q, *J* = 7.1 Hz, 8H), 4.93 (s, 8H), 7.30 (s, 2H); ^{13}C (100 MHz, CDCl3) δ 14.4, 31.2, 35.6, 61.4, 70.2, 92.3, 95.0, 127.6, 139.8, 156.0, 168.5; UV (EtOH) •$_{max}$ nm, (•): 320 (19000), 300 (26500), 285 (25500), 261 (27000). HRMS(FAB+) calcd for $C_{46}H_{66}O_{12}$ $[M]^+$: *m/z* 810.4553, found 810.4564. Crystal data: triclinic, a = 9.7750(10) Å, b = 10.587(2) Å, c = 12.998(2) Å, • = 112.170(10)°, • = 102.190(10)°, • = 96.440(10)°. V = 1189.9(3)Å^3, Z = 1, T = 293(2) K, R_1 = 0.0594, wR_2 = 0.1500, GOF = 1.129 for 263 parameters and 4085 total reflections. Graphite monochromator Mo K• (• = 0.71073 Å) radiation, structure solved by direct methods and refined by full matrix least squares against F^2 for all data using SHELXL software The CIF file is included in Appendix B (Supplemental X-Ray Data).

The other fraction yielded 0.130 g of a white solid (**3.6b**) (blue-fluorescent material): mp 88.4 – 89.1 °C; ^{1}H NMR (400 MHz, $CDCl_3$) δ 1.34 (t, *J* = 7.1 Hz, 12H), 1.38 (s, 36H), 4.32 (q, *J* = 7.1 Hz, 8H), 4.62 (s, 8H), 7.36 (s, 2H); ^{13}C (100 MHz, CDCl3) δ 14.4, 31.2, 35.6, 61.4, 70.2, 92.3, 95.6, 127.6, 139.8, 156.0, 168.5; UV (EtOH) •$_{max}$ nm, (•): 358 (7300) , 284 (24000). HRMS(FAB+) calcd for $C_{46}H_{66}O_{12}$ $[M]^+$: *m/z* 810.4553, found 810.4556.

III.7.h 1-[1,3-Di-(oxoacetonitrile)-2-benzethynyl]-2-(methoxycarbonyl)benzene. To a solution of $CuSO_4$ (0.830 g; 5.20 mmol) in ammonia hydroxide (4 mL) was added a solution of hydroxylamine hydrochloride (0.720 g; 10.4 mmol) in water (13 mL). The reaction mixture was stirred for 10 min and then a solution of the 1,3-di-(oxoacetonitrile)-

2-benzethyne (1.00 g; 4.71 mmol) in ethanol/ethyl acetate (9 mL/6 mL) was added dropwise. The reaction was stirred for 1 h under nitrogen. The solution was filtered to afford 1.0 g (77%) of the copper acetylide as a golden solid.

A solution of the copper acetylide (0.50 g; 1.82 mmol) and methyl 2-iodobenzoate (0.477 g; 1.82 mmol) in pyridine (9 mL) was refluxed under nitrogen for 12 h. The reaction mixture was diluted with ethyl acetate (35 mL), then washed with satd $CuSO_4$ (2 $\times$ 20 mL) and H_2O (1 $\times$ 20 mL). The ethyl acetate layer was concentrated to yield 0.31 g (49%) of a brown solid. ^{1}H NMR (400 MHz, $CDCl_3$) δ 3.95 (s, 3H), 4.99 (s, 4H), 6.87 (d, J = 12 Hz, 2H), 7.36 (t, J = 12 Hz, 1H), 7.41 (t, J = 8 Hz, 1H), 7.53 (t, J = 8 Hz, 1H), 7.70 (d, J = 8 Hz, 1H), 7.99 (d, J = 8 Hz, 1H).

III.7.i 1-[1,3-Di-(2-azidoethoxy)-4,6-di-*tert*-butyl-2-benzethynyl]-2-(methoxycarbonyl)benzene. To a solution of the 1,3-di-(2-azidoethoxy)-4,6-di-*tert*-butyl-2-benzethyne (0.10 g; 0.26 mmol) and methyl 2-iodobenzoate (0.068 g; 0.26 mmol) in benzene (1.5 mL) was added tetrakis(triphenylphosphine) palladium (0.018 g; 0.0156 mmol), cuprous iodide (0.003 g; 0.0158 mmol), and triethylamine (1.9 mL). The reaction mixture was heated to 80 °C for 2 d, and then the crude mixture was separated by preparative TLC (eluted with hexanes–ethyl acetate, 4:1) to afford 0.050 g (37%) of a yellowish solid. ^{1}H NMR (400 MHz, $CDCl_3$) δ 1.41 (s, 18H), 3.64 (t, J = 5 Hz, 4H), 3.91 (s, 3H), 4.48 (t, J = 5 Hz, 4H), 7.31 (s, 1H), 7.43 (t, J = 7.6 Hz, 1H), 7.55 (t, J = 7.6 Hz, 1H), 7.72 (d, J = 7.6 Hz, 1H), 8.02 (d, J = 7.6 Hz, 1H).

Chapter IV: Calculations

IV.1 Calculations on 2-Iodoresorcinols

In this chapter we present computational studies to help answer two questions generated in the previous chapter. Namely, why do the buttressed iodoresorcinols react faster than the unbuttressed iodoresorcinols in the Stille palladium cross-coupling reaction? And, what are the relative energies of the conformations of a model system for the fluorescent tetra esters?

Having observed the rate acceleration of the Stille coupling reaction of the buttressed aryl iodides (as compared to the unbuttressed aryl iodides), the question arose as to the origin of the effect. The rate acceleration could be due to chelation and/or it could be due to electronic effects.

Chelation could occur because of the restricted nature of the side chains motion, i.e. the side chains are held forward. If the side chains interact with the palladium and hold it near the iodine, then this could explain the increased reactivity. However, when the Stille coupling reaction was preformed with cyano side chains, there was still an increase in reactivity over the unbuttressed aryl iodide. As chelation is unlikely with a cyano group, as compared to an ester, there must be other reasons for the acceleration.

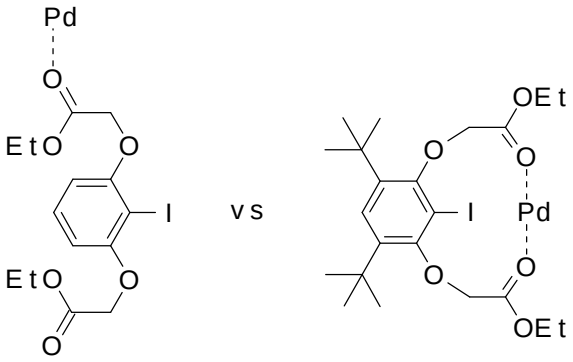

Another factor to consider is the electronic nature of the buttressed system as compared to the unbuttressed system. We know that for unbuttressed iodoresorcinols, the side chains prefer to be coplanar with the aromatic ring. This is not possible in the buttressed iodoresorcinols. The side chains must be "torqued" with respect to the aromatic plane. This being the case, the lone pairs on oxygen are not as available to interact with the aromatic pi system (as oxygen is a resonance donor).

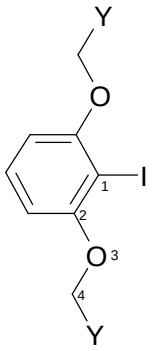

T1,2,3,4 = 180°

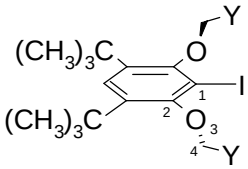

T1,2,3,4 = ~85°

However, oxygen is inductively electron withdrawing. If by torquing (i.e. twisting) the oxygen out of the aromatic plane we reduce the resonance donation of oxygen, then the inductive effect should make the system electron deficient as compared to the unbuttressed systems. As the Stille coupling reaction is facilitated by electron withdrawing substituents, this could explain the enhanced reactivity of the buttressed systems.

In order to explore this possibility, we performed some initial AM1 calculations (on 4,6-di-*tert*-butyl-1,3-dimethoxy-2-iodobenzene) that indicated the reduction potential was lowered as the side chains were pushed forward (from 90° to 0°). This should facilitate the oxidative addition of the palladium catalyst with the buttressed iodoresorcinols.

Due to the number of atoms, it was unfeasible to carry out *ab initio* level calculations on 4,6-di-*tert*-butyl-1,3-dimethoxy-2-iodobenzene directly. So, we used both 4,6-dimethyl-1,3-dimethoxy-2-iodobenzene and 1,3-dimethoxy-2-iodobenzene as model systems. All quantum level calculations were performed at the B3PW91 level of theory with the LANL2DZ basis set (due to the iodine).

First, we minimized the 4,6-dimethyl-1,3-dimethoxy-2-iodobenzene model system (both the syn and anti conformers). This revealed that the side arms are almost perpendicular to the aromatic plane (~95°). We then rotated the side arms from 90° to 0° in 15° increments, allowing complete minimization at each pseudo minimum. We noticed that as the side arms were pushed forward, the reduction potential decreased by approximately 0.4 eV.

However, we realized that this was not a good comparison of buttressed (where the side chains are ~90° to the aromatic plane) versus unbuttressed iodoresorcinols (where the side chains are 180° to the aromatic plane). So we moved to the 1,3-dimethoxy-2-iodobenzene model system. We once again rotated the side arms while maintaining C_2 symmetry (the methyl groups remain on opposite sides of the aromatic plane) or while maintaining C_s symmetry (the methyl groups are on the same side of the aromatic plane). This time the rotation was from 180° to 90° in 10° increments, allowing complete minimization at each pseudo minimum. Once again it was noticed that the reduction potential decreased (see Fig 4.1) from -0.459 eV at 180° to -0.810 (anti) eV or -

0.939 (syn)at 90°, as the arms were pushed forward. It was also noticed that the C_s rotation was accompanied by a downward distortion of the aryl carbon–iodine bond. This bending may weaken the carbon–iodine bond and allow for easier reduction of the C_s conformation (between 0 and 90°) as compared to the reduction of the C_2 conformation.

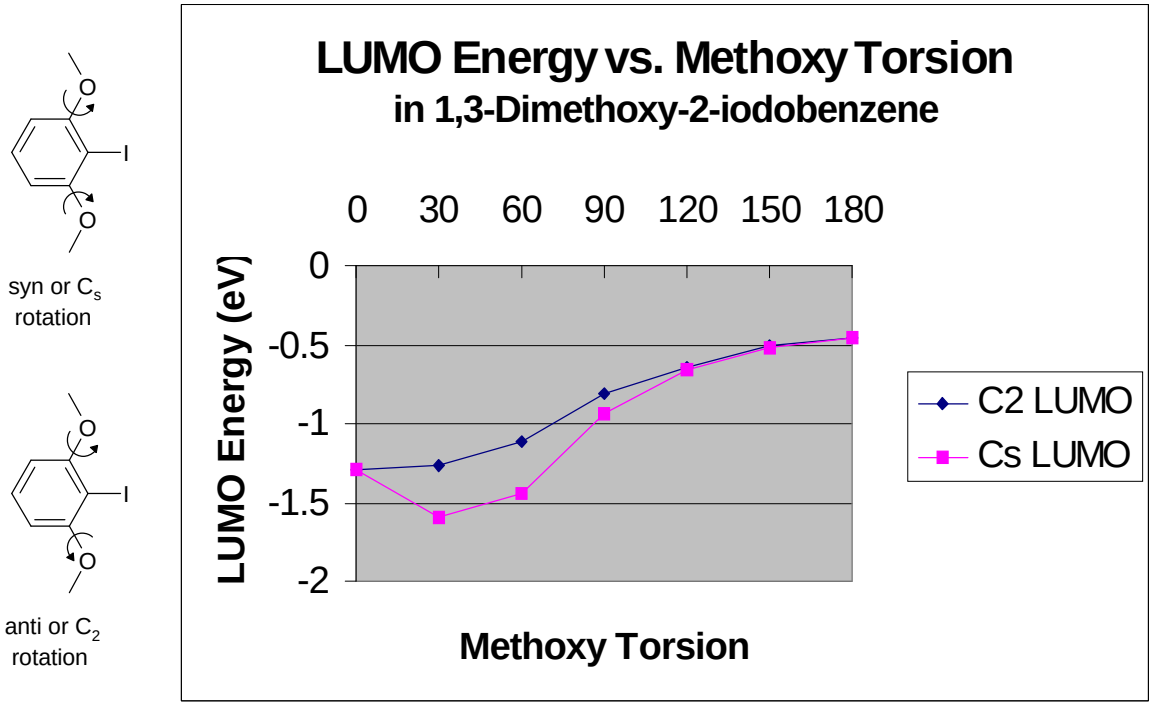

Figure 4.1. The effect of methoxy orientation on reduction potential for 1,3-dimethoxy-2-iodobenzene. Note that the largest differences occur when the methoxys are pushed forward toward the iodine (namely between 0-90°).

Examination of the LUMO orbitals for both the C_2 and C_s rotations, shows that the LUMO is always the σ^* orbital (see Fig 4.2 and Fig 4.3) of the σ bond between the iodine and the aromatic ring carbon. Thus, the oxidative addition of palladium always occurs with insertion into the carbon–iodine bond.

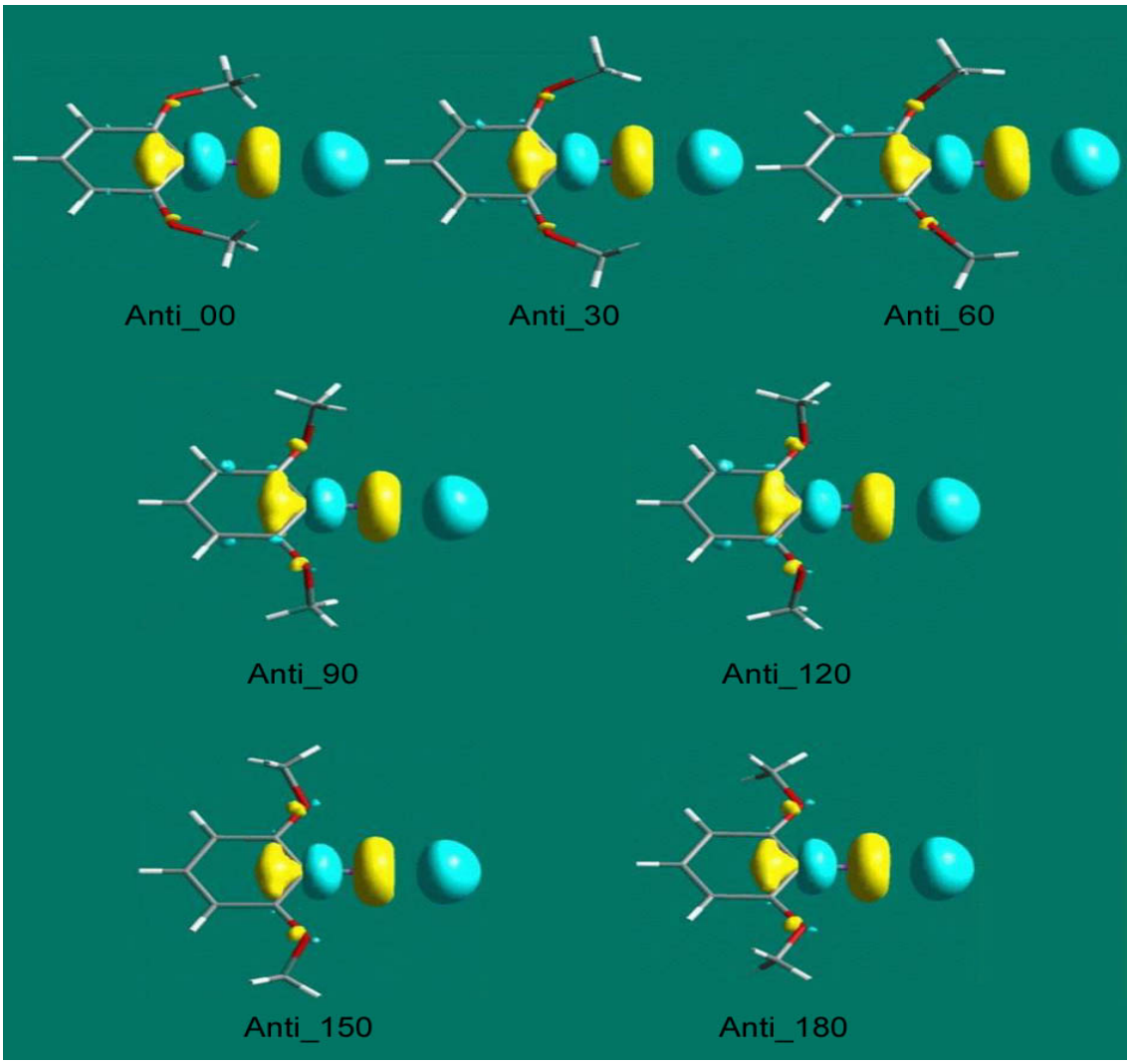

Figure 4.2 Pictorial representation of the LUMOs (always the C–I σ* orbital) during an anti (C_2) rotation as calculated with B3PW91/LanL2DZ.

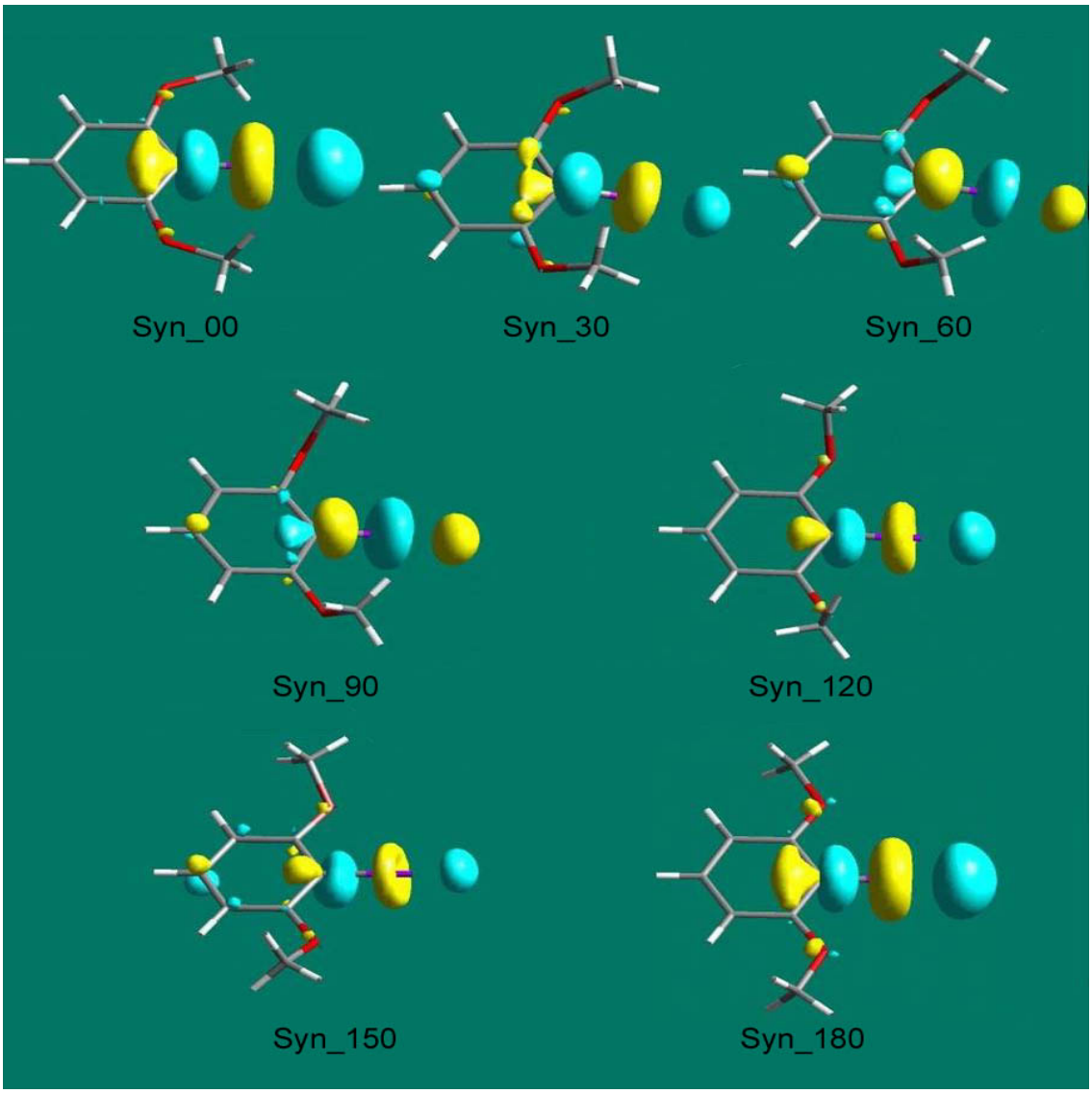

Figure 4.3. Pictorial representation of the LUMOs (always the C–I σ* orbital) during a syn (C_S) rotation as calculated with B3PW91/LanL2DZ. Note the downward bend of the σ* orbital at 30, 60 and 90°.

IV.2 Calculations on the Tetra Ester

As we could not obtain an X-ray crystal structure of the blue-fluorescent tetra ester (**3.6b**), we decided to perform some calculations to verify if our hypothesis (that this material was anti-anti) was correct. First, we performed a Monte-Carlo (MM3) search (as implemented in MacroModel V5.0[95]) to generate 2,000 conformers. The low-energy conformers (within 8 kcal of the global minimum, ~ 70 conformations) obtained, were analyzed by first noting the angle between the aromatic rings and then the relative

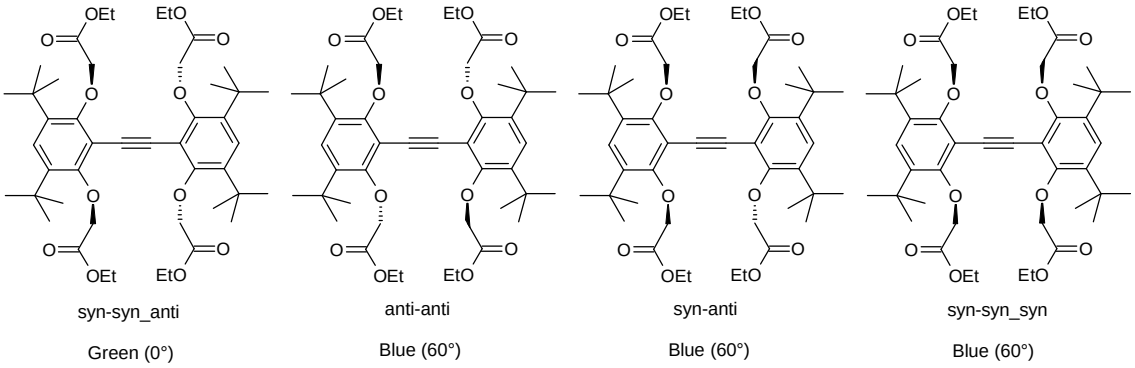

Figure 4.4. Structural families of the tetra-ester (**3.6**).

symmetry of the side chains. After the analysis, we could assign the structures to 4 structural families: syn-syn_anti, anti-anti, syn-anti, and syn-syn_syn. A representative structure (see Fig 4.4) of each family was then minimized at the semi-empirical level (AM1) and the minima verified by frequency calculations. The syn-syn_anti had the expected 0° angle between the aromatic rings. However, the anti-anti, syn-anti, and syn-syn_syn had an angle of ~60° between the aromatic rings.

We also examined a simpler model system, namely 2,2′,4,4′-tetra-*tert*-butyl-1,1′,5,5′-tetramethoxydiphenylacetylene (see Fig. 4.5). We found five distinct minima (verified by frequency calculations): anti-anti_anti (AA_A), anti-anti_syn (AA_S), syn-anti (SA), syn-syn_anti (SS_A), syn-syn_syn (SS_S). The relative energies (in kcals/mol) of the four conformations were: SS_A = 0, AA_A = 0.60, AA_S = 2.40, SA = 3.19, SS_S = 3.47. Attempts to calculate the barrier(s) to rotation about the aryl carbon–oxygen bond (C–O) were unsuccessful, but the barrier appeared to be less than 9

kcal/mol. The calculation of the barrier for rotation about the acetylenic axis was also unsuccessful, but much higher in energy (>15 kcal/mol).

This helps to explain why only the green-fluorescent atropomer (**3.6a**) (SS_A) was successfully separated. Rotation about the acetylenic axis is necessary in order for the SS_A atropomer to interconvert into one of the other atropomers. However the interconversions of AA_A, AA_S, SA and SS_S into each other involve only rotation about the aryl carbon–oxygen bond (C–O). Thus it is expected that the blue-fluorescent material (**3.6b**) is a mixture of the AA_A, AA_S, SA and SS_S atropomers, while the green-fluorescent component is composed of predominately only the SS_A atropomer.

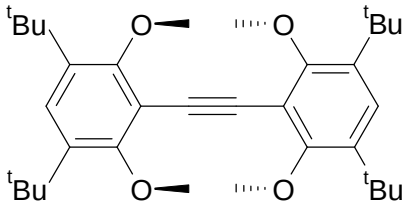

Syn-Syn_Anti (SS_A)

Rel. E = 0.00 kcal/mol

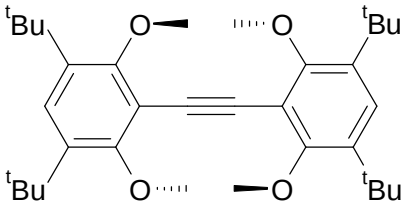

Anti-Anti_Anti (AA_A)

Rel. E = 0.60 kcal/mol

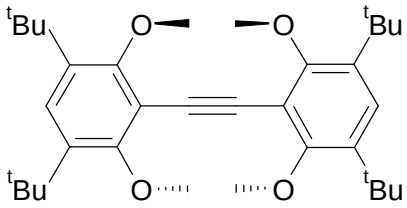

Anti-Anti_Syn (AA_S)

Rel. E = 2.40 kcal/mol

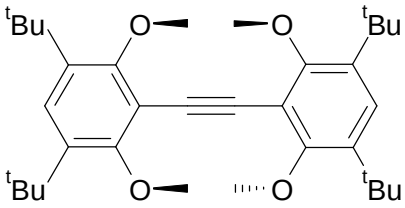

Syn-Anti (SA)

Rel. E = 3.19 kcal/mol

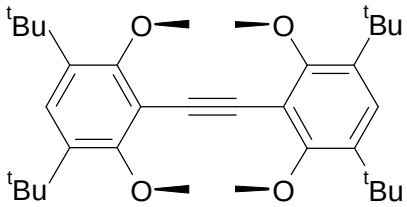

Syn-Syn_Syn (SS_S)

Rel. E = 3.47 kcal/mol

Figure 4.5. Conformations and relative energies of 2,2′,4,4′-tetra-*tert*-butyl-1,1′,5,5′-tetra-methoxy-diarylacetylene.

IV.3 Experimental.

All density functional theory (DFT) and Hartree-Fock (HF) calculations were performed using the Gaussian 98[96] programs. DFT calculations on 1,3-dimethoxy-2-iodobenzene were performed using Becke's Three Parameter Method[97] with the non-local correlation of Perdew/Wang 91[98] (B3PW91) and the LanL2DZ[99-102] basis set. HF calculations on 2,2′,4,4′-tetra-*tert*-butyl-1,1′,5,5′-tetra-methoxy-diphenylacetylene were performed using the 6-31G basis set. Frequency calculations were performed to characterize the stationary points.

IV.3.a XYZ Data for Anti (C_2) rotation of 1,3-dimethoxy-2-iodobenzene.

00 ----------

Center Number	Atomic Number	Coordinates (Angstroms) X	Y	Z
1	53	1.599	0.000	0.000
2	6	-0.553	0.000	0.000
3	6	-1.281	1.227	0.000
4	8	-0.839	2.546	0.000
5	6	0.501	3.105	0.000
6	1	1.062	2.829	0.897
7	1	1.062	2.829	-0.897
8	1	0.322	4.184	0.000
9	6	-2.692	1.206	0.000
10	1	-3.195	2.166	0.000
11	6	-3.389	0.000	0.000
12	6	-2.692	-1.206	0.000
13	1	-3.195	-2.166	0.000
14	6	-1.281	-1.227	0.000
15	8	-0.839	-2.546	0.000
16	6	0.501	-3.105	0.000
17	1	1.062	-2.829	0.897
18	1	0.322	-4.184	0.000
19	1	1.062	-2.829	-0.897
20	1	-4.475	0.000	0.000

30_Anti ----------

Center Number	Atomic Number	Coordinates (Angstroms) X	Y	Z
1	53	-1.602	0.000	0.000
2	6	0.545	0.000	0.000
3	6	1.270	1.216	0.149
4	8	0.793	2.518	0.281
5	6	-0.435	3.076	-0.265
6	1	-0.667	2.668	-1.254
7	1	-1.279	2.923	0.412
8	1	-0.224	4.145	-0.352
9	6	2.680	1.197	0.160
10	1	3.184	2.150	0.270
11	6	3.378	0.000	0.000
12	6	2.680	-1.197	-0.160
13	1	3.184	-2.150	-0.270
14	6	1.270	-1.216	-0.149
15	8	0.793	-2.518	-0.281
16	6	-0.435	-3.076	0.265
17	1	-1.279	-2.923	-0.412
18	1	-0.224	-4.145	0.352
19	1	-0.667	-2.667	1.254
20	1	4.464	0.000	0.000

60_Anti ----------

Center Number	Atomic Number	Coordinates (Angstroms) X	Y	Z
1	53	-1.613	0.000	0.000
2	6	0.519	0.000	0.000
3	6	1.235	1.195	0.258
4	8	0.652	2.433	0.519
5	6	-0.229	3.068	-0.464
6	1	-0.251	2.514	-1.409
7	1	-1.239	3.139	-0.055
8	1	0.175	4.071	-0.636
9	6	2.642	1.181	0.270
10	1	3.152	2.116	0.475
11	6	3.341	0.000	0.000
12	6	2.642	-1.181	-0.270
13	1	3.152	-2.117	-0.476
14	6	1.235	-1.195	-0.258
15	8	0.651	-2.433	-0.518
16	6	-0.229	-3.068	0.465
17	1	-1.239	-3.141	0.055
18	1	0.176	-4.070	0.639
19	1	-0.253	-2.512	1.409
20	1	4.427	0.000	-0.001

90_Anti ----------

Center Number	Atomic Number	Coordinates (Angstroms) X	Y	Z
1	53	-1.684	0.000	0.000
2	6	0.432	0.000	0.000
3	6	1.144	1.186	0.275
4	8	0.457	2.358	0.607
5	6	0.297	3.330	-0.474
6	1	1.274	3.654	-0.856
7	1	-0.298	2.905	-1.291
8	1	-0.230	4.177	-0.033
9	6	2.549	1.182	0.280
10	1	3.071	2.104	0.519
11	6	3.248	0.000	0.000
12	6	2.549	-1.182	-0.280
13	1	3.071	-2.104	-0.519
14	6	1.144	-1.186	-0.275
15	8	0.457	-2.358	-0.607
16	6	0.297	-3.330	0.474
17	1	-0.298	-2.905	1.291
18	1	-0.230	-4.177	0.033
19	1	1.274	-3.654	0.856
20	1	4.334	0.000	0.000

120_Anti ----------

Center Number	Atomic Number	Coordinates (Angstroms) X	Y	Z
1	53	0.000	-1.725	0.000
2	6	0.000	0.388	0.000
3	6	-1.195	1.100	0.233
4	8	-2.357	0.385	0.524
5	6	-3.484	0.552	-0.388
6	1	-3.837	1.591	-0.408
7	1	-3.209	0.236	-1.402
8	1	-4.272	-0.095	0.001
9	6	-1.192	2.506	0.237
10	1	-2.115	3.040	0.444
11	6	0.000	3.202	0.000
12	6	1.193	2.506	-0.237
13	1	2.116	3.039	-0.444
14	6	1.195	1.100	-0.233
15	8	2.357	0.385	-0.524
16	6	3.484	0.551	0.388
17	1	3.209	0.236	1.402
18	1	4.272	-0.095	-0.001
19	1	3.838	1.590	0.408
20	1	0.000	4.289	0.000

150_Anti ----------

Center Number	Atomic Number	Coordinates (Angstroms) X	Y	Z
1	53	0.000	-1.774	0.000
2	6	0.000	0.338	0.000
3	6	-1.210	1.049	0.137
4	8	-2.368	0.301	0.290
5	6	-3.619	0.847	-0.209
6	1	-4.010	1.628	0.457
7	1	-3.497	1.251	-1.222
8	1	-4.313	0.005	-0.223
9	6	-1.211	2.458	0.130
10	1	-2.143	3.003	0.238
11	6	0.000	3.148	0.000
12	6	1.211	2.458	-0.130
13	1	2.143	3.003	-0.238
14	6	1.210	1.049	-0.137
15	8	2.368	0.301	-0.290
16	6	3.619	0.847	0.209
17	1	3.497	1.251	1.222
18	1	4.313	0.005	0.223
19	1	4.010	1.628	-0.457
20	1	0.000	4.235	0.000

180 ----------

Center Number	Atomic Number	Coordinates (Angstroms) X	Y	Z
1	53	0.000	-1.788	0.000
2	6	0.000	0.323	0.000
3	6	-1.219	1.033	0.000
4	8	-2.373	0.271	0.000
5	6	-3.659	0.940	0.000
6	1	-3.788	1.558	0.898
7	1	-3.787	1.557	-0.899
8	1	-4.397	0.136	-0.001
9	6	-1.219	2.443	0.000
10	1	-2.152	2.996	0.000
11	6	0.000	3.130	0.000
12	6	1.219	2.443	0.000
13	1	2.152	2.996	0.000
14	6	1.219	1.033	0.000
15	8	2.373	0.271	-0.001
16	6	3.659	0.940	0.000
17	1	3.787	1.557	0.899
18	1	4.397	0.136	0.001
19	1	3.788	1.558	-0.898
20	1	0.000	4.217	0.000

IV.3.b XYZ Data for Syn (C_S) rotation of 1,3-dimethoxy-2-iodobenzene.

00 ----------

Center Number	Atomic Number	Coordinates (Angstroms) X	Y	Z
1	53	1.599	0.000	0.000
2	6	-0.553	0.000	0.000
3	6	-1.281	1.227	0.000
4	8	-0.839	2.546	0.000
5	6	0.501	3.105	0.000
6	1	1.062	2.829	0.897
7	1	1.062	2.829	-0.897
8	1	0.322	4.184	0.000
9	6	-2.692	1.206	0.000
10	1	-3.195	2.166	0.000
11	6	-3.389	0.000	0.000
12	6	-2.692	-1.206	0.000
13	1	-3.195	-2.166	0.000
14	6	-1.281	-1.227	0.000
15	8	-0.839	-2.546	0.000
16	6	0.501	-3.105	0.000
17	1	1.062	-2.829	0.897
18	1	0.322	-4.184	0.000
19	1	1.062	-2.829	-0.897
20	1	-4.475	0.000	0.000

30_Syn ----------

Center Number	Atomic Number	Coordinates (Angstroms) X	Y	Z
1	53	-1.582	0.000	-0.309
2	6	0.533	0.000	0.064
3	6	1.254	-1.224	-0.001
4	8	0.748	-2.507	0.170
5	6	-0.391	-2.820	1.023
6	1	-0.512	-2.080	1.823
7	1	-1.311	-2.887	0.438
8	1	-0.157	-3.795	1.458
9	6	2.641	-1.211	-0.240
10	1	3.148	-2.169	-0.285
11	6	3.320	0.000	-0.396
12	6	2.641	1.211	-0.240
13	1	3.149	2.168	-0.285
14	6	1.254	1.224	-0.001
15	8	0.748	2.507	0.170
16	6	-0.390	2.820	1.023
17	1	-0.512	2.080	1.823
18	1	-0.156	3.795	1.458
19	1	-1.310	2.888	0.438
20	1	4.388	0.000	-0.594

60_Syn ----------

Center Number	Atomic Number	Coordinates (Angstroms) X	Y	Z
1	53	-1.622	0.000	-0.292
2	6	0.496	0.000	-0.024
3	6	1.211	-1.221	-0.086
4	8	0.629	-2.487	0.000
5	6	-0.118	-2.843	1.206
6	1	0.539	-2.791	2.084
7	1	-0.994	-2.206	1.358
8	1	-0.439	-3.873	1.044
9	6	2.605	-1.212	-0.271
10	1	3.112	-2.170	-0.322
11	6	3.294	0.000	-0.394
12	6	2.605	1.212	-0.271
13	1	3.112	2.170	-0.322
14	6	1.211	1.221	-0.086
15	8	0.628	2.487	0.001
16	6	-0.118	2.843	1.206
17	1	0.538	2.790	2.085
18	1	-0.439	3.874	1.044
19	1	-0.995	2.206	1.358
20	1	4.368	0.000	-0.555

90_Syn ----------

Center Number	Atomic Number	Coordinates (Angstroms) X	Y	Z
1	53	1.667	0.000	-0.183
2	6	-0.452	0.000	-0.148
3	6	-1.163	1.218	-0.176
4	8	-0.496	2.446	-0.213
5	6	-0.184	3.040	1.086
6	1	-1.105	3.243	1.649
7	1	0.472	2.385	1.672
8	1	0.332	3.976	0.866
9	6	-2.568	1.214	-0.233
10	1	-3.083	2.169	-0.279
11	6	-3.266	0.000	-0.266
12	6	-2.568	-1.214	-0.233
13	1	-3.083	-2.169	-0.279
14	6	-1.163	-1.218	-0.176
15	8	-0.496	-2.446	-0.213
16	6	-0.184	-3.040	1.086
17	1	-1.105	-3.243	1.649
18	1	0.332	-3.976	0.866
19	1	0.473	-2.385	1.672
20	1	-4.351	0.000	-0.328

120_Syn ----------

Center Number	Atomic Number	Coordinates (Angstroms) X	Y	Z
1	53	-1.729	-0.001	-0.094
2	6	0.384	0.000	-0.163
3	6	1.095	-1.217	-0.192
4	8	0.379	-2.413	-0.240
5	6	0.579	-3.352	0.857
6	1	1.625	-3.678	0.926
7	1	0.270	-2.902	1.809
8	1	-0.057	-4.209	0.628
9	6	2.501	-1.215	-0.225
10	1	3.034	-2.160	-0.271
11	6	3.196	0.001	-0.236
12	6	2.500	1.217	-0.225
13	1	3.033	2.162	-0.271
14	6	1.094	1.218	-0.192
15	8	0.377	2.413	-0.240
16	6	0.576	3.353	0.857
17	1	1.622	3.680	0.926
18	1	-0.060	4.209	0.628
19	1	0.267	2.902	1.809
20	1	4.282	0.002	-0.277

150_Syn ----------

Center Number	Atomic Number	Coordinates (Angstroms) X	Y	Z
1	53.000	-1.000	-0.775	0.033719
2	6.000	0.000	0.335	-0.10187
3	6.000	1.218	1.045	-0.13323
4	8.000	2.385	0.297	-0.14013
5	6.000	3.578	0.860	0.469077
6	1.000	4.040	1.617	-0.17834
7	1.000	3.350	1.298	1.449217
8	1.000	4.264	0.019	0.585376
9	6.000	1.218	2.455	-0.14489
10	1.000	2.156	3.000	-0.16241
11	6.000	0.000	3.145	-0.14645
12	6.000	-1.218	2.455	-0.14489
13	1.000	-2.155	3.001	-0.16241
14	6.000	-1.218	1.046	-0.13322
15	8.000	-2.384	0.298	-0.14013
16	6.000	-3.578	0.861	0.469076
17	1.000	-4.039	1.618	-0.17834
18	1.000	-4.264	0.021	0.585362
19	1.000	-3.350	1.299	1.449223
20	1.000	0.001	4.231	-0.16023

180 ----------

Center Number	Atomic Number	Coordinates (Angstroms) X	Y	Z
1	53	0.000	-1.788	0.000
2	6	0.000	0.323	0.000
3	6	-1.219	1.033	0.000
4	8	-2.373	0.271	0.000
5	6	-3.659	0.940	0.000
6	1	-3.788	1.558	0.898
7	1	-3.787	1.557	-0.899
8	1	-4.397	0.136	-0.001
9	6	-1.219	2.443	0.000
10	1	-2.152	2.996	0.000
11	6	0.000	3.130	0.000
12	6	1.219	2.443	0.000
13	1	2.152	2.996	0.000
14	6	1.219	1.033	0.000
15	8	2.373	0.271	-0.001
16	6	3.659	0.940	0.000
17	1	3.787	1.557	0.899
18	1	4.397	0.136	0.001
19	1	3.788	1.558	-0.898
20	1	0.000	4.217	0.000

IV.3.c XYZ Data for the minimum conformations of 4,4¢,6,6¢-tetra-*tert*-butyl-1,1¢,3,3¢-tetra-methoxy-diphenylacetylene.

TetraEther_Anti-Anti_Anti ----------

Center Number	Atomic Number	Coordinates (Angstroms) X	Y	Z
1	6	2.031	0.000	0.000
2	6	2.731	1.203	0.137
3	6	4.125	1.233	0.093
4	6	4.767	0.000	0.000
5	6	4.125	-1.233	-0.093
6	6	2.731	-1.203	-0.137
7	8	2.018	2.381	0.260
8	6	4.928	2.552	0.123
9	6	4.928	-2.552	-0.123
10	8	2.018	-2.381	-0.260
11	6	0.599	0.000	0.000
12	6	-0.599	0.000	0.000
13	6	-2.031	0.000	0.000
14	6	-2.731	-1.203	0.137
15	6	-4.125	-1.233	0.093
16	6	-4.767	0.000	0.000
17	6	-4.125	1.233	-0.093
18	6	-2.731	1.203	-0.137
19	8	-2.018	-2.381	0.260
20	6	-4.928	-2.552	0.123
21	6	-4.928	2.552	-0.123
22	8	-2.018	2.381	-0.260
23	6	6.446	2.306	-0.010
24	6	4.504	3.448	-1.064
25	6	4.707	3.303	1.455
26	6	4.504	-3.448	1.064
27	6	4.707	-3.303	-1.455
28	6	6.446	-2.306	0.010
29	6	-6.446	-2.306	-0.010

30	6	-4.504	-3.448	-1.064
31	6	-4.707	-3.303	1.455
32	6	-4.504	3.448	1.064
33	6	-4.707	3.303	-1.455
34	6	-6.446	2.306	0.010
35	1	5.830	0.000	0.000
36	1	-5.830	0.000	0.000
37	1	6.956	3.262	-0.017
38	1	6.842	1.732	0.821
39	1	6.696	1.796	-0.933
40	1	5.069	4.375	-1.047
41	1	4.709	2.950	-2.006
42	1	3.453	3.683	-1.021
43	1	5.342	4.182	1.491
44	1	3.686	3.629	1.563
45	1	4.962	2.672	2.299
46	1	5.069	-4.375	1.047
47	1	4.709	-2.950	2.006
48	1	3.453	-3.683	1.021
49	1	5.342	-4.182	-1.491
50	1	3.686	-3.630	-1.563
51	1	4.962	-2.672	-2.299
52	1	6.956	-3.262	0.017
53	1	6.842	-1.732	-0.821
54	1	6.696	-1.796	0.933
55	1	-6.956	-3.262	-0.017
56	1	-6.842	-1.732	0.821
57	1	-6.696	-1.796	-0.933
58	1	-5.069	-4.375	-1.047
59	1	-4.709	-2.950	-2.006
60	1	-3.453	-3.683	-1.021
61	1	-5.342	-4.182	1.491
62	1	-3.686	-3.629	1.563
63	1	-4.962	-2.672	2.299
64	1	-5.069	4.375	1.047
65	1	-4.709	2.950	2.006
66	1	-3.453	3.683	1.021

67	1	-5.342	4.182	-1.491
68	1	-3.686	3.629	-1.563
69	1	-4.962	2.672	-2.299
70	1	-6.956	3.262	0.017
71	1	-6.842	1.732	-0.821
72	1	-6.696	1.796	0.933
73	6	-1.241	-2.666	1.452
74	1	-1.360	-3.720	1.643
75	1	-0.206	-2.440	1.272
76	1	-1.612	-2.095	2.292
77	6	1.241	-2.666	-1.452
78	1	1.360	-3.720	-1.643
79	1	0.206	-2.440	-1.272
80	1	1.612	-2.095	-2.292
81	6	1.241	2.666	1.452
82	1	1.360	3.720	1.643
83	1	0.206	2.440	1.272
84	1	1.612	2.095	2.292
85	6	-1.241	2.666	-1.452
86	1	-1.360	3.720	-1.643
87	1	-0.206	2.440	-1.272
88	1	-1.611	2.095	-2.291

TetraEther_Anti-Anti_Syn ----------

Center Number	Atomic Number	Coordinates (Angstroms) X	Y	Z
1	6	-2.030	0.000	0.000
2	6	-2.730	-1.011	0.664
3	6	-4.123	-1.067	0.625
4	6	-4.765	0.000	0.000
5	6	-4.123	1.067	-0.625
6	6	-2.730	1.011	-0.664
7	8	-2.009	-1.995	1.322
8	6	-4.924	-2.257	1.199
9	6	-4.924	2.257	-1.199
10	8	-2.009	1.994	-1.322
11	6	-0.596	0.000	0.000
12	6	0.601	0.000	0.000
13	6	2.035	0.000	0.000
14	6	2.734	0.993	0.695
15	6	4.127	0.981	0.753
16	6	4.770	0.000	0.000
17	6	4.127	-0.981	-0.753
18	6	2.734	-0.993	-0.694
19	8	2.023	1.959	1.381
20	6	4.930	1.970	1.628
21	6	4.930	-1.970	-1.628
22	8	2.023	-1.959	-1.381
23	6	-6.441	-2.099	0.958
24	6	-4.479	-3.560	0.494
25	6	-4.721	-2.395	2.724
26	6	-4.479	3.560	-0.494
27	6	-4.721	2.396	-2.724
28	6	-6.440	2.099	-0.958
29	6	6.448	1.698	1.560
30	6	4.712	3.429	1.171
31	6	4.501	1.815	3.106
32	6	4.712	-3.429	-1.171
33	6	4.501	-1.815	-3.106

34	6	6.448	-1.698	-1.560
35	1	-5.828	0.000	0.000
36	1	5.833	0.000	0.000
37	1	-6.949	-2.975	1.341
38	1	-6.848	-1.235	1.471
39	1	-6.678	-2.019	-0.096
40	1	-5.037	-4.403	0.890
41	1	-4.675	-3.500	-0.571
42	1	-3.426	-3.743	0.641
43	1	-5.384	-3.161	3.114
44	1	-3.711	-2.682	2.967
45	1	-4.953	-1.465	3.232
46	1	-5.037	4.403	-0.890
47	1	-4.674	3.500	0.571
48	1	-3.426	3.743	-0.641
49	1	-5.384	3.162	-3.114
50	1	-3.711	2.683	-2.966
51	1	-4.953	1.465	-3.232
52	1	-6.949	2.975	-1.341
53	1	-6.848	1.235	-1.471
54	1	-6.678	2.019	0.096
55	1	6.957	2.393	2.217
56	1	6.696	0.696	1.890
57	1	6.845	1.842	0.561
58	1	5.364	4.091	1.733
59	1	4.947	3.543	0.118
60	1	3.697	3.750	1.337
61	1	5.060	2.508	3.727
62	1	3.447	2.012	3.230
63	1	4.708	0.809	3.457
64	1	5.364	-4.090	-1.732
65	1	4.948	-3.543	-0.118
66	1	3.697	-3.750	-1.337
67	1	5.060	-2.507	-3.727
68	1	3.448	-2.012	-3.230
69	1	4.708	-0.809	-3.456
70	1	6.958	-2.393	-2.216

71	1	6.697	-0.696	-1.890
72	1	6.845	-1.842	-0.561
73	6	1.286	2.980	0.665
74	1	0.334	2.603	0.334
75	1	1.140	3.779	1.373
76	1	1.859	3.337	-0.180
77	6	-1.329	1.674	-2.560
78	1	-1.087	2.622	-3.010
79	1	-0.430	1.115	-2.365
80	1	-1.979	1.110	-3.213
81	6	-1.329	-1.674	2.560
82	1	-1.088	-2.623	3.010
83	1	-0.429	-1.116	2.365
84	1	-1.979	-1.109	3.212
85	6	1.286	-2.980	-0.665
86	1	0.335	-2.604	-0.333
87	1	1.140	-3.779	-1.373
88	1	1.859	-3.337	0.180

TetraEther_Syn-Anti ----------

Center Number	Atomic Number	Coordinates (Angstroms) X	Y	Z
1	6	-2.024	-0.021	0.070
2	6	-2.811	-1.131	0.391
3	6	-4.192	-1.119	0.211
4	6	-4.748	0.099	-0.182
5	6	-4.027	1.263	-0.435
6	6	-2.637	1.167	-0.345
7	8	-2.178	-2.267	0.876
8	6	-5.067	-2.382	0.377
9	6	-4.744	2.585	-0.788
10	8	-1.859	2.279	-0.590
11	6	-0.594	-0.103	0.138
12	6	0.603	-0.144	0.153
13	6	2.037	-0.126	0.134
14	6	2.714	1.051	0.481
15	6	4.096	1.157	0.344
16	6	4.759	0.026	-0.129
17	6	4.147	-1.178	-0.468
18	6	2.761	-1.236	-0.317
19	8	1.989	2.159	0.872
20	6	4.864	2.460	0.659
21	6	4.967	-2.364	-1.019
22	8	2.097	-2.378	-0.706
23	6	-6.545	-2.105	0.026
24	6	-4.563	-3.481	-0.586
25	6	-5.039	-2.911	1.828
26	6	-4.384	3.668	0.255
27	6	-4.349	3.062	-2.203
28	6	-6.279	2.430	-0.775
29	6	6.381	2.309	0.419
30	6	4.366	3.601	-0.258
31	6	4.680	2.855	2.141
32	6	4.817	-3.602	-0.106

33	6	4.504	-2.705	-2.454
34	6	6.475	-2.040	-1.089
35	1	-5.804	0.143	-0.292
36	1	5.814	0.088	-0.242
37	1	-7.104	-3.029	0.115
38	1	-6.997	-1.384	0.698
39	1	-6.661	-1.751	-0.991
40	1	-5.171	-4.374	-0.480
41	1	-4.636	-3.147	-1.616
42	1	-3.535	-3.738	-0.383
43	1	-5.758	-3.716	1.938
44	1	-4.069	-3.303	2.089
45	1	-5.305	-2.129	2.532
46	1	-4.889	4.597	0.010
47	1	-4.708	3.363	1.244
48	1	-3.321	3.849	0.282
49	1	-4.917	3.949	-2.464
50	1	-3.302	3.310	-2.261
51	1	-4.566	2.297	-2.941
52	1	-6.729	3.390	-0.999
53	1	-6.626	1.726	-1.524
54	1	-6.648	2.115	0.194
55	1	6.867	3.249	0.651
56	1	6.821	1.548	1.054
57	1	6.608	2.072	-0.614
58	1	4.912	4.514	-0.041
59	1	4.536	3.350	-1.299
60	1	3.313	3.786	-0.117
61	1	5.278	3.733	2.366
62	1	3.653	3.089	2.366
63	1	5.006	2.053	2.795
64	1	5.451	-4.405	-0.467
65	1	5.119	-3.369	0.910
66	1	3.802	-3.964	-0.090
67	1	5.084	-3.537	-2.841
68	1	3.459	-2.970	-2.476
69	1	4.658	-1.856	-3.112

70	1	7.000	-2.902	-1.484
71	1	6.682	-1.205	-1.748
72	1	6.893	-1.823	-0.112
73	6	1.132	2.167	2.036
74	1	1.387	3.047	2.606
75	1	0.107	2.221	1.713
76	1	1.288	1.284	2.638
77	6	-0.876	2.327	-1.655
78	1	-1.064	3.231	-2.212
79	1	0.106	2.361	-1.217
80	1	-0.967	1.469	-2.304
81	6	-1.675	-2.242	2.231
82	1	-1.429	-3.264	2.470
83	1	-0.795	-1.623	2.297
84	1	-2.432	-1.877	2.910
85	6	1.255	-3.138	0.189
86	1	0.224	-2.883	0.026
87	1	1.423	-4.176	-0.052
88	1	1.531	-2.955	1.219

TetraEther_Syn-Syn_Anti ----------

Center Number	Atomic Number	Coordinates (Angstroms) X	Y	Z
1	6	2.026	0.000	0.140
2	6	2.728	1.210	0.130
3	6	4.117	1.237	0.013
4	6	4.757	0.000	-0.049
5	6	4.117	-1.237	0.013
6	6	2.728	-1.210	0.130
7	8	2.018	2.395	0.171
8	6	4.914	2.555	-0.095
9	6	4.914	-2.556	-0.094
10	8	2.018	-2.395	0.171
11	6	0.596	0.000	0.058
12	6	-0.596	0.000	-0.057
13	6	-2.026	0.000	-0.139
14	6	-2.728	1.210	-0.129
15	6	-4.117	1.237	-0.013
16	6	-4.757	0.000	0.049
17	6	-4.117	-1.237	-0.013
18	6	-2.728	-1.210	-0.130
19	8	-2.018	2.395	-0.170
20	6	-4.914	2.555	0.095
21	6	-4.914	-2.556	0.094
22	8	-2.018	-2.395	-0.171
23	6	6.429	2.303	-0.254
24	6	4.448	3.348	-1.338
25	6	4.732	3.415	1.176
26	6	4.732	-3.414	1.177
27	6	4.448	-3.349	-1.337
28	6	6.429	-2.303	-0.253
29	6	-6.429	2.303	0.253
30	6	-4.448	3.348	1.337
31	6	-4.732	3.415	-1.176
32	6	-4.731	-3.414	-1.177

33	6	-4.448	-3.349	1.336
34	6	-6.429	-2.303	0.252
35	1	5.816	0.000	-0.147
36	1	-5.816	0.000	0.146
37	1	6.936	3.257	-0.338
38	1	6.848	1.784	0.602
39	1	6.655	1.734	-1.148
40	1	5.010	4.274	-1.417
41	1	4.623	2.773	-2.241
42	1	3.397	3.585	-1.280
43	1	5.364	4.295	1.118
44	1	3.713	3.748	1.288
45	1	5.016	2.857	2.062
46	1	5.364	-4.294	1.120
47	1	5.016	-2.856	2.063
48	1	3.713	-3.747	1.289
49	1	5.009	-4.275	-1.416
50	1	3.397	-3.585	-1.278
51	1	4.622	-2.774	-2.240
52	1	6.936	-3.257	-0.337
53	1	6.655	-1.735	-1.148
54	1	6.848	-1.784	0.602
55	1	-6.936	3.257	0.337
56	1	-6.848	1.784	-0.602
57	1	-6.655	1.734	1.148
58	1	-5.010	4.274	1.417
59	1	-4.623	2.773	2.241
60	1	-3.398	3.585	1.279
61	1	-5.364	4.295	-1.119
62	1	-3.713	3.748	-1.288
63	1	-5.016	2.857	-2.062
64	1	-5.364	-4.295	-1.120
65	1	-5.015	-2.856	-2.063
66	1	-3.713	-3.747	-1.289
67	1	-5.010	-4.275	1.416
68	1	-3.398	-3.585	1.278
69	1	-4.623	-2.774	2.240

70	1	-6.936	-3.257	0.336
71	1	-6.655	-1.735	1.147
72	1	-6.848	-1.784	-0.603
73	6	-1.269	2.765	-1.356
74	1	-1.252	3.842	-1.367
75	1	-0.265	2.384	-1.296
76	1	-1.763	2.395	-2.243
77	6	1.269	-2.764	1.357
78	1	1.252	-3.842	1.369
79	1	1.762	-2.393	2.244
80	1	0.265	-2.384	1.296
81	6	1.269	2.765	1.356
82	1	1.762	2.394	2.244
83	1	1.252	3.842	1.368
84	1	0.265	2.384	1.296
85	6	-1.268	-2.764	-1.356
86	1	-0.264	-2.384	-1.295
87	1	-1.253	-3.842	-1.369
88	1	-1.761	-2.392	-2.244

TetraEther_Syn-Syn_Syn ----------

Center Number	Atomic Number	Coordinates (Angstroms) X	Y	Z
1	6	2.029	-0.114	0.145
2	6	2.800	0.941	0.647
3	6	4.173	1.004	0.430
4	6	4.736	-0.069	-0.261
5	6	4.033	-1.173	-0.735
6	6	2.655	-1.180	-0.508
7	8	2.157	1.974	1.313
8	6	5.032	2.213	0.865
9	6	4.746	-2.300	-1.514
10	8	1.899	-2.220	-1.004
11	6	0.597	-0.043	0.205
12	6	-0.597	0.043	0.205
13	6	-2.029	0.114	0.145
14	6	-2.800	-0.941	0.647
15	6	-4.173	-1.004	0.430
16	6	-4.736	0.069	-0.261
17	6	-4.033	1.173	-0.735
18	6	-2.655	1.180	-0.508
19	8	-2.157	-1.974	1.313
20	6	-5.032	-2.213	0.865
21	6	-4.746	2.300	-1.514
22	8	-1.899	2.220	-1.004
23	6	6.513	2.039	0.466
24	6	4.515	3.492	0.168
25	6	4.999	2.402	2.398
26	6	4.577	-3.655	-0.792
27	6	4.174	-2.390	-2.948
28	6	6.263	-2.045	-1.641
29	6	-6.513	-2.039	0.466
30	6	-4.515	-3.492	0.168
31	6	-4.999	-2.402	2.398
32	6	-4.577	3.655	-0.792

33	6	-4.174	2.390	-2.948
34	6	-6.263	2.045	-1.641
35	1	5.784	-0.042	-0.439
36	1	-5.784	0.042	-0.439
37	1	7.065	2.919	0.778
38	1	6.968	1.181	0.948
39	1	6.638	1.941	-0.605
40	1	5.117	4.345	0.467
41	1	4.587	3.392	-0.909
42	1	3.486	3.690	0.425
43	1	5.690	3.187	2.686
44	1	4.018	2.687	2.743
45	1	5.298	1.491	2.906
46	1	5.143	-4.422	-1.311
47	1	4.948	-3.597	0.226
48	1	3.545	-3.967	-0.767
49	1	4.676	-3.181	-3.496
50	1	3.115	-2.593	-2.936
51	1	4.339	-1.458	-3.479
52	1	6.709	-2.860	-2.198
53	1	6.478	-1.128	-2.178
54	1	6.752	-2.003	-0.674
55	1	-7.065	-2.919	0.778
56	1	-6.968	-1.181	0.948
57	1	-6.638	-1.941	-0.606
58	1	-5.117	-4.345	0.467
59	1	-4.587	-3.392	-0.909
60	1	-3.486	-3.690	0.425
61	1	-5.690	-3.187	2.686
62	1	-4.018	-2.687	2.743
63	1	-5.298	-1.491	2.906
64	1	-5.143	4.422	-1.311
65	1	-4.948	3.597	0.226
66	1	-3.545	3.967	-0.767
67	1	-4.676	3.181	-3.496
68	1	-3.115	2.593	-2.936
69	1	-4.339	1.458	-3.479

70	1	-6.709	2.860	-2.198
71	1	-6.478	1.128	-2.178
72	1	-6.752	2.003	-0.674
73	6	-1.580	-1.740	2.615
74	1	-1.466	-2.713	3.065
75	1	-0.619	-1.264	2.522
76	1	-2.238	-1.131	3.220
77	6	1.107	-3.071	-0.144
78	1	1.075	-4.030	-0.634
79	1	1.577	-3.171	0.826
80	1	0.112	-2.679	-0.037
81	6	1.580	1.740	2.615
82	1	1.466	2.713	3.065
83	1	0.619	1.264	2.522
84	1	2.238	1.131	3.220
85	6	-1.107	3.071	-0.144
86	1	-0.112	2.679	-0.037
87	1	-1.075	4.030	-0.634
88	1	-1.577	3.171	0.826

Chapter V: CONCLUSIONS

This project started with 4 major goals:

1) The synthesis of pentasubstituted aromatic building blocks.
2) The coupling of these crowded building blocks into tolanes.
3) Studying any unusual reactivity during the syntheses of these tolanes and crowded building blocks.
4) Studying any unusual structural features or properties of these tolanes and crowded building blocks.

V.1 Synthesis of Pentasubstituted Arenes

The Friedel-Crafts alkylation of resorcinol allows for easy access to 4,6-di-*tert*-butylresorcinol. Although several reports exist of the synthesis, the use of acetic acid gives consistently higher yields. Iodination affords 4,6-di-*tert*-butyl-2-iodoresorcinol in high yields. We had some trouble with highly colored (usually some shade of orange) 4,6-di-*tert*-butyl-2-iodoresorcinol, but careful pH control yields nearly colorless material. While we have exclusively utilized 4,6-di-*tert*-butyl-2-iodoresorcinol (after *O,O*-dialkylation) as a substrate for Pd couplings, there are other chemistries available that could involve this particular aryl iodide.

Alkylation of 4,6-di-*tert*-butyl-2-iodoresorcinol is still challenging, but we have made a few improvements—notably the use of Cs_2CO_3, as the base. However, we are still mainly limited to the use of active electrophiles for alkylation. Nevertheless, we have synthesized a pool of pentasubstituted arenes suitable for elaboration into arylacetylenes and tolanes.

V.2 Synthesis of Arylacetylenes

The Stille palladium cross-coupling reaction of *O,O*-disubstituted-4,6-di-*tert*-butyl-2-iodoresorcinols with tributyltinacetylene, is actually quicker than the same coupling reaction with *O,O*-disubstituted-2-iodoresorcinols. This increased reactivity for the crowded aryl iodides, make possible the synthesis of several crowded arylacetylenes. However, purification of the arylacetylenes is still often very difficult.

V.3 Unusual Reactivity of Crowded Aryl Iodides

To provide an explanation for the increased reactivity, we performed DFT calculations on 1,3-dimethoxy-2-iodobenzene. The results indicated that the reduction potential decreased as the methoxy groups were rotated ("torqued") out of the aromatic plane. This implies that our pentasubstituted resorcinols, in which the oxo side arms are nearly perpendicular to the aromatic plane, should also have a lower reduction potential than the non-buttressed resorcinols (where the oxo side arms are in the aromatic plane). Therefore, the rate increase in the Stille palladium cross-coupling of the buttressed iodoresorcinols, as compared to the non-buttressed iodoresorcinols, may be mostly due to the easier initial reduction of the buttressed iodoresorcinols by the palladium catalyst to an organopalladium species.

The copper/palladium coupling of aryl iodides and arylacetylenes yielded the desired tolanes. However, purification is often difficult and exacerbated by the small amounts of tolane synthesized. The synthesis of the tetra ester was undertaken to see if the Pd/Cu couplings showed a similar enhanced rate of reaction as the Stille coupling of the aryl iodide. While there was no enhancement of the rate, we did notice two fluorescent spots by TLC. This led us to examine the possibility of different atropomers for this tetra ester. Fortunately we were able to separate and grow suitable crystals for X-ray analysis of the green fluorescent atropomer; however, attempts to grow single crystals of the blue fluorescent atropomer(s) were unsuccessful.

V.4 Atropisomerism in Crowded Tolanes

Calculations on a model system of the tetra ester, namely the tetra methylether, showed a surprising number of possible diastereomeric rotamers. The sheer number of stereoisomers suggests why our attempts at separation were unsuccessful. Also the tentative calculated barriers to rotation reveal that simple rotation about the aryl carbon oxygen bond (C–O) is very low, whereas the rotation about the acetylenic axis is much harder. This helps explain why we were able to separate, and obtain a suitable crystal for X-ray analysis, the green fluorescent syn_syn_anti atropomer.

V.5 Final Comments

Although conceptually attractive for studying intramolecular recognition, synthesizing the desired diarylacetylenes required overcoming challenges. The

optimization of the synthesis of 4,6-di-*tert*-butyl-2-iodoresorcinol provided both suitable material and a robust scaffold for further elaboration. Subsequent *O,O* dialkylation provided a pool (5) of bis-functionalized aryl iodides. The bis-ester emerged as the most promising synthon. Stille palladium chemistry on the bis-ester led to the tetra-ester.

Structural and computational studies on the tetra-ester and analogues, suggested a large number of potential stereoisomers (atropomers) exist. Separating the possible atropomers was only partially successful; chromatography did yield one atropomer, which was identified by means of X-ray crystallography, and an inseparable mixture of the other atropomers.

Looking to the future, I have several suggestions. Development of a resin based approach, either resin bound tributyltinacetylene or resin bound aryl iodide,[103] to the synthesis of the aryl ethynes would allow for easier isolation and purification of the aryl ethynes. Likewise, a supported palladium catalyst would simplify the purification of the diarylacetylenes derived from the aryl ethynes. The underlining problem of multiple possible atropomers of the diarylacetylenes is probably only tractable by utilizing rings to constrain the conformational flexibility of the side arms.

REFERENCES

(1) Mathews, C. K.; Van Holde, K. E. *Biochemistry*; 2nd ed.; The Benjamin/Cummings Publishing Co., Inc.: Redwood City CA, 1996.

(2) Murray, J. S.; Politzer, P. *J. Mol. Struct. (Theochem)* **1998**, *425*, 107-114.

(3) Politzer, P.; Murray, J. S. *Fluid Phase Equilibria* **2001**, *185*, 129-137.

(4) Hammett, L. P. *Chem. Rev.* **1935**, *17*, 125.

(5) Hammett, L. P.; Pfluger, H. L. *J. Am. Chem. Soc.* **1933**, *55*, 571.

(6) Swain, C. G.; Lupton, E. C., Jr. *J. Am. Chem. Soc.* **1968**, *90*, 4328.

(7) Swain, C. G.; Unger, S. H.; Rosenquist, N. R.; Swain, M. S. *J. Am. Chem. Soc.* **1983**, *105*, 492.

(8) Kirkwood, J. G.; Westheimer, F. H. *J. Chem. Phys.* **1938**, *6*, 506.

(9) Kirkwood, J. G.; Westheimer, F. H. *J. Chem. Phys.* **1938**, *6*, 513.

(10) Exner, O. *J. Phys. Org. Chem.* **1999**, *12*, 265-274.

(11) Segurado, M. A. P.; Reis, J. C. R.; Oliveira, J. D. G. *J. Chem. Soc., Perkin Trans. 2* **2002**, 323-328.

(12) Charton, M. *Progr. Phys. Org. Chem.* **1981**, *13*, 119.

(13) Beugelman-Verrier, M.; Nicolas, L.; Gaudemer, A.; Parello, J. *Tetrahedron Lett.* **1976**, 361.

(14) Acevedo, S.; Bowden, K. *J. Chem. Soc., Perkin Trans. 2* **1986**, 2051.

(15) Grubbs, E. J.; Fitzgerald, R. *Tetrahedron Lett.* **1968**, 4901.

(16) Grubbs, E. J.; Fitzgerald, R.; Phillips, R. E.; Petty, R. *Tetrahedron* **1971**, *27*, 935.

(17) Grubbs, E. J.; Wang, C. T.; Deardurff, L. A. *J. Org. Chem.* **1984**, *49*, 4080.

(18) Wang, C. T.; Grubbs, E. J. *J. Org. Chem.* **1977**, *42*, 534.

(19) Hine, J. In *Structural Effects on Equilbria in Organic Chemistry*; John Wiley & Sons, Inc.: New York, 1975, p 42.

(20) Rebek, J., Jr.; Duff, R. J.; Gordon, W. E.; Parris, K. *J. Am. Chem. Soc.* **1986**, *108*, 6069-6069.

(21) Gandour, R. D. *Bioorg. Chem.* **1981**, *10*, 169.

(22) Bell, T. W.; Cheng, P. G.; Newcomb, M.; Cram, D. J. *J. Am. Chem. Soc.* **1982**, *104*, 5185-5188.

(23) Zimmerman, S. C.; Cramer, K. D. *J. Am. Chem. Soc.* **1988**, *110*, 5906-5908.

(24) Zimmerman, S. C.; Korthals, J. S.; Cramer, K. D. *Tetrahedron* **1991**, *47*, 2649-2660.

(25) Cloninger, M. J.; Frey, P. A. *Bioorg. Chem.* **1998**, *26*, 323-333.

(26) Tee, O. S. *Adv. Phys. Org. Chem.* **1994**, *29*, 1-85.

(27) Kirby, A. J. *Adv. Phys. Org. Chem.* **1980**, *17*, 183-278.

(28) Czarnik, A. W. *Mol. Struct. Energ.* **1988**, *9*, 75-117.

(29) Gandour, R. D. In *Transition States of Biochemical Processes*; Gandour, R. D., Schowen, R. L., Eds.; Plenum Press: New York, 1978, p 529-552.

(30) Storm, D. R.; Koshland, D. E., Jr. *Proc. Nat. Acad. Sci., USA* **1970**, *66*, 445-452.

(31) Storm, D. R.; Koshland, D. E., Jr. *J. Am. Chem. Soc.* **1972**, *94*, 5805-5814.

(32) Storm, D. R.; Koshland, D. E., Jr. *J. Am. Chem. Soc.* **1972**, *94*, 5815-5825.

(33) Capon, B. *J. Chem. Soc. B* **1971**, 1207-1209.

(34) Bruice, T. C.; Brown, A.; Harris, D. O. *Proc. Nat. Acad. Sci., USA* **1971**, *68*, 658-661.

(35) Bruice, T. C. *The Enzymes*; 3rd ed.; Academic Press: New York, 1970; Vol. 2.

(36) Page, M. I.; Jencks, W. P. *Proc. Nat. Acad. Sci., USA* **1971**, *68*, 1678-1683.

(37) Page, M. I. *Biochem. Biophys. Res. Commun.* **1972**, *49*, 940-944.

(38) Bruice, T. C.; Pandit, U. K. *Proc. Nat. Acad. Sci., USA* **1960**, *46*, 402-404.

(39) Bruice, T. C.; Pandit, U. K. *J. Am. Chem. Soc.* **1960**, *82*, 5858-5865.

(40) Bruice, T. C.; Bradbury, W. C. *J. Am. Chem. Soc.* **1965**, *87*, 4846-4850.

(41) Bruice, T. C.; Bradbury, W. C. *J. Am. Chem. Soc.* **1968**, *90*, 3808-3812.

(42) Bruice, T. C.; Lightstone, F. C. *Acc. Chem. Res.* **1999**, *32*, 127-136.

(43) Jencks, W. P. *Adv. Enzmol. Relat. Areas Mol. Biol.* **1975**, *43*, 219-410.

(44) Milstien, S.; Cohen, L. A. *J. Amer. Chem. Soc.* **1972**, *94*, 9158-9165.

(45) Borchardt, R. T.; Cohen, L. A. *J. Amer. Chem. Soc.* **1972**, *94*, 9166-9174.

(46) Hillery, P. S.; Cohen, L. A. *J. Am. Chem. Soc.* **1983**, *105*, 2760-2770.

(47) Karle, J. M.; Karle, I. L. *J. Am. Chem. Soc.* **1972**, *94*, 9182-9189.

(48) Bruice, T. C. *Annu. Rev. Biochem.* **1976**, *45*, 331-373.

(49) Menger, F. M. *Acc. Chem. Res.* **1985**, *18*, 128-134.

(50) Menger, F. M. *Tetrahedron* **1983**, *39*, 1013-1040.

(51) Tirado-Rives, J.; Gandour, R. D.; Fronczek, F. R. *Tetrahedron Lett.* **1982**, *23*, 1639-1642.

(52) Tirado-Rives, J.; Oliver, M. A.; Fronczek, F. R.; Gandour, R. D. *J. Org. Chem.* **1984**, *49*, 1627-1634.

(53) Tirado-Rives, J. Dissertation, Louisiana State University, 1984.

(54) Oliver, M. A. Dissertation, Louisiana State University, 1986.

(55) Evans, K. L. Dissertation, Loisiana State University, 1993.

(56) Prince, P. Dissertation, Louisiana State University, 1993.

(57) Evans, K. L.; Fronczek, F. R.; Gandour, R. D. *Acta Cryst.* **1995**, *C51*, 983-987.

(58) Okuyama, K.; Hasegawa, T.; Ito, M.; Mikami, K. *J. Phys. Chem.* **1984**, *88*, 1711.

(59) Letsinger, R. L.; Nazy, J. R. *J. Am. Chem. Soc.* **1959**, *81*, 3013-3017.

(60) Letsinger, R. L.; Oftedhal, E. N.; Nazy, J. R. *J. Am. Chem. Soc.* **1965**, *87*, 742-749.

(61) Han, G. Y.; Han, P. F.; Perkin, J.; McBay, H. C. *J. Org. Chem.* **1981**, *46*, 4695-4700.

(62) Kemp, D. S.; Li, Z., Q. *Tetrahedron Lett.* **1995**, *36*, 4175-4178.

(63) Vedejs, E.; Steck, P. L. *Angew. Chem. Int. Engl. Ed.* **1999**, *38*, 2788-2791.

(64) Saied, O.; Simard, M.; Wuest, J. D. *Organometallics* **1996**, *15*, 2345-2349.

(65) Ruggli, P. *Justus Liebigs Ann. Chem.* **1913**, *399*, 174-182.

(66) Ruggli, P. *Justus Liebigs Ann. Chem.* **1913**, *392*, 92-100.

(67) Ruggli, P. *Justus Liebigs Ann. Chem.* **1916**, *412*, 1-13.

(68) Youngs, W. J.; Tessier, C. A.; Bradshaw, J. D. *Chem. Rev.* **1999**, *99*, 3153-3180.

(69) Knops, P.; Voegtle, F. *Chem. Ber.* **1991**, *124*, 1223-1227.

(70) Kelly, R. *Acc. Chem. Res.* **2001**, *34*, 514-522.

(71) Shortreed, M. R.; Swallen, S. F.; Shi, Z.-Y.; Tan, W.; Xu, Z.; Devadoss, C.; Moore, J. M.; Kopelman, R. *J. Phys. Chem. B* **1997**, *101*, 6318-6322.

(72) Swallen, S. F.; Zhu, Z.; Moore, J. M.; Kopelman, R. *J. Phys. Chem. B* **2000**, *104*, 3988-3995.

(73) Raker, J.; Glass, T. E. *J. Org. Chem.* **2001**, *66*, 6504-6512.

(74) Tour, J. M. *Acc. Chem. Res.* **2000**, *33*, 791-804.

(75) Crisp, G. T.; Bubner, T. P. *Tetrahedron* **1997**, *53*, 11899-11912.

(76) Yao, Y.; Tour, J. M. *J. Org. Chem.* **1999**, *64*, 1968-1971.

(77) Brogan, A. Virginia Tech, Blacksburg VA. Compound synthesized during course of undergraduate research, 1998. Graphite monochromator Mo K• (• = 0.71073 Å) radiation, structure solved by direct methods and refined by full matrix least squares against F^2 for all data using SHELXL software. Crystal data: a = 17.2670(10) Å, b = 10.118(2) Å, c = 26.851(2) Å, • = 90.00°, • = 96.37°, • = 90.00°. V = 4662.1(10) $Å^3$, Z = 8, T = 293(2) K, R_1 = 0.0489, wR_2 = 0.1237, GOF = 1.100 for 254 parameters and 3055 total reflections. The CIF file is included in Appendix B (Supplemental X-Ray Data).

(78) Gandour, R. Virginia Tech, Blacksburg VA. Titration carried out over spring break, 2000.

(79) Korneev, S. M.; Nikolaev, V. A. *J. Org. Chem. USSR (Engl. Transl.)* **1990**, *26*, 1724-1728.

(80) Halfpenny, P. J.; Johnson, P. J.; Robinson, M. J. T.; Ward, M. G. *Tetrahedron* **1976**, *32*, 1873-1879.

(81) Thomsen, I.; Torssell, B. G. *Acta Chem. Scand.* **1991**, *45*, 539-542.

(82) Steenken, S.; Neta, P. *J. Phys. Chem.* **1979**, *83*, 1134-1137.

(83) Musso, H.; Maassen, D. *Ann. Chem.* **1965**, *689*, 93-108.

(84) Nabulsi, N. A. R.; Gandour, R. D. *J. Org. Chem.* **1991**, *56*, 2260-2262.

(85) Sharefkin, J. G.; Saltzman, H. *Org. Synth., Coll. Vol.* **1973**, *5*, 660-665.

(86) Glaser, R. *J. Org. Chem.* **2001**, *66*, 771-779.

(87) Farina, V.; Krishnamurthy, V.; Scott, W. J. *Org. React.* **1997**, *50*.

(88) Heck, R. F. *Palladium Reagents in Organic Synthesis*; Academic Press: New York, 1985.

(89) Evans, K. L.; Prince, P.; Huang, E. T.; Boss, K. R.; Gandour, R. D. *Tetrahedron Lett.* **1990**, *31*, 6753-6756.

(90) Prince, P.; Evans, K. L.; Rosas-Garcia, V. M.; Gandour, R. D.; Fronczek, F. R. *Tetrahedron Lett.* **1992**, *34*, 6431-6434.

(91) Saa, J. M.; Martorell, G.; Garcia-Raso, A. *J. Org. Chem.* **1992**, *57*, 678-685.

(92) Biswas, M.; Nguyen, P.; Marder, T. B.; Khundkar, L. R. *J. Phys. Chem. A* **1997**, *101*, 1689-1695.

(93) Zimmerman, H. E.; Dodd, J. R. *J. Am. Chem. Soc.* **1970**, *92*, 6507-6515.

(94) Bürgi, H. B.; Dunitz, J. D. *Acc. Chem. Res.* **1983**, *16*, 153-161.

(95) Mohamadi, F.; Richards, N. G. J.; Guida, W. C.; Liskamp, R.; Lipton, M.; Caufield, C.; Chang, G.; Hendrickson, T.; Still, W. C. *J. Comput. Chem.* **1990**, *11*, 440.

(96) Frisch, M. J. T., G. W.; Schlegel, H. B.; Scuseria, G. E.; Robb, M. A.; Cheeseman, J. R.; Zakrzewski, V. G.; Montgomery, J. A., Jr.; Stratmann, R. E.; Burant, J. C.; Dapprich, S.; Millam, J. M.; Daniels, A. D.; Kudin, K. N.; Strain, M. C.; Farkas, O.; Tomasi, J.; Barone, V.; Cossi, M.; Cammi, R.; Mennucci, B.; Pomelli, C.; Adamo, C.; Clifford, S.; Ochterski, J.; Petersson, G. A.; Ayala, P. Y.; Cui, Q.; Morokuma, K.; Malick, D. K.; Rabuck, A. D.; Raghavachari, K.; Foresman, J. B.; Cioslowski, J.; Ortiz, J. V.; Stefanov, B. B.; Liu, G.; Liashenko, A.; Piskorz, P.; Komaromi, I.; Gomperts, R.; Martin, R. L.; Fox, D. J.; Keith, T.; Al-Laham, M. A.; Peng, C. Y.; Nanayakkara, A.; Gonzalez, C.; Challacombe, M.; Gill, P. M. W.; Johnson, B. G.; Chen, W.; Wong, M. W.;

Andres, J. L.; Head-Gordon, M.; Replogle, E. S.; Pople, J. A. *Gaussian 98, revision A.11.1*; Gaussian, Inc.: Pittsburgh, PA, 1998.

(97) Becke, A. D. *J. Chem. Phys.* **1993**, *98*, 5648-5652.

(98) Perdew, J. P.; Wang, Y. *Phys. Rev. B* **1992**, *45*, 13244.

(99) T. H. Dunning, J.; Hay, P. J. In *Modern Theoretical Chemistry*; H. F. Schaefer, I., Ed.; Plenum: New York, 1976, p 1-28.

(100) Hay, P. J.; Wadt, W. R. *J. Chem. Phys.* **1985**, *82*, 270.

(101) Hay, P. J.; Wadt, W. R. *J. Chem. Phys.* **1985**, *82*, 299.

(102) Wadt, W. R.; Hay, P. J. *J. Chem. Phys.* **1985**, *82*, 284.

(103) Franzén, R. *Can. J. Chem.* **2000**, *78*, 957.

Appendix A (Supplemental NMR Data)

^{1}H NMR for (2-Azidoethoxy-4,6-di-*tert*-butyl-2-iodo-phenoxy)-2-aziodethane (**2.3**)

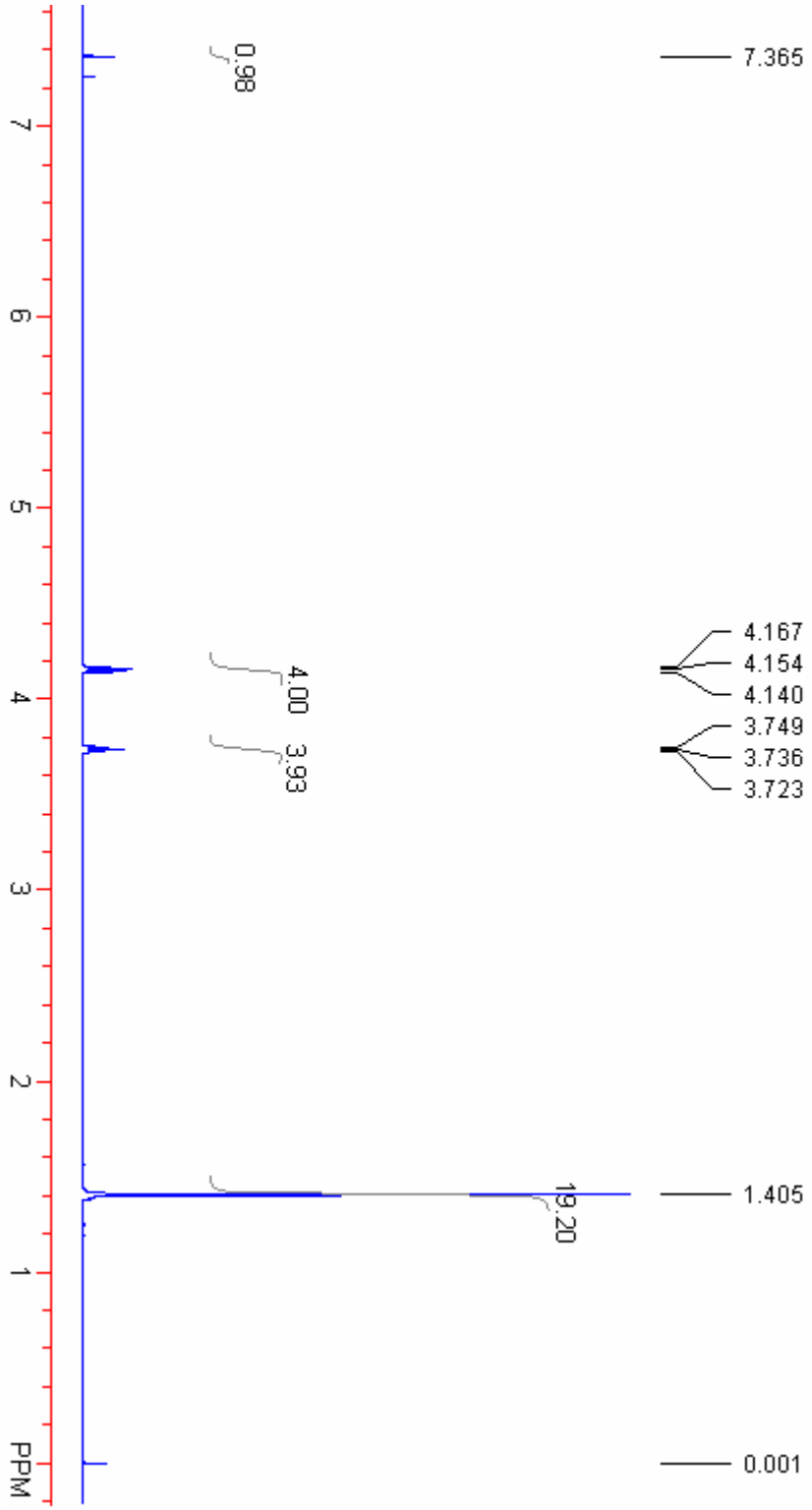

^{13}C NMR for (2-Azidoethoxy-4,6-di-*tert*-butyl-2-iodo-phenoxy)-2-aziodethane (**2.3**)

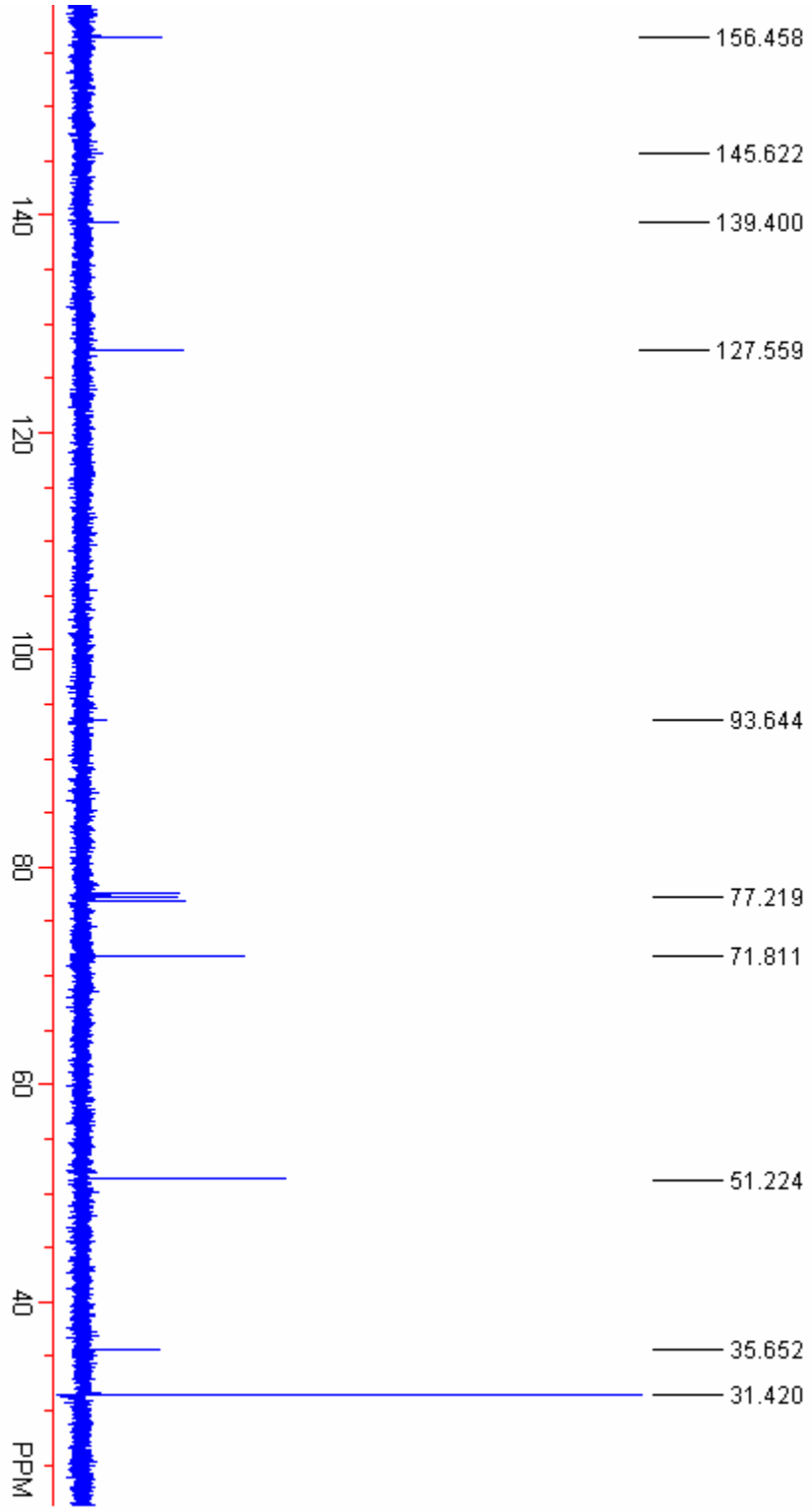

^{1}H NMR for (4,6-Di-*tert*-butyl-2-iodo-1,3-phenylenedioxy)diacetic acid diethyl ester (**2.1**)

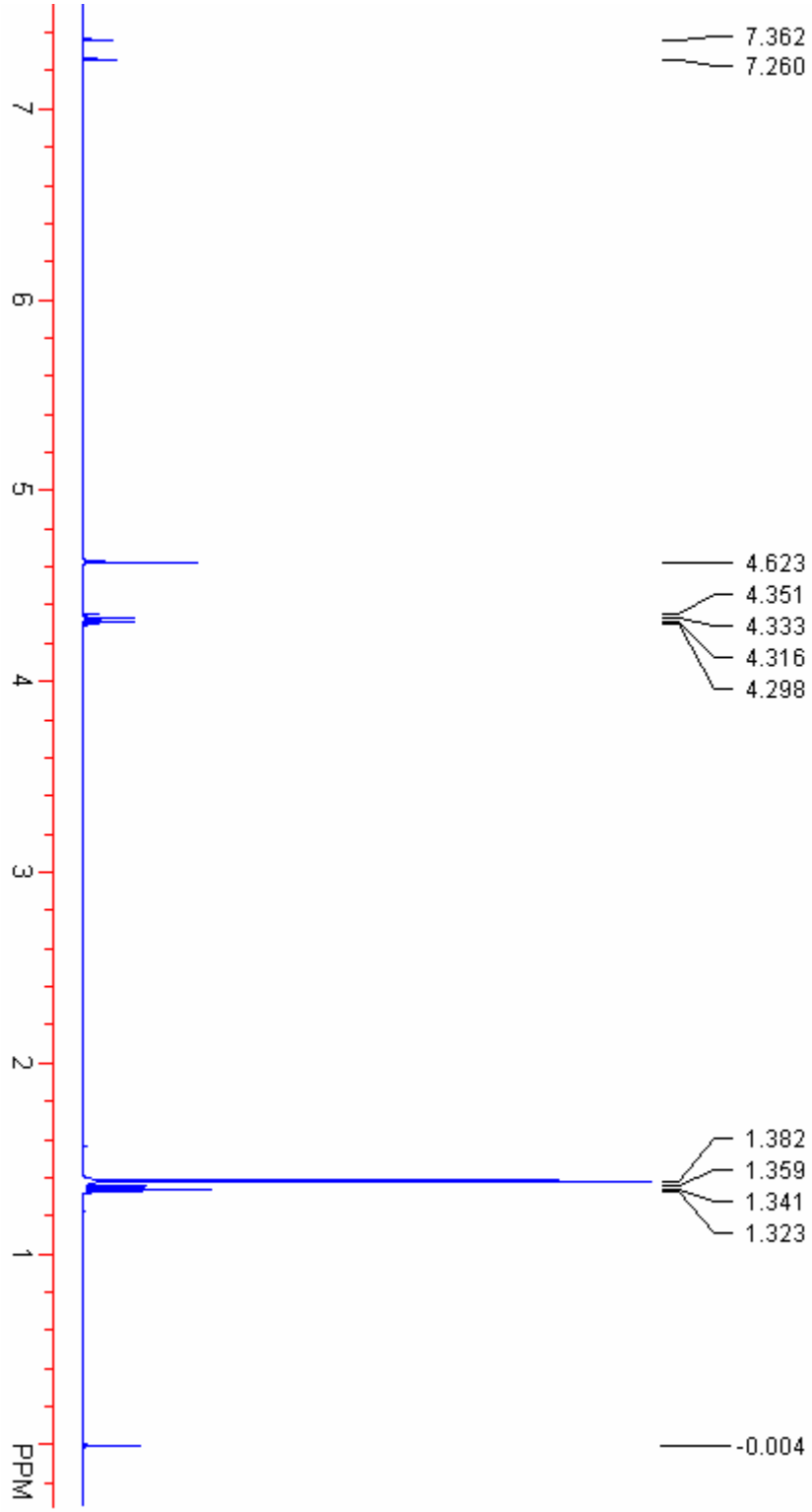

^{13C} NMR for (4,6-Di-*tert*-butyl-2-iodo-1,3-phenylenedioxy)diacetic acid diethyl ester (**2.1**)

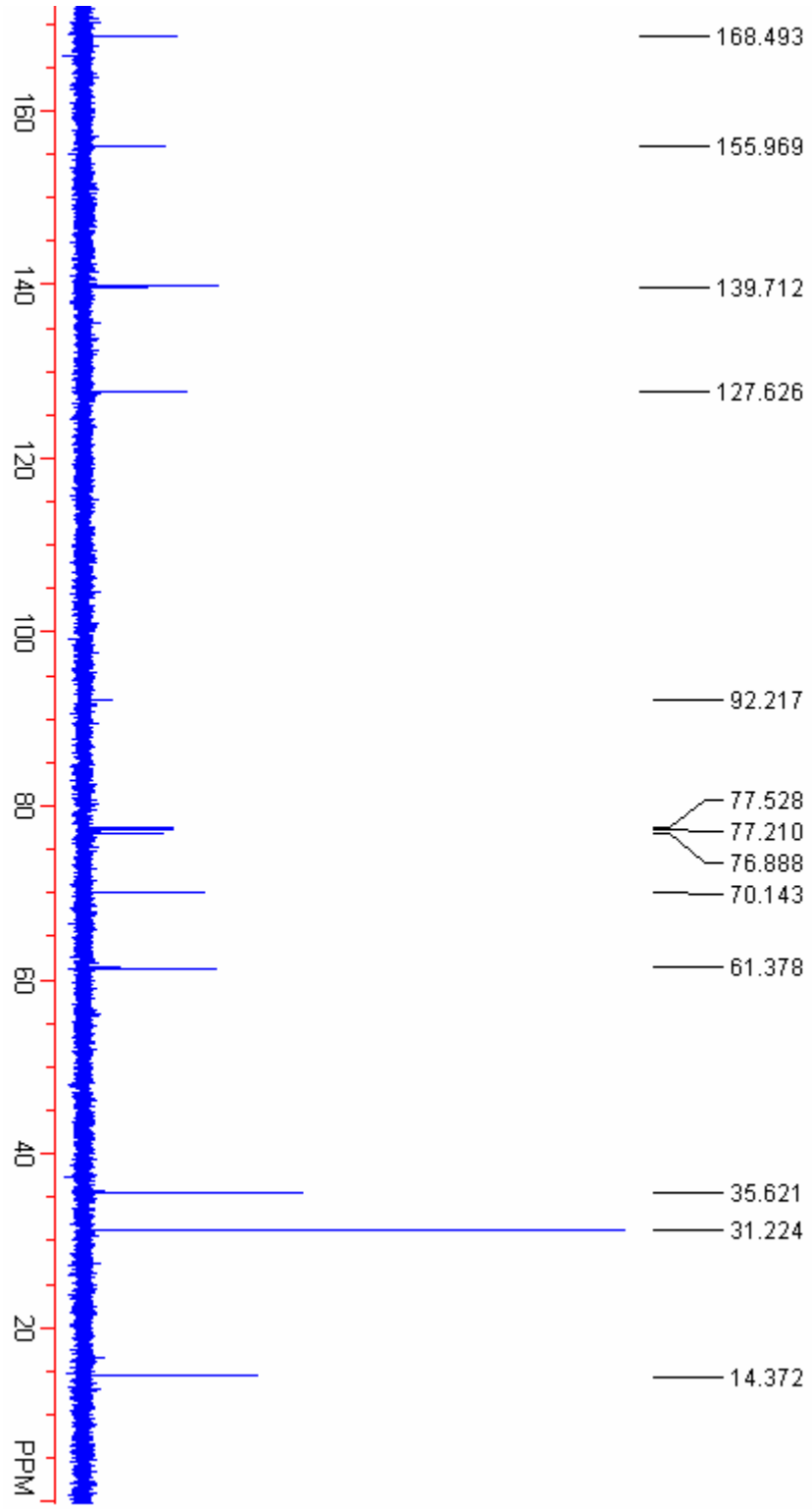

^{1}H NMR for (3-Cyanomethoxy-4,6-di-*tert*-butyl-2-iodo-phenoxy)-acetonitrile (**2.2**)

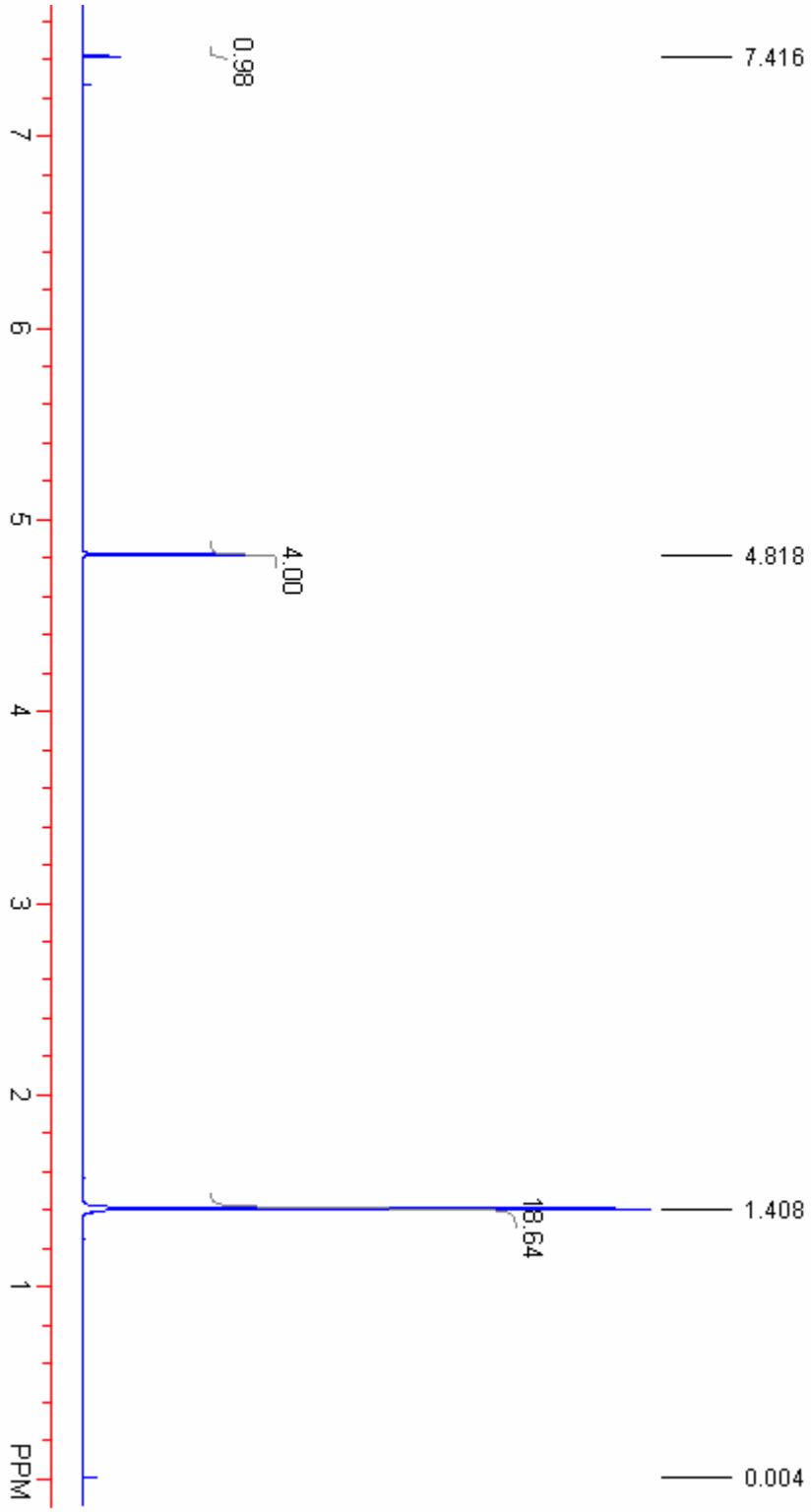

^{13}C NMR for (3-Cyanomethoxy-4,6-di-*tert*-butyl-2-iodo-phenoxy)-acetonitrile (**2.2**)

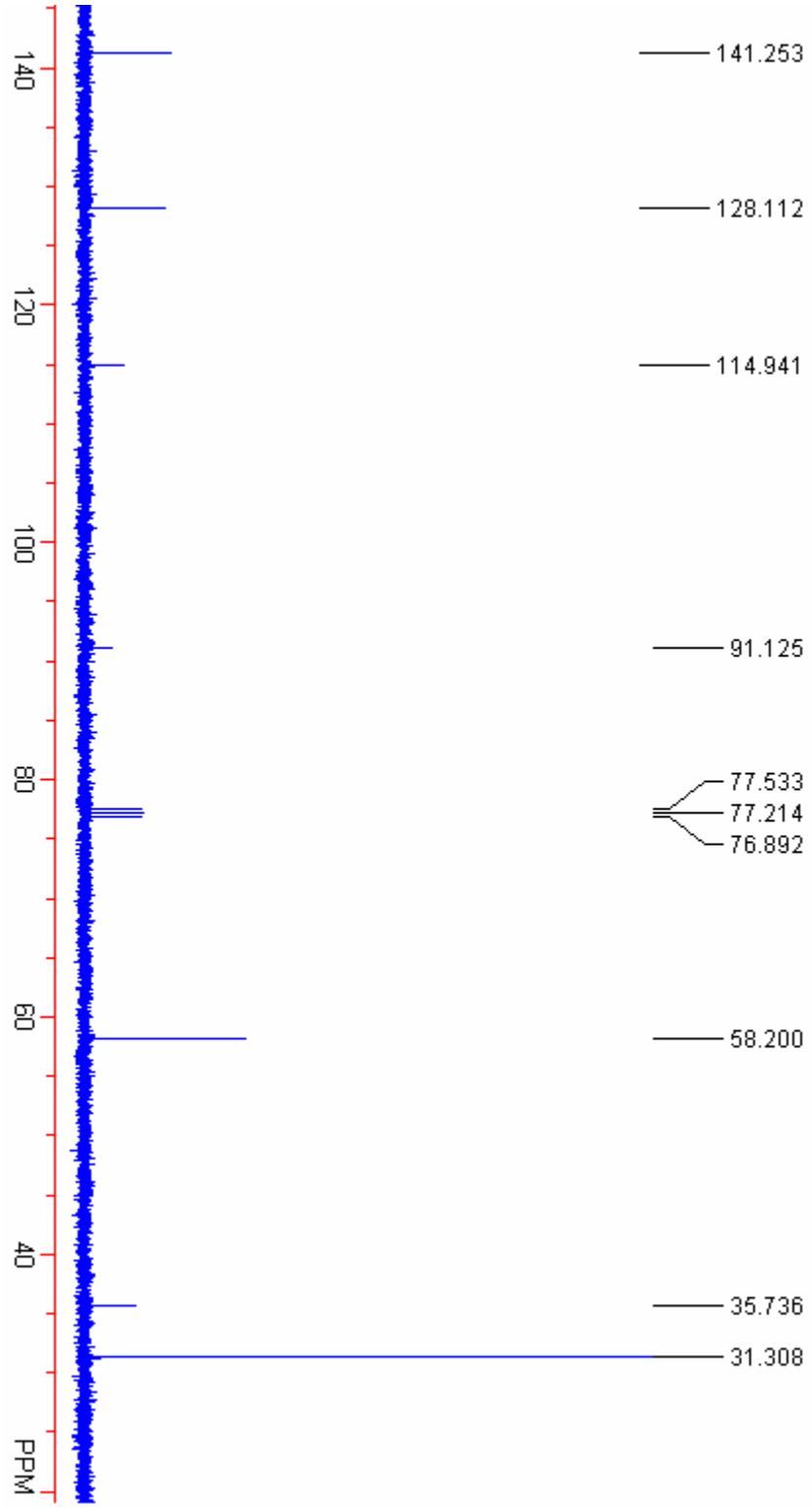

^{1}H NMR for 1,3-Di-(ethoxycarbonylmethoxy-4,6-di-*tert*-butyl-2-benzethyne) (**3.2**)

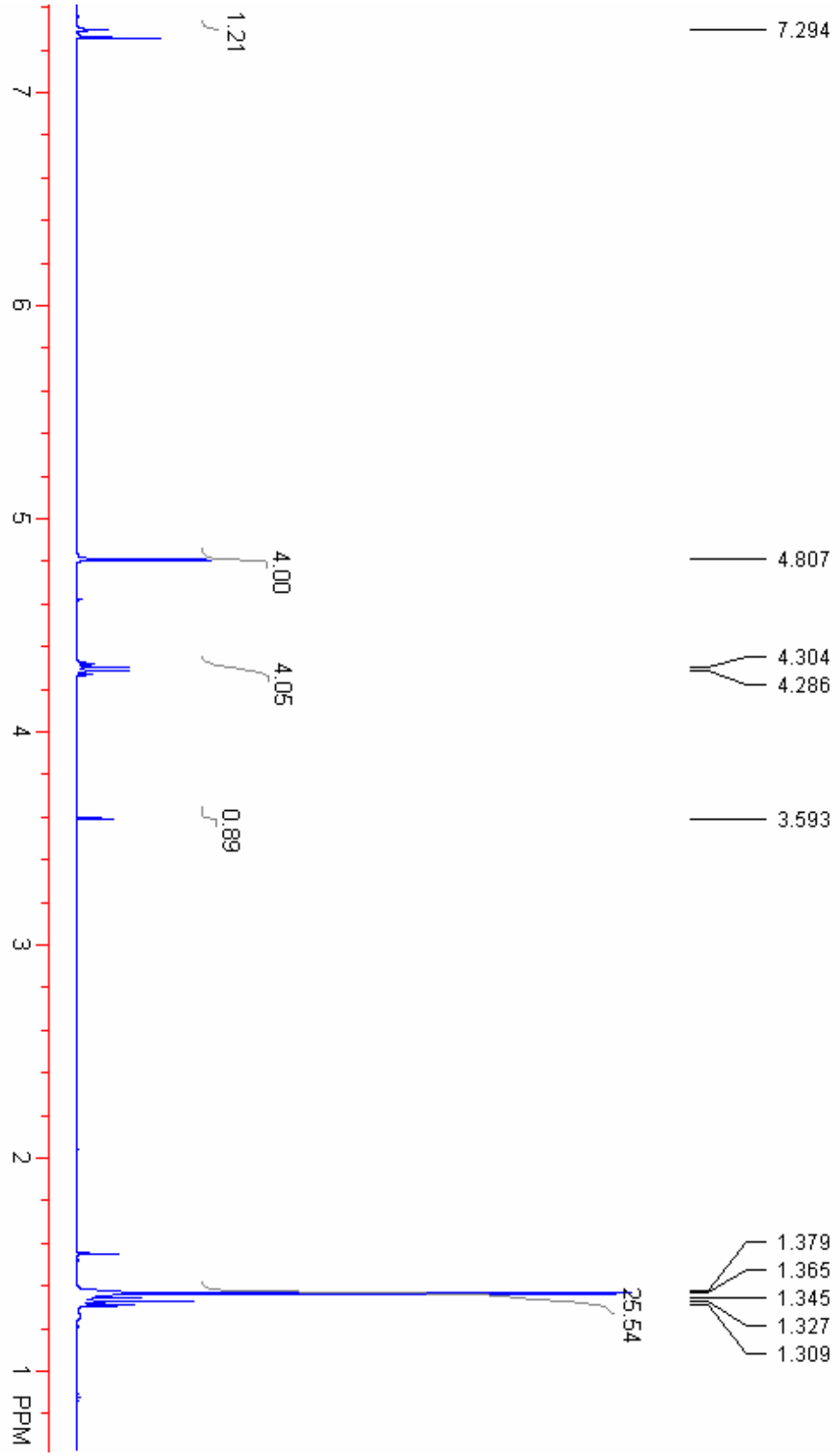

^{13}C NMR for 1,3-Di-(ethoxycarbonylmethoxy-4,6-di-*tert*-butyl-2-benzethyne) (**3.2**)

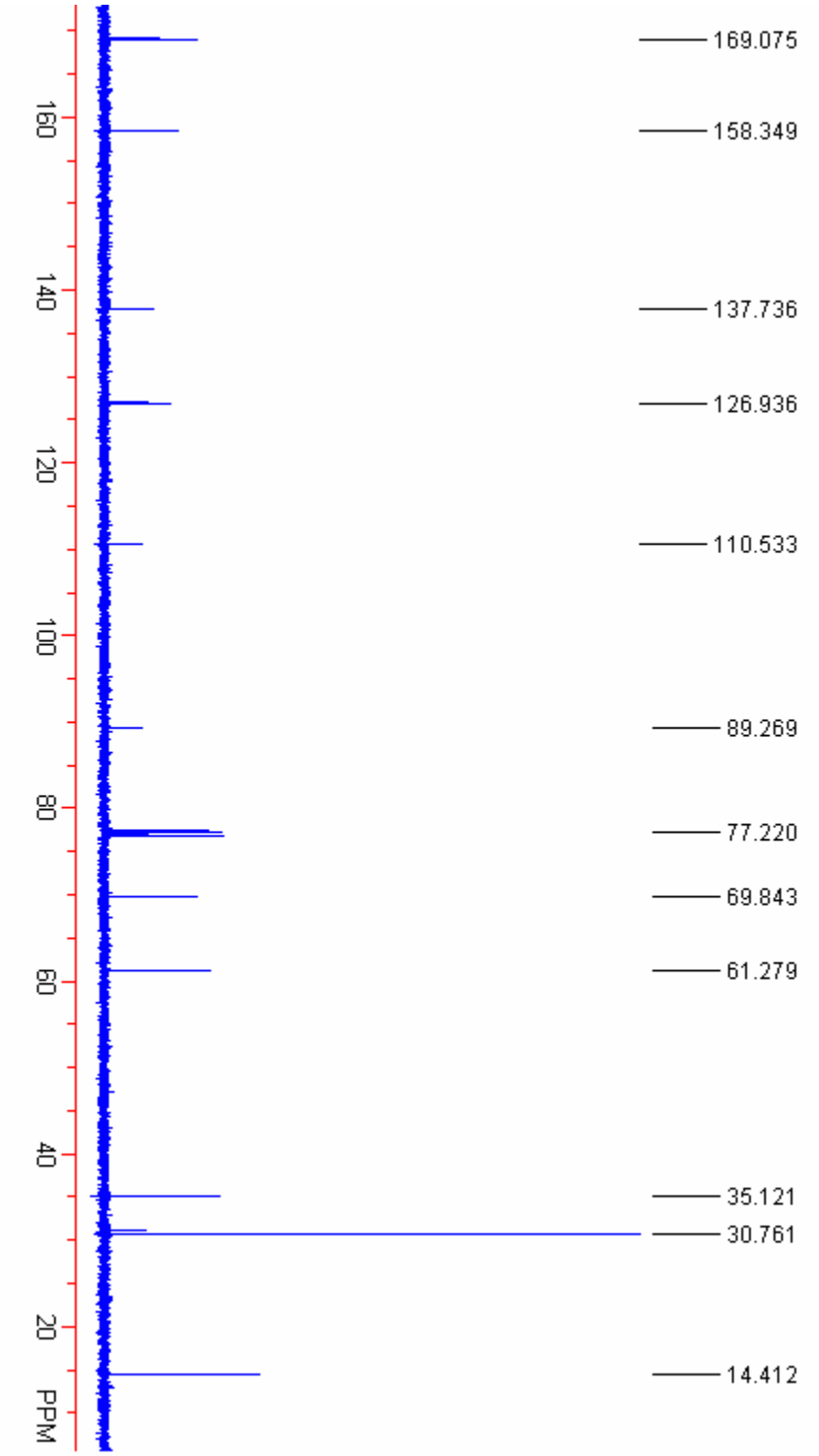

^{1}H NMR for 1,3-Di-(oxoacetonitrile)-4,6-di-*tert*-butyl-2-benzethyne (**3.4**)

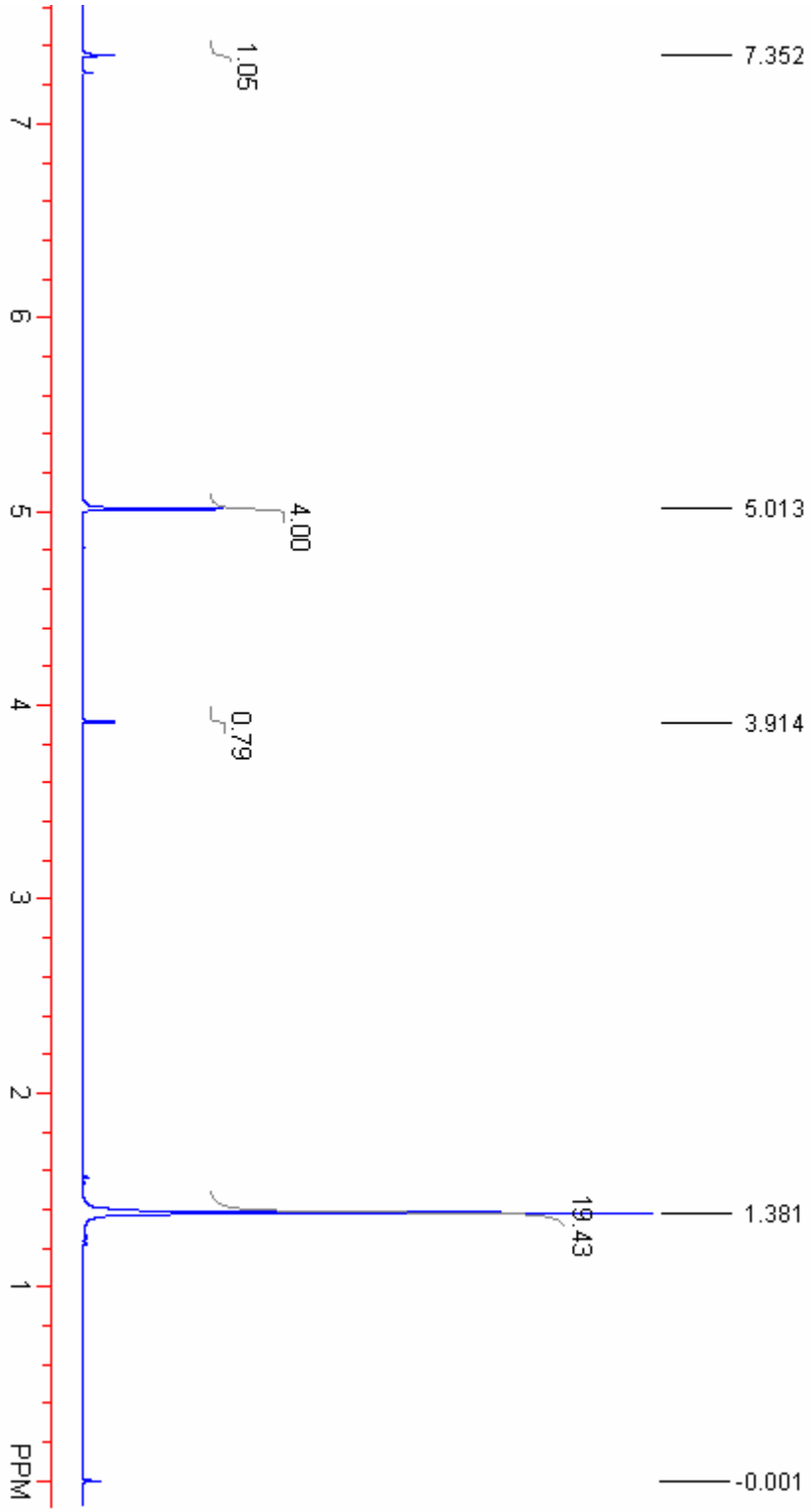

^{131}C NMR for 1,3-Di-(oxoacetonitrile)-4,6-di-*tert*-butyl-2-benzethyne (**3.4**)

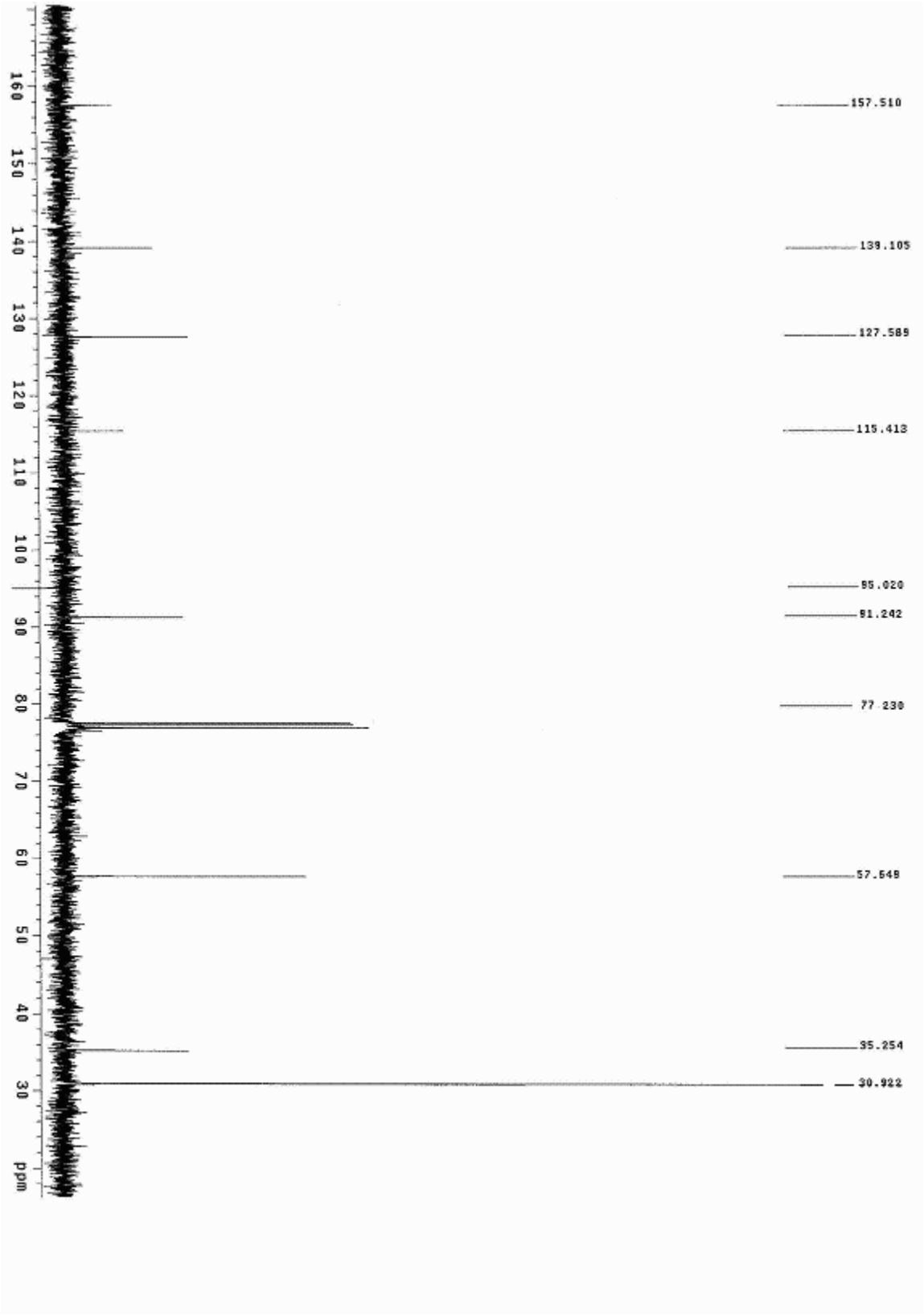

^{1}H NMR for Tetra-Ester (Green) (**3.6a**)

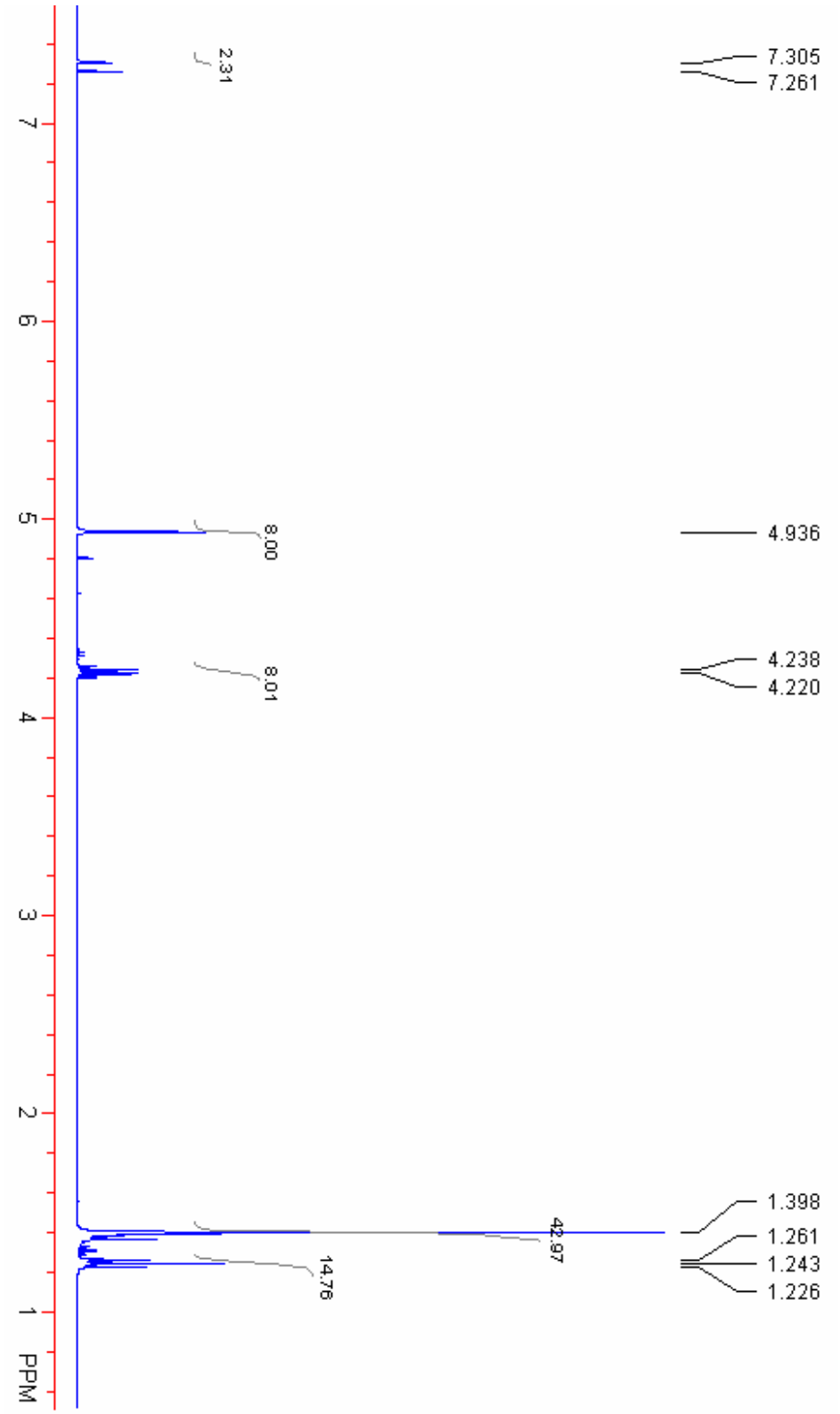

^{13}C NMR for Tetra-Ester (Green) (**3.6a**)

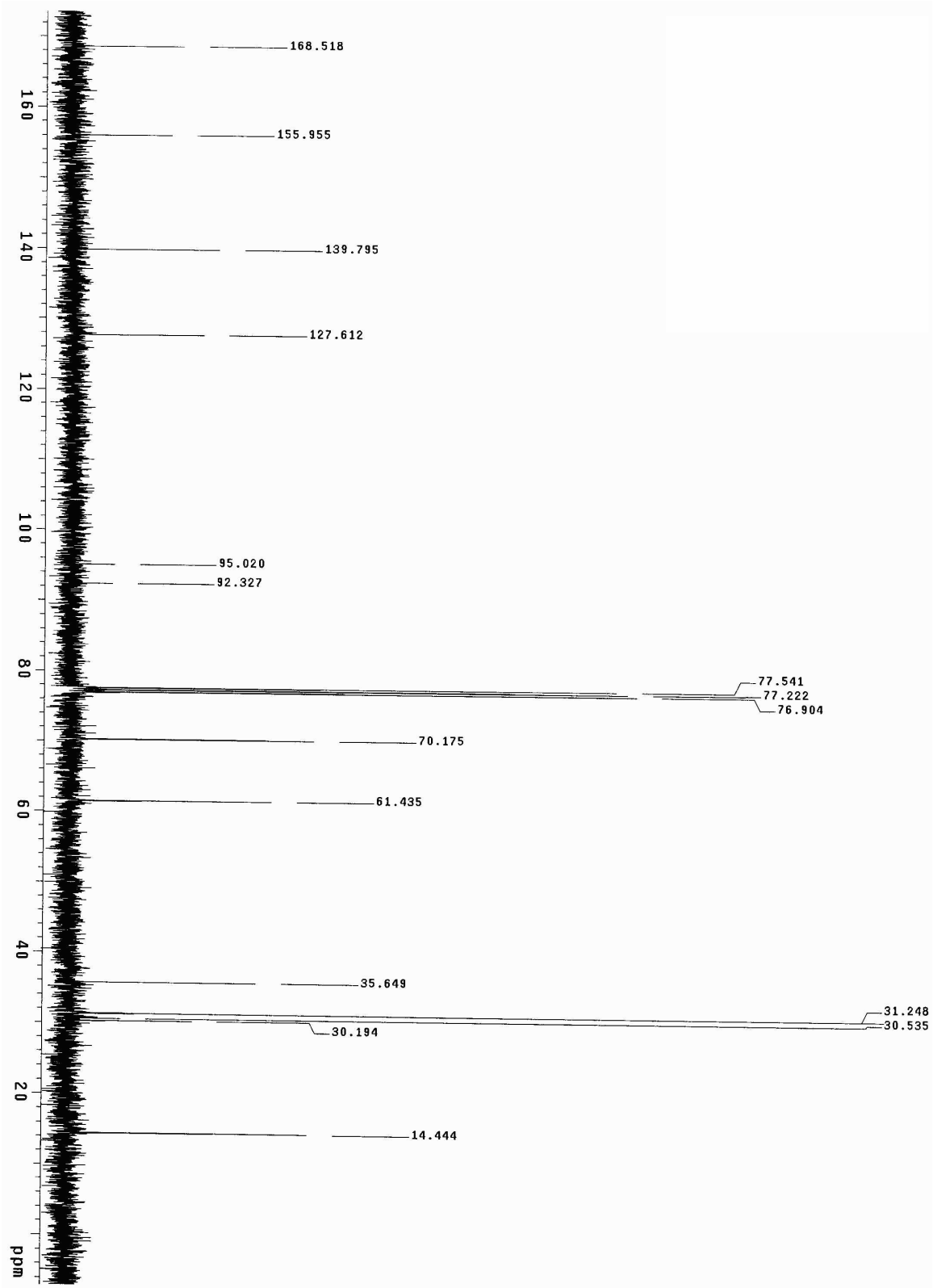

^{1}H NMR for Tetra-Ester (Blue) (**3.6b**)

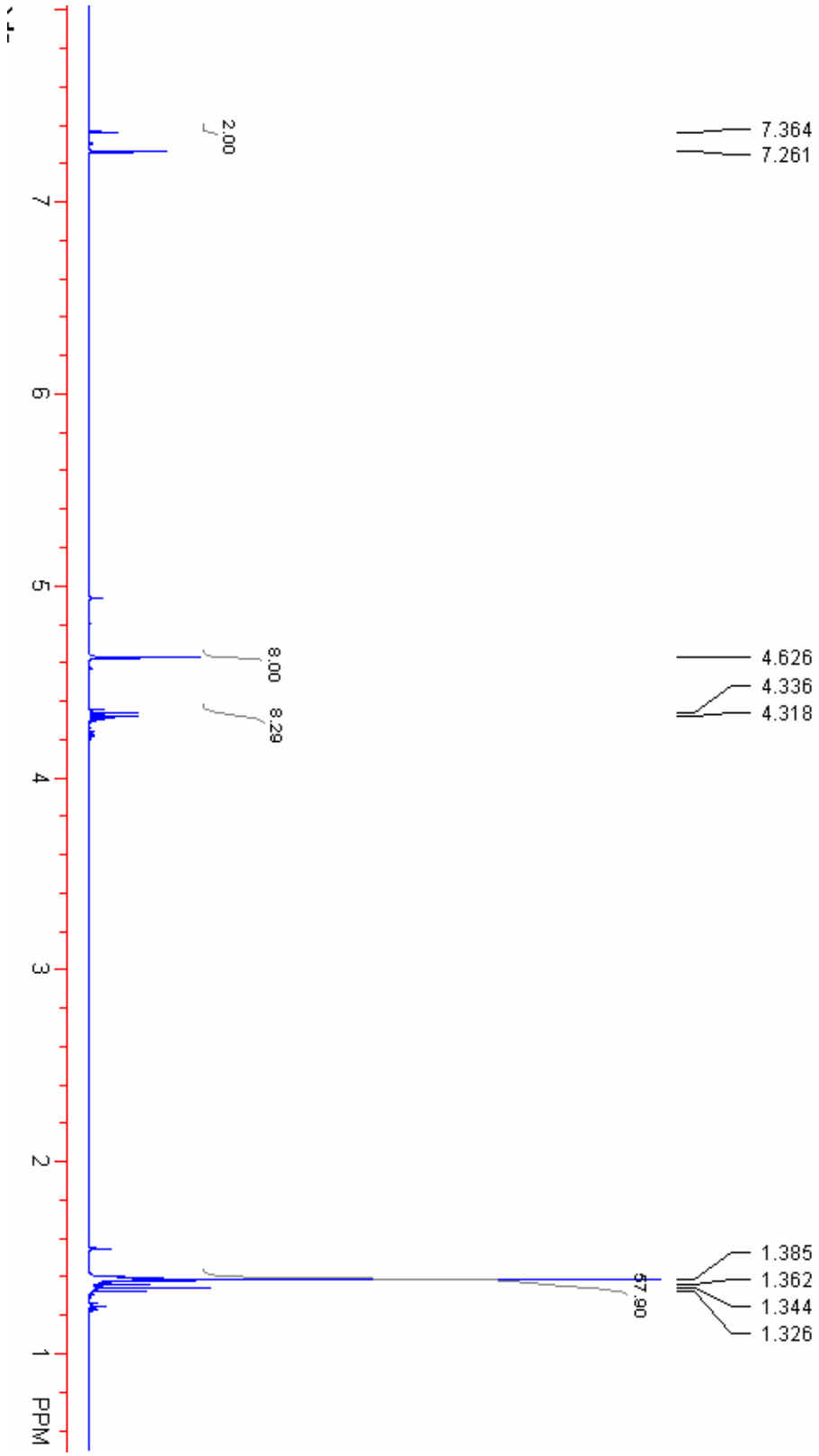

^{13}C NMR for Tetra-Ester (Blue) (**3.6b**)

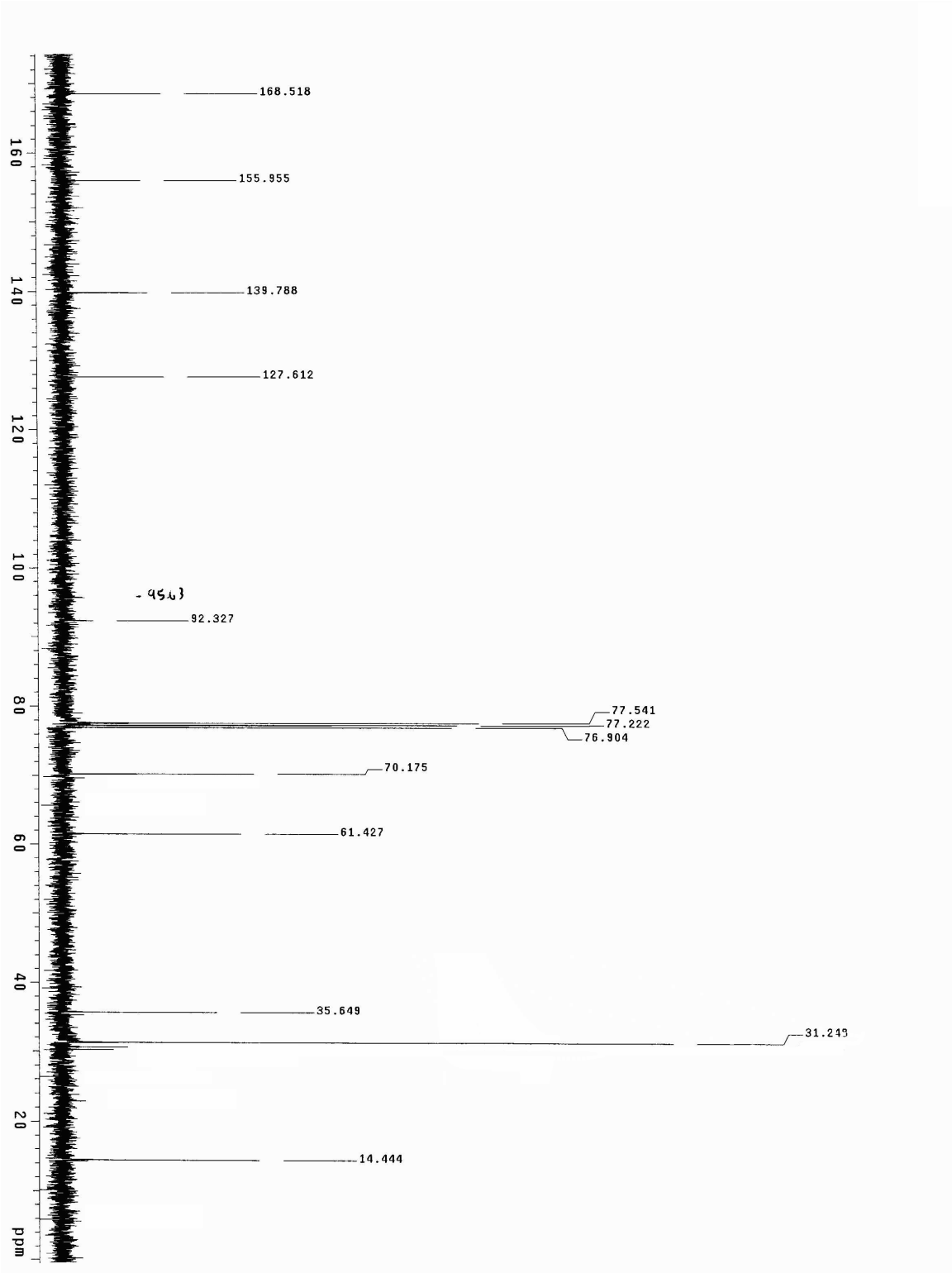

Appendix B (Supplemental X-Ray Data)

Crystallographic data file (**CIF**) for (4,6-di-*tert*-butyl-*m*-phenylenedioxy)diacetic acid diethyl ester:

```
data_diester

_audit_creation_method           SHELXL
_chemical_name_systematic
;
 ?
;
_chemical_name_common            ?
_chemical_formula_moiety         ?
_chemical_formula_structural     ?
_chemical_formula_analytical     ?
_chemical_formula_sum            'C22 H34 O6'
_chemical_formula_weight         394.49
_chemical_melting_point          ?
_chemical_compound_source        ?

loop_
 _atom_type_symbol
 _atom_type_description
 _atom_type_scat_dispersion_real
 _atom_type_scat_dispersion_imag
 _atom_type_scat_source
 'C'  'C'   0.0033   0.0016
 'International Tables Vol C Tables 4.2.6.8 and 6.1.1.4'
 'H'  'H'   0.0000   0.0000
 'International Tables Vol C Tables 4.2.6.8 and 6.1.1.4'
 'O'  'O'   0.0106   0.0060
 'International Tables Vol C Tables 4.2.6.8 and 6.1.1.4'

_symmetry_cell_setting           ?
_symmetry_space_group_name_H-M    ?

loop_
 _symmetry_equiv_pos_as_xyz
 'x, y, z'
 '-x, y, -z+1/2'
 'x+1/2, y+1/2, z'
 '-x+1/2, y+1/2, -z+1/2'
 '-x, -y, -z'
```

```
 'x, -y, z-1/2'
 '-x+1/2, -y+1/2, -z'
 'x+1/2, -y+1/2, z-1/2'

_cell_length_a                    17.2670(10)
_cell_length_b                    10.118(2)
_cell_length_c                    26.851(2)
_cell_angle_alpha                 90.00
_cell_angle_beta                  96.37
_cell_angle_gamma                 90.00
_cell_volume                      4662.1(10)
_cell_formula_units_Z             8
_cell_measurement_temperature     293(2)
_cell_measurement_reflns_used     ?
_cell_measurement_theta_min       ?
_cell_measurement_theta_max       ?

_exptl_crystal_description        ?
_exptl_crystal_colour             ?
_exptl_crystal_size_max           ?
_exptl_crystal_size_mid           ?
_exptl_crystal_size_min           ?
_exptl_crystal_density_meas       ?
_exptl_crystal_density_diffrn     1.124
_exptl_crystal_density_method     ?
_exptl_crystal_F_000              1712
_exptl_absorpt_coefficient_mu     0.081
_exptl_absorpt_correction_type    ?
_exptl_absorpt_correction_T_min   ?
_exptl_absorpt_correction_T_max   ?

_exptl_special_details
;
 ?
;

_diffrn_ambient_temperature       293(2)
_diffrn_radiation_wavelength      0.71073
_diffrn_radiation_type            MoK\a
_diffrn_radiation_source          'fine-focus sealed tube'
_diffrn_radiation_monochromator   graphite
_diffrn_measurement_device        ?
_diffrn_measurement_method        ?
_diffrn_standards_number          ?
_diffrn_standards_interval_count  ?
_diffrn_standards_interval_time   ?
```

```
_diffrn_standards_decay_%          ?
_diffrn_reflns_number              3885
_diffrn_reflns_av_R_equivalents    0.1283
_diffrn_reflns_av_sigmaI/netI      0.0486
_diffrn_reflns_limit_h_min         -1
_diffrn_reflns_limit_h_max         18
_diffrn_reflns_limit_k_min         -1
_diffrn_reflns_limit_k_max         10
_diffrn_reflns_limit_l_min         -28
_diffrn_reflns_limit_l_max         28
_diffrn_reflns_theta_min           2.34
_diffrn_reflns_theta_max           22.55
_reflns_number_total               3055
_reflns_number_observed            2205
_reflns_observed_criterion         >2sigma(I)

_computing_data_collection         ?
_computing_cell_refinement         ?
_computing_data_reduction          ?
_computing_structure_solution      'SHELXS-86 (Sheldrick, 1990)'
_computing_structure_refinement    'SHELXL-93 (Sheldrick, 1993)'
_computing_molecular_graphics      ?
_computing_publication_material    ?

_refine_special_details
;
 Refinement on F^2^ for ALL reflections except for 255 with very negative F^2^
 or flagged by the user for potential systematic errors.  Weighted R-factors
 wR and all goodnesses of fit S are based on F^2^, conventional R-factors R
 are based on F, with F set to zero for negative F^2^. The observed criterion
 of F^2^ > 2sigma(F^2^) is used only for calculating _R_factor_obs etc. and is
 not relevant to the choice of reflections for refinement.  R-factors based
 on F^2^ are statistically about twice as large as those based on F, and R-
 factors based on ALL data will be even larger.
;

_refine_ls_structure_factor_coef  Fsqd
_refine_ls_matrix_type            full
_refine_ls_weighting_scheme
 'calc w=1/[\s^2^(Fo^2^)+(0.0621P)^2^+2.9109P] where P=(Fo^2^+2Fc^2^)/3'
_atom_sites_solution_primary      direct
_atom_sites_solution_secondary    difmap
_atom_sites_solution_hydrogens    geom
_refine_ls_hydrogen_treatment     ?
_refine_ls_extinction_method      SHELXL
_refine_ls_extinction_coef        0.0054(5)
```

```
_refine_ls_extinction_expression
 'Fc^*^=kFc[1+0.001xFc^2^\l^3^/sin(2\q)]^-1/4^'
_refine_ls_number_reflns          2800
_refine_ls_number_parameters      254
_refine_ls_number_restraints      0
_refine_ls_R_factor_all           0.0734
_refine_ls_R_factor_obs           0.0489
_refine_ls_wR_factor_all          0.1434
_refine_ls_wR_factor_obs          0.1237
_refine_ls_goodness_of_fit_all    1.032
_refine_ls_goodness_of_fit_obs    1.100
_refine_ls_restrained_S_all       1.067
_refine_ls_restrained_S_obs       1.100
_refine_ls_shift/esd_max          0.000
_refine_ls_shift/esd_mean         0.000

loop_
 _atom_site_label
 _atom_site_type_symbol
 _atom_site_fract_x
 _atom_site_fract_y
 _atom_site_fract_z
 _atom_site_U_iso_or_equiv
 _atom_site_thermal_displace_type
 _atom_site_occupancy
 _atom_site_calc_flag
 _atom_site_refinement_flags
 _atom_site_disorder_group
C1 C 0.84220(15) 0.4991(2) 0.40071(9) 0.0558(6) Uani 1 d . .
C2 C 0.83807(15) 0.4109(2) 0.43959(9) 0.0566(7) Uani 1 d . .
H2A H 0.83062(15) 0.4426(2) 0.47123(9) 0.068 Uiso 1 calc R .
C3 C 0.84481(14) 0.2765(2) 0.43225(9) 0.0512(6) Uani 1 d . .
C4 C 0.85524(14) 0.2251(2) 0.38546(9) 0.0519(6) Uani 1 d . .
C5 C 0.85924(15) 0.3186(2) 0.34788(9) 0.0579(7) Uani 1 d . .
H5A H 0.86612(15) 0.2867(2) 0.31618(9) 0.069 Uiso 1 calc R .
C6 C 0.85398(15) 0.4547(2) 0.35302(9) 0.0564(7) Uani 1 d . .
O1 O 0.83397(12) 0.6337(2) 0.40717(7) 0.0746(6) Uani 1 d . .
C7 C 0.8222(2) 0.6791(3) 0.45560(10) 0.0673(8) Uani 1 d . .
H7A H 0.7808(2) 0.6281(3) 0.46800(10) 0.081 Uiso 1 calc R .
H7B H 0.8058(2) 0.7708(3) 0.45352(10) 0.081 Uiso 1 calc R .
C8 C 0.8944(2) 0.6677(3) 0.49167(11) 0.0694(8) Uani 1 d . .
O2 O 0.95894(14) 0.6702(3) 0.48018(9) 0.1100(8) Uani 1 d . .
O3 O 0.87659(12) 0.6564(2) 0.53816(7) 0.0829(6) Uani 1 d . .
C9 C 0.9420(2) 0.6533(5) 0.57782(14) 0.128(2) Uani 1 d . .
H9A H 0.9702(2) 0.5708(5) 0.57624(14) 0.154 Uiso 1 calc R .
H9B H 0.9775(2) 0.7254(5) 0.57321(14) 0.154 Uiso 1 calc R .
```

C10 C 0.9132(3) 0.6652(5) 0.62552(14) 0.141(2) Uani 1 d . .
H10A H 0.9561(3) 0.6631(5) 0.65152(14) 0.211 Uiso 1 calc R .
H10B H 0.8785(3) 0.5931(5) 0.63006(14) 0.211 Uiso 1 calc R .
H10C H 0.8857(3) 0.7473(5) 0.62703(14) 0.211 Uiso 1 calc R .
O4 O 0.83875(11) 0.1888(2) 0.47092(6) 0.0627(5) Uani 1 d . .
C11 C 0.8567(2) 0.2348(3) 0.52041(8) 0.0597(7) Uani 1 d . .
H11A H 0.8171(2) 0.2966(3) 0.52867(8) 0.072 Uiso 1 calc R .
H11B H 0.9065(2) 0.2801(3) 0.52370(8) 0.072 Uiso 1 calc R .
C12 C 0.85999(15) 0.1189(3) 0.55510(10) 0.0624(7) Uani 1 d . .
O5 O 0.85242(13) 0.0056(2) 0.54359(7) 0.0839(6) Uani 1 d . .
O6 O 0.87178(12) 0.1634(2) 0.60196(7) 0.0783(6) Uani 1 d . .
C13 C 0.8729(2) 0.0653(3) 0.64117(11) 0.0920(10) Uani 1 d . .
H13A H 0.9163(2) 0.0052(3) 0.63949(11) 0.110 Uiso 1 calc R .
H13B H 0.8250(2) 0.0145(3) 0.63738(11) 0.110 Uiso 1 calc R .
C14 C 0.8810(3) 0.1348(5) 0.68906(12) 0.142(2) Uani 1 d . .
H14A H 0.8819(3) 0.0719(5) 0.71587(12) 0.213 Uiso 1 calc R .
H14B H 0.8377(3) 0.1938(5) 0.69036(12) 0.213 Uiso 1 calc R .
H14C H 0.9286(3) 0.1845(5) 0.69247(12) 0.213 Uiso 1 calc R .
C15 C 0.8592(2) 0.0761(2) 0.37573(10) 0.0654(7) Uani 1 d . .
C16 C 0.9231(2) 0.0096(3) 0.41106(11) 0.0793(9) Uani 1 d . .
H16A H 0.9240(2) -0.0833(3) 0.40395(11) 0.119 Uiso 1 calc R .
H16B H 0.9129(2) 0.0227(3) 0.44512(11) 0.119 Uiso 1 calc R .
H16C H 0.9727(2) 0.0477(3) 0.40630(11) 0.119 Uiso 1 calc R .
C17 C 0.7803(2) 0.0139(3) 0.38306(13) 0.0947(10) Uani 1 d . .
H17A H 0.7400(2) 0.0555(3) 0.36091(13) 0.142 Uiso 1 calc R .
H17B H 0.7698(2) 0.0262(3) 0.41712(13) 0.142 Uiso 1 calc R .
H17C H 0.7816(2) -0.0789(3) 0.37573(13) 0.142 Uiso 1 calc R .
C18 C 0.8769(2) 0.0478(3) 0.32199(11) 0.1039(13) Uani 1 d . .
H18A H 0.8377(2) 0.0883(3) 0.29873(11) 0.156 Uiso 1 calc R .
H18B H 0.8769(2) -0.0459(3) 0.31646(11) 0.156 Uiso 1 calc R .
H18C H 0.9270(2) 0.0834(3) 0.31717(11) 0.156 Uiso 1 calc R .
C19 C 0.8618(2) 0.5501(3) 0.30902(10) 0.0672(8) Uani 1 d . .
C20 C 0.8734(2) 0.4749(3) 0.26067(11) 0.0987(11) Uani 1 d . .
H20A H 0.9191(2) 0.4205(3) 0.26629(11) 0.148 Uiso 1 calc R .
H20B H 0.8797(2) 0.5370(3) 0.23439(11) 0.148 Uiso 1 calc R .
H20C H 0.8287(2) 0.4204(3) 0.25114(11) 0.148 Uiso 1 calc R .
C21 C 0.7887(2) 0.6350(3) 0.29813(11) 0.0880(10) Uani 1 d . .
H21A H 0.7442(2) 0.5788(3) 0.29040(11) 0.132 Uiso 1 calc R .
H21B H 0.7943(2) 0.6918(3) 0.27012(11) 0.132 Uiso 1 calc R .
H21C H 0.7817(2) 0.6877(3) 0.32702(11) 0.132 Uiso 1 calc R .
C22 C 0.9333(2) 0.6381(3) 0.32141(12) 0.0885(10) Uani 1 d . .
H22A H 0.9788(2) 0.5839(3) 0.32819(12) 0.133 Uiso 1 calc R .
H22B H 0.9266(2) 0.6908(3) 0.35036(12) 0.133 Uiso 1 calc R .
H22C H 0.9393(2) 0.6950(3) 0.29347(12) 0.133 Uiso 1 calc R .

loop_

```
 _atom_site_aniso_label
 _atom_site_aniso_U_11
 _atom_site_aniso_U_22
 _atom_site_aniso_U_33
 _atom_site_aniso_U_23
 _atom_site_aniso_U_13
 _atom_site_aniso_U_12
C1 0.063(2) 0.0462(14) 0.058(2) 0.0015(13) 0.0082(12) 0.0015(12)
C2 0.069(2) 0.053(2) 0.0491(14) -0.0012(12) 0.0153(12) 0.0003(13)
C3 0.0529(15) 0.0481(15) 0.0532(15) 0.0058(12) 0.0091(11) -0.0065(12)
C4 0.0556(15) 0.0494(14) 0.0506(14) 0.0014(12) 0.0052(11) -0.0044(12)
C5 0.063(2) 0.062(2) 0.0497(14) -0.0056(13) 0.0094(12) 0.0007(13)
C6 0.065(2) 0.053(2) 0.0517(15) 0.0026(12) 0.0087(12) -0.0031(13)
O1 0.114(2) 0.0488(11) 0.0637(12) 0.0041(9) 0.0205(11) 0.0083(10)
C7 0.088(2) 0.049(2) 0.067(2) -0.0026(13) 0.017(2) 0.0067(14)
C8 0.072(2) 0.058(2) 0.081(2) -0.0077(15) 0.021(2) -0.0111(15)
O2 0.077(2) 0.138(2) 0.119(2) -0.004(2) 0.0316(14) -0.022(2)
O3 0.0751(13) 0.104(2) 0.0695(13) -0.0074(11) 0.0090(10) -0.0150(12)
C9 0.089(3) 0.197(5) 0.092(3) -0.027(3) -0.018(2) -0.022(3)
C10 0.123(3) 0.215(5) 0.081(3) -0.004(3) -0.002(2) -0.021(3)
O4 0.0833(13) 0.0537(11) 0.0518(10) 0.0046(8) 0.0106(9) -0.0060(9)
C11 0.064(2) 0.062(2) 0.054(2) 0.0055(13) 0.0102(12) -0.0067(13)
C12 0.057(2) 0.072(2) 0.061(2) 0.008(2) 0.0150(13) -0.0026(15)
O5 0.115(2) 0.0623(13) 0.0768(13) 0.0102(11) 0.0196(12) -0.0029(12)
O6 0.1004(15) 0.0827(14) 0.0530(12) 0.0133(10) 0.0140(10) -0.0081(11)
C13 0.104(3) 0.109(3) 0.065(2) 0.027(2) 0.021(2) -0.002(2)
C14 0.204(5) 0.160(4) 0.060(2) 0.006(2) 0.009(2) -0.070(4)
C15 0.084(2) 0.049(2) 0.062(2) -0.0050(13) 0.0069(14) -0.0031(14)
C16 0.095(2) 0.059(2) 0.085(2) -0.002(2) 0.011(2) 0.014(2)
C17 0.099(3) 0.062(2) 0.119(3) -0.001(2) -0.006(2) -0.018(2)
C18 0.178(4) 0.062(2) 0.073(2) -0.015(2) 0.019(2) 0.009(2)
C19 0.086(2) 0.061(2) 0.056(2) 0.0072(13) 0.0165(14) -0.006(2)
C20 0.156(3) 0.083(2) 0.062(2) 0.010(2) 0.033(2) -0.010(2)
C21 0.105(3) 0.085(2) 0.074(2) 0.025(2) 0.007(2) 0.001(2)
C22 0.100(2) 0.075(2) 0.093(2) 0.012(2) 0.026(2) -0.017(2)

_geom_special_details
;
 All esds (except the esd in the dihedral angle between two l.s. planes)
 are estimated using the full covariance matrix.  The cell esds are taken
 into account individually in the estimation of esds in distances, angles
 and torsion angles; correlations between esds in cell parameters are only
 used when they are defined by crystal symmetry.  An approximate (isotropic)
 treatment of cell esds is used for estimating esds involving l.s. planes.
;
```

```
loop_
 _geom_bond_atom_site_label_1
 _geom_bond_atom_site_label_2
 _geom_bond_distance
 _geom_bond_site_symmetry_2
 _geom_bond_publ_flag
C1 C2 1.381(3) . ?
C1 O1 1.382(3) . ?
C1 C6 1.393(3) . ?
C2 C3 1.381(3) . ?
C3 O4 1.379(3) . ?
C3 C4 1.390(3) . ?
C4 C5 1.390(3) . ?
C4 C15 1.533(3) . ?
C5 C6 1.389(3) . ?
C6 C19 1.543(3) . ?
O1 C7 1.415(3) . ?
C7 C8 1.495(4) . ?
C8 O2 1.190(3) . ?
C8 O3 1.323(3) . ?
O3 C9 1.464(4) . ?
C9 C10 1.429(5) . ?
O4 C11 1.410(3) . ?
C11 C12 1.495(4) . ?
C12 O5 1.190(3) . ?
C12 O6 1.331(3) . ?
O6 C13 1.446(3) . ?
C13 C14 1.459(4) . ?
C15 C16 1.529(4) . ?
C15 C17 1.534(4) . ?
C15 C18 1.534(4) . ?
C19 C21 1.528(4) . ?
C19 C22 1.529(4) . ?
C19 C20 1.537(4) . ?

loop_
 _geom_angle_atom_site_label_1
 _geom_angle_atom_site_label_2
 _geom_angle_atom_site_label_3
 _geom_angle
 _geom_angle_site_symmetry_1
 _geom_angle_site_symmetry_3
 _geom_angle_publ_flag
C2 C1 O1 121.8(2) . . ?
C2 C1 C6 120.8(2) . . ?
O1 C1 C6 117.4(2) . . ?
```

```
C3 C2 C1 121.1(2) . . ?
O4 C3 C2 120.8(2) . . ?
O4 C3 C4 117.9(2) . . ?
C2 C3 C4 121.3(2) . . ?
C3 C4 C5 115.0(2) . . ?
C3 C4 C15 122.4(2) . . ?
C5 C4 C15 122.6(2) . . ?
C6 C5 C4 126.4(2) . . ?
C5 C6 C1 115.4(2) . . ?
C5 C6 C19 122.2(2) . . ?
C1 C6 C19 122.4(2) . . ?
C1 O1 C7 117.6(2) . . ?
O1 C7 C8 112.1(2) . . ?
O2 C8 O3 124.7(3) . . ?
O2 C8 C7 124.6(3) . . ?
O3 C8 C7 110.7(2) . . ?
C8 O3 C9 116.6(3) . . ?
C10 C9 O3 109.5(3) . . ?
C3 O4 C11 118.0(2) . . ?
O4 C11 C12 108.5(2) . . ?
O5 C12 O6 124.9(3) . . ?
O5 C12 C11 126.7(3) . . ?
O6 C12 C11 108.3(3) . . ?
C12 O6 C13 116.4(2) . . ?
O6 C13 C14 107.7(3) . . ?
C16 C15 C4 111.7(2) . . ?
C16 C15 C17 109.3(2) . . ?
C4 C15 C17 108.9(2) . . ?
C16 C15 C18 107.3(2) . . ?
C4 C15 C18 111.2(2) . . ?
C17 C15 C18 108.4(3) . . ?
C21 C19 C22 110.1(2) . . ?
C21 C19 C20 107.4(3) . . ?
C22 C19 C20 107.1(2) . . ?
C21 C19 C6 111.0(2) . . ?
C22 C19 C6 109.6(2) . . ?
C20 C19 C6 111.6(2) . . ?

_refine_diff_density_max    0.212
_refine_diff_density_min   -0.122
_refine_diff_density_rms    0.036
# END OF CIF
```

Crystallographic data file (**CIF**) for (4,6-Di-*tert*-butyl-2-Iodo-1,3-phenylenedioxy)di-*N*-phenylformamide :

```
data_bis-carbamate

_audit_creation_method            SHELXL
_chemical_name_systematic
;
 ?
;
_chemical_name_common             ?
_chemical_compound_source         'Local laboratory'
_chemical_formula_moiety          'C28 H31 I N2 O4'
_chemical_formula_structural      ?
_chemical_formula_analytical      ?
_chemical_formula_sum             'C28 H31 I N2 O4'
_chemical_formula_weight          586.45
_chemical_melting_point           ?

loop_
 _atom_type_symbol
 _atom_type_description
 _atom_type_scat_dispersion_real
 _atom_type_scat_dispersion_imag
 _atom_type_scat_source
 'C'  'C'   0.0033   0.0016
 'International Tables Vol C Tables 4.2.6.8 and 6.1.1.4'
 'H'  'H'   0.0000   0.0000
 'International Tables Vol C Tables 4.2.6.8 and 6.1.1.4'
 'N'  'N'   0.0061   0.0033
 'International Tables Vol C Tables 4.2.6.8 and 6.1.1.4'
 'O'  'O'   0.0106   0.0060
 'International Tables Vol C Tables 4.2.6.8 and 6.1.1.4'
 'I'  'I'  -0.4742   1.8119
 'International Tables Vol C Tables 4.2.6.8 and 6.1.1.4'

_symmetry_cell_setting            Orthorhombic
_symmetry_space_group_name_Hall     '-P 2n 2ab'
_symmetry_space_group_name_H-M    Pbcn

loop_
 _symmetry_equiv_pos_as_xyz
 'x, y, z'
 '-x+1/2, -y+1/2, z+1/2'
 '-x, y, -z+1/2'
```

```
 'x+1/2, -y+1/2, -z'
 '-x, -y, -z'
 'x-1/2, y-1/2, -z-1/2'
 'x, -y, z-1/2'
 '-x-1/2, y-1/2, z'

_cell_length_a                    26.419(5)
_cell_length_b                    9.774(2)
_cell_length_c                    10.195(2)
_cell_angle_alpha                 90
_cell_angle_beta                  90
_cell_angle_gamma                 90
_cell_volume                      2632.5(9)
_cell_formula_units_Z             4
_cell_measurement_temperature     100
_cell_measurement_reflns_used     25
_cell_measurement_theta_min       11.8
_cell_measurement_theta_max       21.0

_exptl_crystal_description        fragment
_exptl_crystal_colour             colorless
_exptl_crystal_size_max           0.50
_exptl_crystal_size_mid           0.38
_exptl_crystal_size_min           0.25
_exptl_crystal_density_meas       'not measured'
_exptl_crystal_density_diffrn     1.480
_exptl_crystal_density_method     ?
_exptl_crystal_F_000              1192
_exptl_absorpt_coefficient_mu     1.252
_exptl_absorpt_correction_type    'psi-scan'
_exptl_absorpt_process_details    '(North et al., 1968)'
_exptl_absorpt_correction_T_min   0.651
_exptl_absorpt_correction_T_max   0.730

_exptl_special_details
;
 ?
;

_diffrn_ambient_temperature       100
_diffrn_radiation_wavelength      0.71073
_diffrn_radiation_type            MoK\a
_diffrn_radiation_source          'fine-focus sealed tube'
_diffrn_radiation_monochromator   graphite
_diffrn_measurement_device        'Enraf-Nonius CAD4'
_diffrn_measurement_method        '\w-2\q scans'
```

```
_diffrn_standards_number          3
_diffrn_standards_interval_count  100
_diffrn_standards_interval_time   ?
_diffrn_standards_decay_%         <2
_diffrn_reflns_number             3824
_diffrn_reflns_av_R_equivalents   0.025
_diffrn_reflns_av_sigmaI/netI     0.0242
_diffrn_reflns_limit_h_min        0
_diffrn_reflns_limit_h_max        37
_diffrn_reflns_limit_k_min        -13
_diffrn_reflns_limit_k_max        0
_diffrn_reflns_limit_l_min        0
_diffrn_reflns_limit_l_max        14
_diffrn_reflns_theta_min          2.99
_diffrn_reflns_theta_max          30.0
_reflns_number_total              3824
_reflns_number_observed           2944
_reflns_observed_criterion        I>2\s(I)

_computing_data_collection        'XPRESS'
_computing_cell_refinement        'XCAD4'
_computing_data_reduction         'Siemens SHELXTL'
_computing_structure_solution     'SHELXS-86 (Sheldrick, 1990)'
_computing_structure_refinement   'SHELXL-93 (Sheldrick, 1993)'
_computing_molecular_graphics     'Siemens SHELXTL'
_computing_publication_material   'Siemens SHELXTL'

_refine_special_details
;
 Refinement on F^2^ for ALL reflections except for 0 with very negative F^2^
 or flagged by the user for potential systematic errors.  Weighted R-factors
 wR and all goodnesses of fit S are based on F^2^, conventional R-factors R
 are based on F, with F set to zero for negative F^2^. The observed criterion
 of F^2^ > 2sigma(F^2^) is used only for calculating _R_factor_obs etc. and is
 not relevant to the choice of reflections for refinement.  R-factors based
 on F^2^ are statistically about twice as large as those based on F, and R-
 factors based on ALL data will be even larger.
;

_refine_ls_structure_factor_coef  Fsqd
_refine_ls_matrix_type            full
_refine_ls_weighting_scheme
 'calc w=1/[\s^2^(Fo^2^)+(0.0458P)^2^+3.1122P] where P=(Fo^2^+2Fc^2^)/3'
_atom_sites_solution_primary      direct
_atom_sites_solution_secondary    difmap
_atom_sites_solution_hydrogens    difmap
```

```
_refine_ls_hydrogen_treatment     refall
_refine_ls_extinction_method      ?
_refine_ls_extinction_coef        ?
_refine_ls_extinction_expression  ?
_refine_ls_number_reflns          3824
_refine_ls_number_parameters      223
_refine_ls_number_restraints      0
_refine_ls_R_factor_all           0.0496
_refine_ls_R_factor_obs           0.0327
_refine_ls_wR_factor_all          0.0924
_refine_ls_wR_factor_obs          0.0804
_refine_ls_goodness_of_fit_all    1.013
_refine_ls_goodness_of_fit_obs    1.014
_refine_ls_restrained_S_all       1.013
_refine_ls_restrained_S_obs       1.014
_refine_ls_shift/esd_max          -0.004
_refine_ls_shift/esd_mean         0.001

loop_
 _atom_site_label
 _atom_site_type_symbol
 _atom_site_fract_x
 _atom_site_fract_y
 _atom_site_fract_z
 _atom_site_U_iso_or_equiv
 _atom_site_thermal_displace_type
 _atom_site_occupancy
 _atom_site_calc_flag
 _atom_site_refinement_flags
 _atom_site_disorder_group
I1 I 0.5000 0.11729(2) 0.7500 0.02306(9) Uani 1 d S .
C4 C 0.5000 -0.3774(3) 0.7500 0.0147(5) Uani 1 d S .
O1 O 0.57386(6) -0.0932(2) 0.6133(2) 0.0152(3) Uani 1 d . .
C12 C 0.58158(8) -0.3911(2) 0.6132(2) 0.0151(4) Uani 1 d . .
C6 C 0.66842(8) 0.1682(2) 0.6137(2) 0.0155(4) Uani 1 d . .
O2 O 0.61797(6) -0.0262(2) 0.7949(2) 0.0184(3) Uani 1 d . .
N1 N 0.63260(7) 0.0641(2) 0.5890(2) 0.0160(4) Uani 1 d . .
C2 C 0.53859(8) -0.1674(2) 0.6862(2) 0.0135(4) Uani 1 d . .
C3 C 0.53932(8) -0.3104(2) 0.6834(2) 0.0137(4) Uani 1 d . .
C15 C 0.57154(10) -0.5462(2) 0.6150(2) 0.0194(4) Uani 1 d . .
C14 C 0.58464(10) -0.3506(3) 0.4676(2) 0.0218(5) Uani 1 d . .
C9 C 0.73727(10) 0.3824(2) 0.6448(3) 0.0276(6) Uani 1 d . .
C13 C 0.63246(10) -0.3646(3) 0.6807(3) 0.0234(5) Uani 1 d . .
C5 C 0.60935(8) -0.0171(2) 0.6787(2) 0.0149(4) Uani 1 d . .
C8 C 0.72463(10) 0.3371(3) 0.5208(3) 0.0264(5) Uani 1 d . .
C7 C 0.69044(10) 0.2303(2) 0.5044(2) 0.0211(5) Uani 1 d . .
```

C11 C 0.68111(9) 0.2132(2) 0.7391(2) 0.0192(4) Uani 1 d . .
C1 C 0.5000 -0.0960(3) 0.7500 0.0148(5) Uani 1 d S .
C10 C 0.71534(10) 0.3205(3) 0.7530(3) 0.0240(5) Uani 1 d . .
H15C H 0.5983(12) -0.5875(30) 0.5735(30) 0.021(7) Uiso 1 d . .
H13C H 0.6298(13) -0.3875(29) 0.7734(29) 0.023(8) Uiso 1 d . .
H15B H 0.5412(11) -0.5675(30) 0.5666(28) 0.019(7) Uiso 1 d . .
H15A H 0.5708(11) -0.5751(32) 0.7059(32) 0.022(7) Uiso 1 d . .
H7C H 0.5508(12) -0.3714(29) 0.4264(31) 0.026(8) Uiso 1 d . .
H8B H 0.6135(12) -0.4039(31) 0.4237(32) 0.028(8) Uiso 1 d . .
H11 H 0.6662(12) 0.1679(35) 0.8082(33) 0.029(8) Uiso 1 d . .
H13B H 0.6574(12) -0.4234(34) 0.6365(32) 0.033(9) Uiso 1 d . .
H14A H 0.5934(11) -0.2548(33) 0.4525(30) 0.027(8) Uiso 1 d . .
H4 H 0.5000 -0.4740(50) 0.7500 0.024(11) Uiso 1 d S .
H13 H 0.7398(13) 0.3756(31) 0.4435(36) 0.038(10) Uiso 1 d . .
H14 H 0.7211(13) 0.3457(37) 0.8345(37) 0.039(9) Uiso 1 d . .
H7 H 0.6815(11) 0.2018(31) 0.4258(31) 0.026(8) Uiso 1 d . .
H9 H 0.7611(12) 0.4584(33) 0.6569(31) 0.033(9) Uiso 1 d . .
H13A H 0.6446(11) -0.2772(33) 0.6708(29) 0.025(8) Uiso 1 d . .
H1N H 0.6243(11) 0.0548(31) 0.5153(28) 0.016(7) Uiso 1 d . .

loop_
 _atom_site_aniso_label
 _atom_site_aniso_U_11
 _atom_site_aniso_U_22
 _atom_site_aniso_U_33
 _atom_site_aniso_U_23
 _atom_site_aniso_U_13
 _atom_site_aniso_U_12
I1 0.02073(12) 0.00731(11) 0.0411(2) 0.000 0.00141(10) 0.000
C4 0.0196(14) 0.0095(13) 0.0149(12) 0.000 0.0004(12) 0.000
O1 0.0169(7) 0.0120(7) 0.0165(7) 0.0016(6) 0.0006(6) -0.0037(6)
C12 0.0178(10) 0.0114(9) 0.0163(10) 0.0001(8) 0.0021(8) 0.0013(7)
C6 0.0132(9) 0.0108(9) 0.0226(10) 0.0003(8) 0.0008(8) 0.0001(7)
O2 0.0224(8) 0.0173(8) 0.0155(7) 0.0026(6) -0.0016(6) -0.0015(6)
N1 0.0192(9) 0.0151(9) 0.0137(8) 0.0009(7) -0.0010(7) -0.0038(7)
C2 0.0157(9) 0.0116(9) 0.0133(9) 0.0017(7) -0.0006(7) -0.0023(7)
C3 0.0177(10) 0.0104(9) 0.0130(9) 0.0006(7) -0.0003(7) 0.0007(7)
C15 0.0255(11) 0.0130(10) 0.0196(11) -0.0002(8) 0.0036(9) 0.0027(9)
C14 0.0277(12) 0.0195(11) 0.0183(11) 0.0010(9) 0.0075(9) 0.0021(10)
C9 0.0220(12) 0.0151(12) 0.046(2) -0.0030(10) -0.0001(11) -0.0039(9)
C13 0.0207(11) 0.0204(12) 0.0291(13) -0.0012(10) -0.0004(10) 0.0036(9)
C5 0.0153(9) 0.0113(9) 0.0181(10) 0.0006(8) 0.0007(8) 0.0012(8)
C8 0.0260(12) 0.0178(11) 0.0355(14) 0.0005(10) 0.0087(11) -0.0049(10)
C7 0.0231(11) 0.0164(11) 0.0238(11) 0.0009(9) 0.0027(9) -0.0044(9)
C11 0.0204(10) 0.0151(10) 0.0222(11) -0.0009(9) -0.0023(9) -0.0012(8)
C1 0.0192(14) 0.0060(11) 0.0192(13) 0.000 -0.0028(12) 0.000

C10 0.0228(11) 0.0175(11) 0.0316(12) -0.0051(11) -0.0076(10) -0.0017(9)

_geom_special_details
;
All esds (except the esd in the dihedral angle between two l.s. planes)
are estimated using the full covariance matrix. The cell esds are taken
into account individually in the estimation of esds in distances, angles
and torsion angles; correlations between esds in cell parameters are only
used when they are defined by crystal symmetry. An approximate (isotropic)
treatment of cell esds is used for estimating esds involving l.s. planes.
;

loop_
_geom_bond_atom_site_label_1
_geom_bond_atom_site_label_2
_geom_bond_distance
_geom_bond_site_symmetry_2
_geom_bond_publ_flag
I1 C1 2.084(3) . ?
C4 C3 1.403(2) 3_656 ?
C4 C3 1.403(2) . ?
O1 C5 1.370(3) . ?
O1 C2 1.395(2) . ?
C12 C13 1.532(3) . ?
C12 C14 1.538(3) . ?
C12 C15 1.539(3) . ?
C12 C3 1.543(3) . ?
C6 C11 1.393(3) . ?
C6 C7 1.395(3) . ?
C6 N1 1.413(3) . ?
O2 C5 1.210(3) . ?
N1 C5 1.357(3) . ?
C2 C1 1.396(3) . ?
C2 C3 1.398(3) . ?
C9 C8 1.381(4) . ?
C9 C10 1.385(4) . ?
C8 C7 1.390(3) . ?
C11 C10 1.392(3) . ?
C1 C2 1.396(3) 3_656 ?

loop_
_geom_angle_atom_site_label_1
_geom_angle_atom_site_label_2
_geom_angle_atom_site_label_3
_geom_angle
_geom_angle_site_symmetry_1

```
 _geom_angle_site_symmetry_3
 _geom_angle_publ_flag
C3 C4 C3 124.4(3) 3_656 . ?
C5 O1 C2 118.7(2) . . ?
C13 C12 C14 110.1(2) . . ?
C13 C12 C15 108.2(2) . . ?
C14 C12 C15 105.9(2) . . ?
C13 C12 C3 109.9(2) . . ?
C14 C12 C3 110.8(2) . . ?
C15 C12 C3 111.9(2) . . ?
C11 C6 C7 119.7(2) . . ?
C11 C6 N1 123.5(2) . . ?
C7 C6 N1 116.8(2) . . ?
C5 N1 C6 127.2(2) . . ?
O1 C2 C1 118.4(2) . . ?
O1 C2 C3 120.0(2) . . ?
C1 C2 C3 121.3(2) . . ?
C2 C3 C4 116.5(2) . . ?
C2 C3 C12 122.0(2) . . ?
C4 C3 C12 121.5(2) . . ?
C8 C9 C10 119.2(2) . . ?
O2 C5 N1 128.1(2) . . ?
O2 C5 O1 124.4(2) . . ?
N1 C5 O1 107.4(2) . . ?
C9 C8 C7 120.5(2) . . ?
C8 C7 C6 120.1(2) . . ?
C6 C11 C10 119.2(2) . . ?
C2 C1 C2 120.0(3) 3_656 . ?
C2 C1 I1 120.00(13) 3_656 . ?
C2 C1 I1 120.00(13) . . ?
C9 C10 C11 121.3(2) . . ?

loop_
 _geom_torsion_atom_site_label_1
 _geom_torsion_atom_site_label_2
 _geom_torsion_atom_site_label_3
 _geom_torsion_atom_site_label_4
 _geom_torsion
 _geom_torsion_site_symmetry_1
 _geom_torsion_site_symmetry_2
 _geom_torsion_site_symmetry_3
 _geom_torsion_site_symmetry_4
 _geom_torsion_publ_flag
 C11 C6 N1 C5 -7.4(4) . . . . ?
 C7 C6 N1 C5 174.6(2) . . . . ?
 C5 O1 C2 C1 72.9(2) . . . . ?
```

```
 C5 O1 C2 C3 -113.5(2) . . . . ?
 O1 C2 C3 C4 -174.63(15) . . . . ?
 C1 C2 C3 C4 -1.2(3) . . . . ?
 O1 C2 C3 C12 6.5(3) . . . . ?
 C1 C2 C3 C12 179.9(2) . . . . ?
 C3 C4 C3 C2 0.59(14) 3_656 . . . ?
 C3 C4 C3 C12 179.5(2) 3_656 . . . ?
 C13 C12 C3 C2 64.3(3) . . . . ?
 C14 C12 C3 C2 -57.6(3) . . . . ?
 C15 C12 C3 C2 -175.5(2) . . . . ?
 C13 C12 C3 C4 -114.6(2) . . . . ?
 C14 C12 C3 C4 123.5(2) . . . . ?
 C15 C12 C3 C4 5.6(3) . . . . ?
 C6 N1 C5 O2 -7.9(4) . . . . ?
 C6 N1 C5 O1 173.7(2) . . . . ?
 C2 O1 C5 O2 12.7(3) . . . . ?
 C2 O1 C5 N1 -168.8(2) . . . . ?
 C10 C9 C8 C7 -0.2(4) . . . . ?
 C9 C8 C7 C6 0.3(4) . . . . ?
 C11 C6 C7 C8 -0.4(4) . . . . ?
 N1 C6 C7 C8 177.6(2) . . . . ?
 C7 C6 C11 C10 0.6(3) . . . . ?
 N1 C6 C11 C10 -177.3(2) . . . . ?
 O1 C2 C1 C2 174.2(2) . . . 3_656 ?
 C3 C2 C1 C2 0.63(15) . . . 3_656 ?
 O1 C2 C1 I1 -5.8(2) . . . . ?
 C3 C2 C1 I1 -179.37(15) . . . . ?
 C8 C9 C10 C11 0.4(4) . . . . ?
 C6 C11 C10 C9 -0.6(4) . . . . ?

_refine_diff_density_max    0.895
_refine_diff_density_min   -1.695
_refine_diff_density_rms    0.095
# END OF CIF
```

Crystallographic data file (**CIF**) for **3.6a**:

```
data_Tetra-Ester(Green)

_audit_creation_method            SHELXL
_chemical_name_systematic
;
 ?
;
_chemical_name_common             ?
_chemical_formula_moiety          ?
_chemical_formula_structural      ?
_chemical_formula_analytical      ?
_chemical_formula_sum             'C46 H66 O12'
_chemical_formula_weight          810.99
_chemical_melting_point           ?
_chemical_compound_source         ?

loop_
 _atom_type_symbol
 _atom_type_description
 _atom_type_scat_dispersion_real
 _atom_type_scat_dispersion_imag
 _atom_type_scat_source
 'C'  'C'   0.0033   0.0016
 'International Tables Vol C Tables 4.2.6.8 and 6.1.1.4'
 'H'  'H'   0.0000   0.0000
 'International Tables Vol C Tables 4.2.6.8 and 6.1.1.4'
 'O'  'O'   0.0106   0.0060
 'International Tables Vol C Tables 4.2.6.8 and 6.1.1.4'

_symmetry_cell_setting            Triclinic
_symmetry_space_group_name_H-M    P-1

loop_
 _symmetry_equiv_pos_as_xyz
 'x, y, z'
 '-x, -y, -z'

_cell_length_a                    9.7750(10)
_cell_length_b                    10.587(2)
_cell_length_c                    12.998(2)
_cell_angle_alpha                 112.170(10)
_cell_angle_beta                  102.190(10)
_cell_angle_gamma                 96.440(10)
_cell_volume                      1189.9(3)
```

```
_cell_formula_units_Z            1
_cell_measurement_temperature     293(2)
_cell_measurement_reflns_used     20
_cell_measurement_theta_min       5.40
_cell_measurement_theta_max       12.46

_exptl_crystal_description        Clear_flat_plate
_exptl_crystal_colour             colorless
_exptl_crystal_size_max           0.2
_exptl_crystal_size_mid           0.6
_exptl_crystal_size_min           0.8
_exptl_crystal_density_meas       ?
_exptl_crystal_density_diffrn     1.132
_exptl_crystal_density_method     ?
_exptl_crystal_F_000              438
_exptl_absorpt_coefficient_mu     0.081
_exptl_absorpt_correction_type    none
_exptl_absorpt_correction_T_min   ?
_exptl_absorpt_correction_T_max   ?

_exptl_special_details
;
 ?
;

_diffrn_ambient_temperature       293(2)
_diffrn_radiation_wavelength      0.71073
_diffrn_radiation_type            MoK\a
_diffrn_radiation_source          'fine-focus sealed tube'
_diffrn_radiation_monochromator   graphite
_diffrn_measurement_device        'Siemens P4'
_diffrn_measurement_method        '\w scans'
_diffrn_standards_number          3
_diffrn_standards_interval_count  197
_diffrn_standards_interval_time   ?
_diffrn_standards_decay_%         8.75
_diffrn_reflns_number             4877
_diffrn_reflns_av_R_equivalents   0.0353
_diffrn_reflns_av_sigmaI/netI     0.0473
_diffrn_reflns_limit_h_min        -1
_diffrn_reflns_limit_h_max        11
_diffrn_reflns_limit_k_min        -11
_diffrn_reflns_limit_k_max        11
_diffrn_reflns_limit_l_min        -15
_diffrn_reflns_limit_l_max        15
_diffrn_reflns_theta_min          1.76
```

```
_diffrn_reflns_theta_max          25.00
_reflns_number_total              4085
_reflns_number_observed           2653
_reflns_observed_criterion        >2sigma(I)

_computing_data_collection        'Siemens XSCANS'
_computing_cell_refinement        'Siemens XSCANS'
_computing_data_reduction         'Siemens SHELXTL'
_computing_structure_solution     'SHELXS-86 (Sheldrick, 1990)'
_computing_structure_refinement   'SHELXL-93 (Sheldrick, 1993)'
_computing_molecular_graphics     'Siemens SHELXTL'
_computing_publication_material   'Siemens SHELXTL'

_refine_special_details
;
 Refinement on F^2^ for ALL reflections except for 459 with very negative F^2^
 or flagged by the user for potential systematic errors.  Weighted R-factors
 wR and all goodnesses of fit S are based on F^2^, conventional R-factors R
 are based on F, with F set to zero for negative F^2^. The observed criterion
 of F^2^ > 2sigma(F^2^) is used only for calculating _R_factor_obs etc. and is
 not relevant to the choice of reflections for refinement.  R-factors based
 on F^2^ are statistically about twice as large as those based on F, and R-
 factors based on ALL data will be even larger.
;

_refine_ls_structure_factor_coef  Fsqd
_refine_ls_matrix_type            full
_refine_ls_weighting_scheme
 'calc w=1/[\s^2^(Fo^2^)+(0.0715P)^2^+0.3991P] where P=(Fo^2^+2Fc^2^)/3'
_atom_sites_solution_primary      direct
_atom_sites_solution_secondary    difmap
_atom_sites_solution_hydrogens    geom
_refine_ls_hydrogen_treatment     ?
_refine_ls_extinction_method      SHELXL
_refine_ls_extinction_coef        0.0254(37)
_refine_ls_extinction_expression
 'Fc^*^=kFc[1+0.001xFc^2^\l^3^/sin(2\q)]^-1/4^'
_refine_ls_number_reflns          3626
_refine_ls_number_parameters      263
_refine_ls_number_restraints      0
_refine_ls_R_factor_all           0.0946
_refine_ls_R_factor_obs           0.0594
_refine_ls_wR_factor_all          0.1815
_refine_ls_wR_factor_obs          0.1500
_refine_ls_goodness_of_fit_all    1.039
_refine_ls_goodness_of_fit_obs    1.129
```

```
_refine_ls_restrained_S_all       1.087
_refine_ls_restrained_S_obs       1.129
_refine_ls_shift/esd_max         -0.013
_refine_ls_shift/esd_mean         0.002

loop_
 _atom_site_label
 _atom_site_type_symbol
 _atom_site_fract_x
 _atom_site_fract_y
 _atom_site_fract_z
 _atom_site_U_iso_or_equiv
 _atom_site_thermal_displace_type
 _atom_site_occupancy
 _atom_site_calc_flag
 _atom_site_refinement_flags
 _atom_site_disorder_group
C1 C 0.5119(2) 0.2075(2) 0.5849(2) 0.0481(6) Uani 1 d . .
C2 C 0.4034(2) 0.2671(2) 0.5443(2) 0.0502(6) Uani 1 d . .
C3 C 0.3858(2) 0.3979(3) 0.6121(2) 0.0528(6) Uani 1 d . .
C4 C 0.4890(3) 0.4692(3) 0.7180(2) 0.0580(7) Uani 1 d . .
H4A H 0.4785(3) 0.5567(3) 0.7654(2) 0.070 Uiso 1 calc R .
C5 C 0.6066(3) 0.4211(3) 0.7594(2) 0.0545(6) Uani 1 d . .
C6 C 0.6154(2) 0.2876(2) 0.6904(2) 0.0505(6) Uani 1 d . .
O1 O 0.3053(2) 0.1875(2) 0.43760(14) 0.0562(5) Uani 1 d . .
C8 C 0.2434(4) 0.0969(3) 0.2327(2) 0.0728(8) Uani 1 d . .
C9 C 0.1904(6) -0.0327(5) 0.0305(3) 0.129(2) Uani 1 d . .
H9A H 0.1122(6) -0.0968(5) 0.0316(3) 0.154 Uiso 1 calc R .
H9B H 0.1512(6) 0.0372(5) 0.0094(3) 0.154 Uiso 1 calc R .
C10 C 0.2619(8) -0.1065(6) -0.0515(4) 0.190(3) Uani 1 d . .
H10A H 0.1952(8) -0.1511(6) -0.1270(4) 0.285 Uiso 1 calc R .
H10B H 0.2998(8) -0.1757(6) -0.0303(4) 0.285 Uiso 1 calc R .
H10C H 0.3387(8) -0.0421(6) -0.0523(4) 0.285 Uiso 1 calc R .
O4 O 0.7229(2) 0.2289(2) 0.73039(14) 0.0567(5) Uani 1 d . .
C12 C 0.9525(3) 0.1756(3) 0.7324(3) 0.0695(8) Uani 1 d . .
C13 C 1.1670(5) 0.0961(7) 0.7238(5) 0.183(3) Uani 1 d . .
H13A H 1.2358(5) 0.1823(7) 0.7475(5) 0.220 Uiso 1 calc R .
H13B H 1.1590(5) 0.0850(7) 0.7931(5) 0.220 Uiso 1 calc R .
C14 C 1.2136(7) -0.0009(8) 0.6660(6) 0.210(3) Uani 1 d . .
H14A H 1.3046(7) -0.0022(8) 0.7110(6) 0.315 Uiso 1 calc R .
H14B H 1.2251(7) 0.0104(8) 0.5983(6) 0.315 Uiso 1 calc R .
H14C H 1.1477(7) -0.0872(8) 0.6435(6) 0.315 Uiso 1 calc R .
C15 C 0.7175(3) 0.5129(3) 0.8762(2) 0.0673(8) Uani 1 d . .
C16 C 0.8644(3) 0.5421(3) 0.8582(3) 0.0848(10) Uani 1 d . .
H16A H 0.8596(3) 0.5873(3) 0.8063(3) 0.127 Uiso 1 calc R .
H16B H 0.8946(3) 0.4558(3) 0.8258(3) 0.127 Uiso 1 calc R .
```

H16C H 0.9318(3) 0.6017(3) 0.9311(3) 0.127 Uiso 1 calc R .
C17 C 0.7239(4) 0.4411(4) 0.9586(2) 0.0918(10) Uani 1 d . .
H17A H 0.6308(4) 0.4231(4) 0.9697(2) 0.138 Uiso 1 calc R .
H17B H 0.7912(4) 0.5005(4) 1.0316(2) 0.138 Uiso 1 calc R .
H17C H 0.7536(4) 0.3545(4) 0.9264(2) 0.138 Uiso 1 calc R .
C18 C 0.6781(4) 0.6547(3) 0.9348(3) 0.1005(12) Uani 1 d . .
H18A H 0.5854(4) 0.6397(3) 0.9474(3) 0.151 Uiso 1 calc R .
H18B H 0.6760(4) 0.7039(3) 0.8859(3) 0.151 Uiso 1 calc R .
H18C H 0.7481(4) 0.7089(3) 1.0076(3) 0.151 Uiso 1 calc R .
C19 C 0.2578(3) 0.4592(3) 0.5750(2) 0.0619(7) Uani 1 d . .
C20 C 0.2613(3) 0.4804(3) 0.4657(3) 0.0816(9) Uani 1 d . .
H20A H 0.3494(3) 0.5422(3) 0.4797(3) 0.122 Uiso 1 calc R .
H20B H 0.1821(3) 0.5202(3) 0.4450(3) 0.122 Uiso 1 calc R .
H20C H 0.2546(3) 0.3921(3) 0.4039(3) 0.122 Uiso 1 calc R .
C21 C 0.1190(3) 0.3615(4) 0.5548(3) 0.0912(11) Uani 1 d . .
H21A H 0.1181(3) 0.3490(4) 0.6241(3) 0.137 Uiso 1 calc R .
H21B H 0.1118(3) 0.2728(4) 0.4932(3) 0.137 Uiso 1 calc R .
H21C H 0.0393(3) 0.4009(4) 0.5343(3) 0.137 Uiso 1 calc R .
C22 C 0.2613(4) 0.6021(4) 0.6699(3) 0.0943(11) Uani 1 d . .
H22A H 0.3482(4) 0.6659(4) 0.6845(3) 0.141 Uiso 1 calc R .
H22B H 0.2573(4) 0.5916(4) 0.7395(3) 0.141 Uiso 1 calc R .
H22C H 0.1805(4) 0.6377(4) 0.6450(3) 0.141 Uiso 1 calc R .
C23 C 0.5066(2) 0.0616(2) 0.5241(2) 0.0499(6) Uani 1 d . .
C7 C 0.3628(3) 0.1565(3) 0.3420(2) 0.0704(8) Uani 1 d . .
H7A H 0.4234(3) 0.0899(3) 0.3414(2) 0.085 Uiso 1 calc R .
H7B H 0.4208(3) 0.2408(3) 0.3478(2) 0.085 Uiso 1 calc R .
O2 O 0.1224(3) 0.1076(3) 0.2260(2) 0.1071(9) Uani 1 d . .
O3 O 0.2944(3) 0.0343(2) 0.1445(2) 0.0967(8) Uani 1 d . .
C11 C 0.8148(3) 0.1813(3) 0.6595(2) 0.0626(7) Uani 1 d . .
H11A H 0.8332(3) 0.2442(3) 0.6234(2) 0.075 Uiso 1 calc R .
H11B H 0.7696(3) 0.0893(3) 0.5990(2) 0.075 Uiso 1 calc R .
O5 O 0.9886(3) 0.2228(3) 0.8356(2) 0.1075(9) Uani 1 d . .
O6 O 1.0268(2) 0.1093(3) 0.6645(2) 0.0949(7) Uani 1 d . .

loop_
 _atom_site_aniso_label
 _atom_site_aniso_U_11
 _atom_site_aniso_U_22
 _atom_site_aniso_U_33
 _atom_site_aniso_U_23
 _atom_site_aniso_U_13
 _atom_site_aniso_U_12
C1 0.0403(12) 0.0472(13) 0.0492(13) 0.0158(11) 0.0056(10) 0.0080(10)
C2 0.0407(13) 0.0521(14) 0.0475(13) 0.0152(11) 0.0044(11) 0.0044(11)
C3 0.0450(13) 0.0541(15) 0.0568(14) 0.0201(12) 0.0123(11) 0.0138(11)
C4 0.058(2) 0.0521(14) 0.0549(14) 0.0132(12) 0.0134(12) 0.0147(12)

C5 0.0529(14) 0.0537(15) 0.0480(13) 0.0164(11) 0.0057(11) 0.0100(12)
C6 0.0437(13) 0.0540(14) 0.0487(13) 0.0193(11) 0.0061(11) 0.0103(11)
O1 0.0448(9) 0.0621(10) 0.0493(9) 0.0164(8) 0.0018(8) 0.0084(8)
C8 0.080(2) 0.064(2) 0.057(2) 0.0199(14) -0.001(2) 0.008(2)
C9 0.174(4) 0.111(3) 0.053(2) 0.008(2) -0.003(2) 0.002(3)
C10 0.313(9) 0.161(5) 0.064(3) 0.011(3) 0.031(4) 0.096(5)
O4 0.0496(10) 0.0622(11) 0.0516(9) 0.0200(8) 0.0043(8) 0.0171(8)
C12 0.052(2) 0.063(2) 0.077(2) 0.0204(15) 0.001(2) 0.0142(14)
C13 0.117(4) 0.233(7) 0.158(5) 0.027(4) 0.010(3) 0.120(4)
C14 0.157(5) 0.274(9) 0.191(6) 0.063(6) 0.044(5) 0.141(6)
C15 0.072(2) 0.059(2) 0.0491(15) 0.0089(12) -0.0002(13) 0.0092(14)
C16 0.067(2) 0.076(2) 0.076(2) 0.016(2) -0.009(2) -0.010(2)
C17 0.107(3) 0.099(2) 0.054(2) 0.026(2) 0.005(2) 0.015(2)
C18 0.113(3) 0.073(2) 0.066(2) -0.006(2) -0.011(2) 0.024(2)
C19 0.0510(15) 0.062(2) 0.072(2) 0.0258(13) 0.0124(13) 0.0212(13)
C20 0.079(2) 0.088(2) 0.094(2) 0.051(2) 0.020(2) 0.037(2)
C21 0.051(2) 0.097(2) 0.142(3) 0.063(2) 0.028(2) 0.026(2)
C22 0.085(2) 0.087(2) 0.101(2) 0.024(2) 0.019(2) 0.049(2)
C23 0.0388(12) 0.0536(13) 0.0487(14) 0.0174(11) 0.0017(10) 0.0095(12)
C7 0.061(2) 0.090(2) 0.054(2) 0.0265(15) 0.0082(13) 0.0166(15)
O2 0.074(2) 0.133(2) 0.0770(15) 0.0241(14) -0.0123(12) 0.0118(15)
O3 0.124(2) 0.097(2) 0.0511(12) 0.0166(11) 0.0118(12) 0.0261(14)
C11 0.0462(14) 0.073(2) 0.059(2) 0.0220(13) 0.0047(12) 0.0141(13)
O5 0.084(2) 0.132(2) 0.0727(15) 0.0188(14) -0.0134(12) 0.0453(15)
O6 0.0618(13) 0.119(2) 0.099(2) 0.0363(14) 0.0167(12) 0.0428(13)

_geom_special_details
;
All esds (except the esd in the dihedral angle between two l.s. planes)
are estimated using the full covariance matrix. The cell esds are taken
into account individually in the estimation of esds in distances, angles
and torsion angles; correlations between esds in cell parameters are only
used when they are defined by crystal symmetry. An approximate (isotropic)
treatment of cell esds is used for estimating esds involving l.s. planes.
;

loop_
_geom_bond_atom_site_label_1
_geom_bond_atom_site_label_2
_geom_bond_distance
_geom_bond_site_symmetry_2
_geom_bond_publ_flag
C1 C6 1.402(3) . ?
C1 C2 1.402(3) . ?
C1 C23 1.434(3) . ?
C2 O1 1.388(3) . ?

```
C2 C3 1.386(3) . ?
C3 C4 1.392(3) . ?
C3 C19 1.544(3) . ?
C4 C5 1.396(3) . ?
C5 C6 1.383(3) . ?
C5 C15 1.543(3) . ?
C6 O4 1.386(3) . ?
O1 C7 1.413(3) . ?
C8 O2 1.188(4) . ?
C8 O3 1.321(4) . ?
C8 C7 1.495(4) . ?
C9 C10 1.429(6) . ?
C9 O3 1.464(4) . ?
O4 C11 1.417(3) . ?
C12 O5 1.195(3) . ?
C12 O6 1.311(3) . ?
C12 C11 1.496(4) . ?
C13 C14 1.222(6) . ?
C13 O6 1.473(5) . ?
C15 C16 1.520(4) . ?
C15 C17 1.524(4) . ?
C15 C18 1.541(4) . ?
C19 C21 1.520(4) . ?
C19 C20 1.526(4) . ?
C19 C22 1.541(4) . ?
C23 C23 1.193(4) 2_656 ?

loop_
 _geom_angle_atom_site_label_1
 _geom_angle_atom_site_label_2
 _geom_angle_atom_site_label_3
 _geom_angle
 _geom_angle_site_symmetry_1
 _geom_angle_site_symmetry_3
 _geom_angle_publ_flag
C6 C1 C2 119.6(2) . . ?
C6 C1 C23 120.8(2) . . ?
C2 C1 C23 119.3(2) . . ?
O1 C2 C3 119.9(2) . . ?
O1 C2 C1 118.5(2) . . ?
C3 C2 C1 121.3(2) . . ?
C2 C3 C4 115.7(2) . . ?
C2 C3 C19 122.4(2) . . ?
C4 C3 C19 121.9(2) . . ?
C3 C4 C5 125.8(2) . . ?
C6 C5 C4 116.0(2) . . ?
```

```
C6 C5 C15 123.0(2) . . ?
C4 C5 C15 121.0(2) . . ?
C5 C6 O4 119.1(2) . . ?
C5 C6 C1 121.2(2) . . ?
O4 C6 C1 119.6(2) . . ?
C2 O1 C7 114.9(2) . . ?
O2 C8 O3 125.4(3) . . ?
O2 C8 C7 125.3(3) . . ?
O3 C8 C7 109.3(3) . . ?
C10 C9 O3 108.3(4) . . ?
C6 O4 C11 116.9(2) . . ?
O5 C12 O6 125.5(3) . . ?
O5 C12 C11 125.7(3) . . ?
O6 C12 C11 108.8(3) . . ?
C14 C13 O6 114.8(5) . . ?
C16 C15 C17 109.9(3) . . ?
C16 C15 C18 107.4(3) . . ?
C17 C15 C18 107.4(3) . . ?
C16 C15 C5 110.2(2) . . ?
C17 C15 C5 110.4(2) . . ?
C18 C15 C5 111.4(2) . . ?
C21 C19 C20 110.3(3) . . ?
C21 C19 C22 107.8(3) . . ?
C20 C19 C22 107.6(3) . . ?
C21 C19 C3 109.3(2) . . ?
C20 C19 C3 110.7(2) . . ?
C22 C19 C3 111.1(2) . . ?
C23 C23 C1 175.3(3) 2_656 . ?
O1 C7 C8 109.5(2) . . ?
C8 O3 C9 116.4(3) . . ?
O4 C11 C12 109.0(2) . . ?
C12 O6 C13 115.4(3) . . ?

_refine_diff_density_max    0.304
_refine_diff_density_min   -0.267
_refine_diff_density_rms    0.037
                                    # END OF CIF
```

VITA

Brett Kite was born in Radford, Virginia on December 15, 1970 to Bertram W. Kite, Jr. and Alice Lowers Kite. He received his B.S. in chemistry from Virginia Polytechnic Institute and State University in 1992. After the departure of his original advisor, he joined Dr. Richard D. Gandour's research group at Virginia Tech in 1993. He received his Ph.D. in chemistry from Virginia Tech Polytechnic Institute and State University in 2006.